

# Simulation of gas-assisted injection moulding

**Citation for published version (APA):**

Haagh, G. A. A. V. (1998). *Simulation of gas-assisted injection moulding*. [Phd Thesis 1 (Research TU/e / Graduation TU/e), Mechanical Engineering]. Technische Universiteit Eindhoven.  
<https://doi.org/10.6100/IR509070>

**DOI:**

[10.6100/IR509070](https://doi.org/10.6100/IR509070)

**Document status and date:**

Published: 01/01/1998

**Document Version:**

Publisher's PDF, also known as Version of Record (includes final page, issue and volume numbers)

**Please check the document version of this publication:**

- A submitted manuscript is the version of the article upon submission and before peer-review. There can be important differences between the submitted version and the official published version of record. People interested in the research are advised to contact the author for the final version of the publication, or visit the DOI to the publisher's website.
- The final author version and the galley proof are versions of the publication after peer review.
- The final published version features the final layout of the paper including the volume, issue and page numbers.

[Link to publication](#)

**General rights**

Copyright and moral rights for the publications made accessible in the public portal are retained by the authors and/or other copyright owners and it is a condition of accessing publications that users recognise and abide by the legal requirements associated with these rights.

- Users may download and print one copy of any publication from the public portal for the purpose of private study or research.
- You may not further distribute the material or use it for any profit-making activity or commercial gain
- You may freely distribute the URL identifying the publication in the public portal.

If the publication is distributed under the terms of Article 25fa of the Dutch Copyright Act, indicated by the "Taverne" license above, please follow below link for the End User Agreement:

[www.tue.nl/taverne](http://www.tue.nl/taverne)

**Take down policy**

If you believe that this document breaches copyright please contact us at:

[openaccess@tue.nl](mailto:openaccess@tue.nl)

providing details and we will investigate your claim.

# Simulation of Gas-Assisted Injection Moulding

Gerard Haugh

# **Simulation of Gas-Assisted Injection Moulding**

CIP-DATA LIBRARY TECHNISCHE UNIVERSITEIT EINDHOVEN

Simulation of gas-assisted injection moulding /

Gerardus Antonius Adrianus Victor Haagh. – Eindhoven : Technische Universiteit Eindhoven, 1998. – XVIII, 109 p. – With ref. – With summary in Dutch.

Proefschrift. – ISBN 90-386-0620-6

NUGI 841

Trefwoorden: gasinjectiespuitgieten / spuitgieten ; kunststoffen / numerieke simulatie

Subject headings: gas-assisted injection moulding / injection moulding ; plastics / numerical simulation

This research was financially supported by the Graduate School Polymer Technology Netherlands (PTN).

Druk: Universiteitsdrukkerij TU Eindhoven

# Simulation of Gas-Assisted Injection Moulding

PROEFSCHRIFT

ter verkrijging van de graad van doctor  
aan de Technische Universiteit Eindhoven,  
op gezag van de Rector Magnificus, prof.dr. M. Rem,  
voor een commissie aangewezen door het College voor Promoties  
in het openbaar te verdedigen op  
donderdag 5 maart 1998 om 16.00 uur

door

Gerardus Antonius Adrianus Victor Haagh

geboren te Dongen

Dit proefschrift is goedgekeurd door de promotoren:

prof.dr.ir. H.E.H. Meijer

prof.dr.ir. F.P.T. Baaijens

en de copromotor:

dr.ir. F.N. van de Vosse

*De kennis der natuur is ons niet  
aangeboren en ze komt ons ook niet  
aangewaaid in het studeervertrek.  
Zij moet door zwoegen en sloven  
verworven worden (...).*

E.J. Dijksterhuis – De  
mechanisering van het  
wereldbeeld, (I:102).

*Voor mijn ouders*





# Contents

<b>Summary</b>	<b>xi</b>
<b>Samenvatting</b>	<b>xiii</b>
<b>Notation</b>	<b>xv</b>
<b>1 Introduction</b>	<b>1</b>
1.1 Injection moulding processes	1
1.2 Gas-assisted injection moulding	4
1.2.1 Process characteristics	5
1.2.2 Advantages	6
1.2.3 Practical aspects	9
1.3 Gas penetration into a viscous fluid	11
1.4 A review of gas-assisted injection moulding modelling	16
1.5 Objective	20
<b>2 Modelling</b>	<b>23</b>
2.1 Mould filling simulation: a moving boundary problem	24
2.2 Governing equations	25
2.3 Flow problem	26
2.3.1 Polymer domain	28
2.3.2 Air domain	29
2.3.3 Boundary conditions	30
2.3.4 Interfacial conditions	30
2.4 Material label convection problem	31
2.5 Temperature problem	32
2.5.1 Polymer domain	33
2.5.2 Air domain	34
2.5.3 Initial and boundary conditions	35
2.6 Residual stresses	35

2.6.1	The compressible Leonov model	36
2.6.2	Flow-induced stresses	38
2.6.3	Thermally and pressure-induced stresses	38
2.6.4	Initial and boundary conditions	40
2.7	Conclusions	41
<b>3</b>	<b>Methods</b>	<b>43</b>
3.1	Numerical methods	43
3.1.1	Stokes equation	43
3.1.2	Convection equation	45
3.1.3	Temperature equation	47
3.1.4	Residual stresses	48
3.2	Implementation	49
3.3	Experimental methods	50
3.3.1	Cylinder set-up	51
3.3.2	Plaque-with-rib set-up	52
3.3.3	Material properties	53
<b>4</b>	<b>Results</b>	<b>57</b>
4.1	Simulation of general mould filling phenomena	57
4.1.1	Filling of an axisymmetric cylinder	58
4.1.2	Flow in a bifurcation	60
4.1.3	Filling of a three-dimensional rectangular cavity	61
4.1.4	Discussion	61
4.2	Simulation of gas-assisted injection moulding phenomena	63
4.2.1	GAIM of an axisymmetric cylinder	63
4.2.2	Gas flow around a sharp corner	66
4.2.3	Bifurcation of the gas flow	66
4.2.4	GAIM of a three-dimensional rectangular cavity	68
4.2.5	Discussion	68
4.3	Experimental validation	71
4.3.1	Axisymmetric cylinder	71
4.3.2	Plaque-with-rib	75
4.3.3	Discussion	77
4.4	A test case for residual stress computations	82
<b>5</b>	<b>Conclusions and Recommendations</b>	<b>85</b>
5.1	Conclusions	85
5.2	Recommendations	88

<b>References</b>	<b>91</b>
<b>A The effect of compressibility on the momentum equation</b>	<b>99</b>
<b>B Convergence test</b>	<b>101</b>
<b>C The fingering effect</b>	<b>105</b>
<b>Dankwoord</b>	<b>107</b>
<b>Curriculum Vitae</b>	<b>109</b>



# Summary

A three-dimensional computational model for Gas-Assisted Injection Moulding (GAIM) processes is developed. From the simulations of a number of typical benchmark problems and from the comparison of numerical with experimental results, it is concluded that this model provides a sound basis for the predictive simulation of these processes.

In gas-assisted injection moulding, gas is injected into a mould that has been filled partially with a polymer melt. The gas drives the molten polymer core further into the mould until it is filled completely, thus yielding a product with a polymer skin and a hollow core. While the polymer is cooled in the mould, the gas is used to transmit the packing pressure to the polymer skin. Once the polymer skin has been solidified completely, the gas pressure is released, and the product can be ejected.

A major characteristic of GAIM is that the pressure gradient in the gas core is negligibly small compared to the pressure gradient in the polymer melt, due to the very large polymer/gas viscosity ratio. The gas penetrates in the direction of the least flow resistance, which is typically found in the thicker parts of the mould, such as ribs or specially designed gas leading channels.

The negligible pressure gradient in the gas core is the basis for most of the advantages of the GAIM process. First of all, it leads to a reduction in both the injection and packing pressure. Moreover, the pressure is distributed more uniformly over the mould. This may reduce residual stresses and warpage. Also, the sink marks at the thick-walled parts will be reduced, as the polymer shrinkage will be compensated by an enlargement of the gas core. Furthermore, cooling times may be decreased, yielding shorter cycle times. Finally, GAIM allows for (partially) thick-walled products that are to be avoided in conventional injection moulding; therefore it enhances the product design possibilities. On the other hand, the characteristics of GAIM complicate the control of the process. Because the direction of the lowest flow resistance along which the gas front proceeds is unique, splitting of the gas flow may lead to uncontrolled gas penetration.

Although gas-assisted injection moulding has been practised in industry for more than a decade, the process is not completely understood, particularly with respect to the gas penetration mechanism. Consequently, mould design and process control are often governed by trial-and-error, and reliable information on the gas distribution and the

final product properties can often only be obtained from experiments. To gain a better understanding of the gas-assisted injection moulding process, to improve the process control, and to predict the final product properties, we have developed a simulation tool for the GAIM process.

An important quantity in GAIM is the residual wall thickness, which is the thickness of the polymer layer that is left behind at the mould walls after the gas front has passed. This thickness does not only determine the ratio of polymer and gas to be injected, but also affects the final product properties. The pressure at the gas front induces velocities in the gas front vicinity that have a significant component in the thickness direction. Moreover, gas penetration typically takes place in the thick-walled parts of a mould. Therefore, GAIM is characterised by three-dimensional (flow) phenomena.

Because of this 3-D character, the  $2\frac{1}{2}$ -D approach — which is the state-of-the-art in modelling ‘conventional’ injection moulding processes — is inadequate for GAIM modelling. Therefore, we have developed a computational model that is able to deal with (non-isothermal) three-dimensional flow, in order to correctly predict the gas distribution in GAIM products. This model employs a pseudo-concentration method, in which the governing equations are solved on a fixed grid that covers the entire mould. Both the air downstream of the polymer front and the gas are represented by a fictitious fluid that does not contribute to the pressure drop in the mould. A material label  $c$  (the ‘pseudo-concentration’) is introduced to distinguish the polymer from the gas (and air), and all material properties are defined as a function of this material label. The moving polymer flow front is modelled by introducing a material label dependent boundary condition at the mould walls, which prescribes free slip in the air domain, and no slip in the polymer domain.

Validation of the model has been carried out by comparing simulation results to both isothermal and non-isothermal gas injection experiments. For isothermal gas injection, the agreement between experimental and numerical values is excellent. Non-isothermal conditions, however, were accompanied by experimental difficulties that complicated the control over the gas penetration. The experimental and numerical results do exhibit similar trends, but the quantitative agreement is not as good as for the isothermal cases.

In conclusion, the developed model enables the simulation of gas-assisted injection moulding processes. In contradiction to other models that have been reported in the literature, this model yields the gas penetration from the actual process physics (not from a presupposed gas distribution). Moreover, it is able to deal with the 3-D character of the process, and incorporates temperature effects and generalised Newtonian viscosity behaviour. As such, this model can be regarded as a starting point for a design tool for gas-assisted injection moulding products; in this respect, a model for 3-D residual stress computations is proposed that fits within the pseudo-concentration approach. It is recommended, however, to improve the computational efficiency of the code before using it for simulations on more complex (industrial) GAIM products.

# Samenvatting

Er is een drie-dimensionaal rekenmodel ontwikkeld voor gasinjectiespuitgieten (een overigens zwakke vertaling van de veel betere Engelse term *Gas-Assisted Injection Moulding*). Uit simulaties van een aantal typische *benchmark* problemen en uit de vergelijking van numerieke met experimentele resultaten kan geconcludeerd worden, dat dit model een goede basis biedt om met behulp van simulaties voorspellingen te doen over dit proces.

Bij gasinjectiespuitgieten wordt gas geïnjecteerd in een matrijs die slechts gedeeltelijk gevuld is met kunststof. Het gas duwt de gesmolten polymeerkern verder de matrijs in, totdat die geheel gevuld is. Het resultaat is een kunststof product met een holle kern. Terwijl de kunststof vervolgens afkoelt in de matrijs, wordt de nadruk via het gas overgebracht op de polymeerlaag aan de wanden. Wanneer het polymeer geheel gestold is, kan het nadrukken beëindigd en het product uitgeworpen worden.

Een belangrijk kenmerk van gasinjectiespuitgieten is, dat de drukval in het gas verwaarloosbaar klein is ten opzichte van de drukval in de kunststof smelt vanwege de hoge viscositeitsverhouding van polymeer en gas. Het gas dringt de smelt binnen langs de weg van de minste stromingsweerstand, die typisch leidt door de dikwandige delen van de matrijs zoals ribben en speciaal ontworpen gasgeleidingskanalen.

De meeste voordelen van gasinjectiespuitgieten komen voort uit de verwaarloosbare drukval in het gas. Allereerst verlaagt die de benodigde injectie- en nadruk, die bovendien gelijkmatiger over de matrijs verdeeld wordt. Hierdoor kunnen restspanningen en kromtrekken verminderd worden. Ook kan het ontstaan van krimpholtes aan het oppervlak van dikwandige delen tegengegaan worden, omdat de krimp van het kunststof opvangen wordt door een vergroting van de gasholte. Verder kan de koeltijd — en daarmee de cyclustijd — verkort worden. En tot slot wordt de ontwerpvrijheid vergroot, omdat gasinjectiespuitgieten dikwandige delen mogelijk maakt die bij conventioneel spuitgieten vermeden dienen te worden. Daar staat tegenover, dat het proces moeilijk te sturen is: omdat de weg van de minste weerstand voor het binnendringende gas eenduidig is, kan het opsplitsen van de gasstroom tot een ongecontroleerd proces leiden.

Hoewel gasinjectiespuitgieten al ruim tien jaar in de industrie wordt toegepast, is er nog geen volledig inzicht in het proces, met name in het binnendringen van het gas. Derhalve worden matrijsontwerp en procesbesturing vaak uitgevoerd op basis van *trial-*

*and-error*, en kunnen betrouwbare gegevens over de gasverdeling in het product en de uiteindelijke producteigenschappen alleen proefondervindelijk verkregen worden. Om het proces beter te kunnen begrijpen en beheersen, en om de producteigenschappen te voorspellen, is een simulatiegereedschap voor gasinjectiespuitgieten ontwikkeld.

Een belangrijke grootheid in het proces is de restwanddikte, ofwel de polymeerlaagdikte die overblijft aan de wand nadat het gasfront gepasseerd is. Deze restwanddikte bepaalt niet alleen de verhouding waarin polymeer en gas ingespoten moeten worden, maar beïnvloedt ook de producteigenschappen. De druk aan het gasfront leidt tot snelheden in de buurt van dat front die aanzienlijke componenten in de dikterichting hebben. Omdat het gas bovendien binnendringt in de dikwandige delen van de matrijs, wordt gasinjectiespuitgieten gekenmerkt door drie-dimensionale stromingsverschijnselen.

Vanwege dit 3-D karakter is de  $2\frac{1}{2}$ -D-benadering — die standaard is bij de modellering van 'conventionele' spuitgietsprocessen — niet toereikend voor de modellering van gasinjectiespuitgieten. Daarom is een rekenmodel ontwikkeld voor drie-dimensionale (niet-isotherme) stromingen, om de gasverdeling in gasinjectiespuitgietsproducten correct te voorspellen. Dit model maakt gebruik van een pseudo-concentratiemethode, waarin de relevante vergelijkingen worden opgelost op een vast rooster dat de hele matrijsholte beslaat. Zowel de lucht vóór het polymeerfront als het gas worden beschreven door een fictieve vloeistof, die niet bijdraagt aan de drukval in de matrijs. Er wordt een materiaal-label  $c$  (de 'pseudo-concentratie') geïntroduceerd waarmee het polymeer van het gas (en de lucht) onderscheiden wordt, en alle materiaaleigenschappen worden gedefinieerd als functies van dit materiaal-label. Een bewegend polymeerfront wordt gemodelleerd door de randvoorwaarde aan de matrijswanden te laten afhangen van de materiaal-labels, zodat in het luchtdomein vrije slip, en in het polymeerdomein geen slip optreedt.

Het model is gevalideerd door resultaten van simulaties te vergelijken met zowel isotherme als niet-isotherme gasinjectie-experimenten. Voor isotherme gasinjectie komen numerieke en experimentele resultaten uitstekend overeen. De niet-isotherme experimenten gingen echter gepaard met experimentele problemen die de beheersing van het proces bemoeilijkten. De simulaties en experimenten tonen weliswaar dezelfde trends, maar de kwantitatieve overeenstemming is minder goed dan onder isotherme condities.

Concluderend kan gesteld worden, dat het ontwikkelde model in staat is om gasinjectiespuitgietsprocessen na te bootsen. In tegenstelling tot andere modellen die in de literatuur verschenen zijn, volgt de manier waarop het gas binnendringt uit de fysica van het proces (en niet uit een vooronderstelde gasverdeling). Bovendien kan het model overweg met het 3-D karakter van het proces, en met temperatuureffecten en gegeneraliseerd Newtons viscositeitsgedrag. Als zodanig kan het dienen als een aanzet tot een ontwerp-gereedschap voor gasinjectiespuitgietsproducten; met het oog daarop wordt ook een model voor 3-D restspanningsberekeningen voorgesteld dat bij de pseudo-concentratiemethode aansluit. Het is echter aan te bevelen om de efficiëntie van de code te verbeteren voordat simulaties aan ingewikkelder (industriële) producten worden uitgevoerd.



# Notation

## General notation

$a, \alpha, A$	scalars (regular Latin and Greek symbols)
$\underline{a}$	column
$A$	matrix (upright regular Latin capitals)
$\mathbf{a}$	vector (bold Latin symbols)
$\mathbf{A}, \boldsymbol{\alpha}$	second order tensors (bold Latin capitals, bold Greek symbols)

## Latin symbols

$A$	$\text{m}^2$	area
$c$	–	material label
$c_p$	$\text{J kg}^{-1} \text{K}^{-1}$	specific heat capacity
$e$	$\text{J kg}^{-1}$	specific internal energy
$e$		computational element domain
$g$	$\text{m s}^{-2}$	gravitational acceleration
$h$	$\text{m}$	channel height; characteristic element length
$h_r$	$\text{J kg}^{-1}$	reaction heat
$H$	$\text{m}$	characteristic thickness
$J$	–	volumetric change
$L$	$\text{m}$	characteristic length
$n$	–	power-law exponent
$m$	–	number of modes
$p$	$\text{Pa}$	pressure
$r$	$\text{W kg}^{-1}$	thermal radiation
$R$	$\text{m}$	radius
$R$	$\text{N s m}^{-1}$	flow resistance
$R_c$	$\text{s}^{-1}$	reaction rate
$t$	$\text{s}$	time
$T$	$\text{K}$	temperature

$T_g$	K	glass transition temperature
$(\Delta T)_0$	K	characteristic temperature difference
$u, v, w$	$\text{m s}^{-1}$	velocity components in $x$ -, $y$ -, and $z$ -direction, respectively
$U$	$\text{m s}^{-1}$	characteristic velocity
$v$	$\text{m}^3 \text{kg}^{-1}$	specific volume
$x, y, z$	m	spatial coordinates

**Greek symbols**

$\alpha$	$\text{K}^{-1}$	linear thermal expansion coefficient
$\epsilon$	–	characteristic height-to-length ratio
$\varepsilon$	–	residual wall thickness ratio
$\gamma$	$\text{N m}^{-1}$	interfacial tension
$\Gamma$		boundary
$\eta$	$\text{Pa s}$	shear viscosity
$\kappa$	$\text{Pa}^{-1}$	compressibility coefficient
$\lambda$	$\text{W m}^{-1} \text{K}^{-1}$	heat conduction coefficient
$\mu$	$\text{Pa s}$	bulk viscosity
$\phi$	–	cross-sectional liquid fraction; shape function
$\Phi$	$\text{m}^3 \text{s}^{-1}$	volume flow
$\theta$	s	relaxation time
$\rho$	$\text{kg m}^{-3}$	density
$\tau$	s	characteristic time
$\psi$	–	(pressure) shape function
$\Omega$		computational domain

**Vectors and tensors**

$\mathbf{0}$	–	null vector or tensor
$\mathbf{B}$	–	Finger (or left Cauchy-Green) strain tensor
$\mathbf{D}$	$\text{s}^{-1}$	rate-of-deformation tensor
$\mathbf{F}$	–	deformation gradient tensor
$\mathbf{h}$	$\text{W m}^{-2}$	heat flux vector
$\mathbf{I}$	–	unit tensor
$\mathbf{L}$	$\text{s}^{-1}$	velocity gradient tensor
$\mathbf{n}$	m	normal vector
$\mathbf{W}$	$\text{s}^{-1}$	spin tensor
$\boldsymbol{\sigma}$	$\text{Pa}$	Cauchy stress tensor
$\boldsymbol{\tau}$	$\text{Pa}$	extra stress tensor

**Dimensionless numbers**

$Br$	Brinkman number = $\frac{\text{viscous dissipation}}{\text{heat conduction}}$
$Ca$	Capillary number = $\frac{\text{viscous force}}{\text{interfacial tension force}}$
$De$	Deborah number = $\frac{\text{relaxation time}}{\text{process time}}$
$Fo$	Fourier number = $\frac{\text{elapsed time}}{\text{characteristic cooling time}}$
$Fr$	Froude number = $\frac{\text{inertia force}}{\text{gravity force}}$
$Gc$	Gay-Lussac number = characteristic thermal expansion
$Pe$	Péclet number = $\frac{\text{heat convection}}{\text{heat conduction}}$
$Re$	Reynolds number = $\frac{\text{inertia force}}{\text{viscous force}}$
$Sr$	Strouhal number = $\frac{\text{instationary inertia force}}{\text{stationary inertia force}}$

**Superscripts**

$(e)$	with respect to a single element
$n$	at time level $n$
*	dimensionless variable

**Subscripts**

$e$	entrance; elastic
$i$ (or $j$ )	$i^{\text{th}}$ (or $j^{\text{th}}$ ) component of a column or matrix
$m$	melt
$n$	in normal direction
$p$	plastic
$s$	solid (= in glass state)
$t$	in tangential direction(s)
$v$	air vent; viscous
$ve$	viscoelastic
$w$	wall
0	characteristic value; reference value

**Operators and functions**

$\dot{a}$	material time derivative of $a$
$\frac{\partial a}{\partial t}$	spatial time derivative of $a$
$\Delta a$	difference in $a$

$\nabla$	$m^{-1}$	gradient operator
$ a $		absolute value of $a$
$\mathcal{O}(a)$		order of magnitude of $a$
#		number of
$\mathbf{A}^c$		transpose of tensor $\mathbf{A}$
$\mathbf{A}^d$		deviatoric part of tensor $\mathbf{A}$ ( $\mathbf{A}^d = \mathbf{A} - \frac{1}{3}\text{tr}(\mathbf{A})$ )
$\text{tr}(\mathbf{A})$		trace (or first invariant) of tensor $\mathbf{A}$
$II_{\mathbf{A}}$		second invariant of tensor $\mathbf{A}$
$\det(\mathbf{A})$		determinant (or third invariant) of tensor $\mathbf{A}$

# Chapter 1

## Introduction

### 1.1 Injection moulding processes

In injection moulding of plastics, a hot, molten polymer is injected under high pressure into a cooled mould. There, the polymer cools and solidifies to attain its final shape. The process allows for the moulding of complex-shaped products with several functions integrated into a single part, with short cycle times and relatively high dimensional accuracy at low cost. Injection moulded products can vary in size from a few square millimeters to approximately  $1 \text{ m}^2$  (with the thickness being in the order of millimeters), and their moulding cycle time ranges from a few seconds to minutes.

The injection moulding process can be subdivided into four stages: (1) injection, (2) packing, (3) cooling, and (4) ejection. In the first stage, the polymer melt is actually injected into the mould. The polymer is usually supplied as granulate, which is heated and mixed by an extruder to obtain a homogeneous melt. The melt is transported towards a (closed) nozzle at the end of the extruder barrel, where it is collected while the extruder screw retracts. As soon as a sufficient amount of polymer melt is obtained, the nozzle opens and the screw acts as a ram plunger that drives the melt into the mould at high pressure (usually a few hundred bar). A non-return valve prevents back-flow of the melt into the screw channel. The polymer injection is characterised by high melt deformation rates (typical shear rates of  $10^5 \text{ s}^{-1}$  near the injection gate), high temperature gradients, and high cooling rates near the mould walls. This causes the polymer molecules to be stretched, after which this orientation is partly frozen-in, *e.g.*, near the cooled mould walls.

Once the mould has been completely filled, the product enters the packing stage. In this stage, the polymer is cooled further, which is accompanied by shrinkage. As long as the injection gate is not 'frozen' (*i.e.*, not closed off by solidified material), some polymer can still be injected to compensate for this shrinkage. This requires a much

higher pressure than during the injection stage (up to 1000 bar), because the polymer viscosity has increased with the decreasing temperature, yielding large pressure gradients over the mould length, even at low melt flow velocities. The differential shrinkage caused by inhomogeneous cooling, combined with the presence of high pressures, gives rise to thermally and pressure-induced residual stresses, which mainly develop during this stage. Also the (minor) flow due to packing can still induce molecular orientation that is partly frozen in.

As soon as the injection gate freezes, the packing pressure can be released and the polymer cools further during the cooling stage. Due to the low thermal conductivity of polymers, this stage dominates the product cycle time. Therefore, injection moulding products are designed to be built up of thin-walled parts in order to keep the cooling times as short as possible.

When the polymer has cooled sufficiently, the product is ejected from the mould. Although ejection itself is trivial, it is at this stage that any product imperfections become visible. Most notably any warpage caused by the residual stress distribution in the product may manifest itself, but also shrinkage (particularly near ribs and bosses where so-called *sink marks* may appear), and surface defects such as weld lines and differences in colour and gloss. Moreover, during its life cycle the product's dimensions are likely to change due to physical aging and the relaxation of frozen-in orientation.

Thus, although injection moulding has proven its usefulness for the (mass) production of polymer products, still some aspects of the process require extra consideration and precautions:

- the relatively long cooling times, which dominate the moulding cycle time;
- the high pressures required, particularly during the packing stage;
- the necessarily stiff (heavy) and complex moulds, which are consequently expensive;
- the possible occurrence of product defects, such as warpage, sink marks, surface imperfections, and dimensional instability.

The first two aspects are more or less counteracting. Short cooling times can best be obtained by using the smallest part thicknesses possible. But as the pressure scales with  $h^{-3}$  ( $h$  being the part thickness), the pressure and the machine size are minimised by making the wall thickness as large as possible. As a rule of thumb, the lower and upper limits for part thicknesses are in the order of 0.5mm and 5mm respectively.

The mould geometry, the process conditions, and the material behaviour do not only affect the injection moulding process itself; they also have a profound influence on the final product properties. Complex moulds are most likely to yield weld lines; mass accumulations occurring at ribs, corners and bosses give rise to sink marks as a result

of shrinkage; and residual stresses due to differential shrinkage are a notorious source of product warpage. The non-trivial relations between process conditions and product properties, together with the complex mould geometries and material behaviour, can make the prediction of the process and product properties a precarious job, for which moulding experience alone is often inadequate. Moreover, since complex moulds are expensive and iterative mould testing is time-consuming, trial-and-error methods for process and product optimisation are to be avoided for economic reasons.

Instead, several methods have been developed to simulate injection moulding processes. In first instance, such simulations focused on the process itself, *i.e.*, on the prediction of process times, filling patterns, and pressures, in order to optimise the process (Manziona, 1987; Boshouwers and van der Werf, 1988; Sitters, 1988). Some of the injection moulding simulation codes have been commercialised successfully, particularly the Moldflow (see Manziona, 1987, chap. 4; Kennedy, 1993) and C-MOLD packages (see Manziona, 1987, chap. 7; Hieber and Shen, 1980; Chiang *et al.*, 1991). In recent years, the research objectives have been shifted towards the prediction of the final product properties, such as residual stresses and orientation, warpage, and dimensional stability (Flaman, 1990; Baaijens, 1991; Douven, 1991; Zoetelief, 1995; Caspers, 1995).

Over the years, many variants of the injection moulding process have emerged that try to circumvent the disadvantages of conventional injection moulding that were shortly discussed above. For instance, in Reaction Injection Moulding (RIM) two or more low-viscous components are injected into the mould, where they react to yield the final product material (Macosko, 1989). Usually, the injection pressure and temperature are much lower than in conventional injection moulding, and the mould walls are heated to initiate or accelerate the curing reaction. A process that bears some resemblance to the RIM process is Structural Foam Moulding (SFM), in which a short shot of material is injected that reacts to emit gas yielding a foam in the product core. The expanding foam completes the mould filling, compensates for shrinkage, and provides the packing pressure. Hence, this process enables the moulding of thick-walled products without sink marks, but at the cost of longer cooling times because the foam is an excellent thermal insulator. A variant to the SFM process was developed by the ICI company, who injected the foaming material into a mould that had been partially filled with a (non-foaming) thermoplastic, in order to obtain a 'sandwich' construction of thermoplastic at the walls and a foamed core.

Maintaining the principle of an expanding gas to take care of filling and packing, it was almost self-evident to replace the core foam in the ICI sandwich moulding process by a pressurised gas to be injected directly into the mould (Meridies, 1981). The process that was thus obtained has become known as gas-assisted injection moulding, and will be the subject of this thesis.

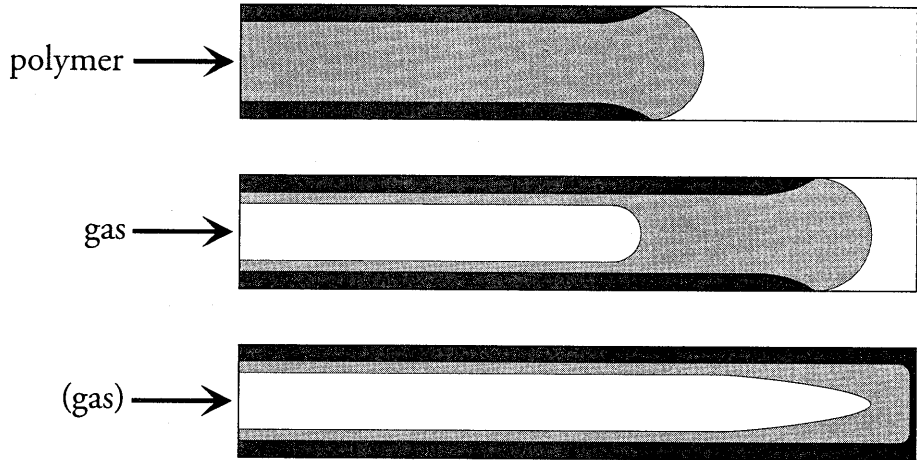


**Figure 1.1:** The principle of gas-assisted injection moulding: polymer injection (top), gas injection (middle), and packing (bottom). Light grey = polymer melt, dark grey = solidified polymer, white = gas/air.

## 1.2 Gas-assisted injection moulding

In Gas-Assisted Injection Moulding (GAIM), gas is injected into a mould that has been partially filled with polymer (see Figure 1.1). The gas drives the molten polymer core further into the mould, until it is filled completely. The penetrating gas leaves behind a polymer layer at the mould walls, yielding a product with a polymer skin and an inner gas channel. The gas can either be injected through a needle in the extruder nozzle, or directly into the mould through separate gas injection needles. Usually, nitrogen gas is used to avoid burning effects.

After the mould has been entirely filled, gas is used to transmit the packing pressure to the polymer that is being cooled. Any shrinkage of the polymer material near the gas channel is compensated for by an enlargement of the gas core. Once all polymer material has solidified, the gas pressure is released. The product is then further cooled until it has retained sufficient rigidity to eject it from the mould.

Among the different names that have been used for this process (such as 'gas injection moulding' and 'controlled internal pressure moulding') the term *gas-assisted injection moulding* is preferred in this thesis, as it is not only the most commonly used name, but also the best description of the process: the gas merely *assists* in the mould filling and packing, and after the gas pressure has been released, most of it leaves the mould.



### 1.2.1 Process characteristics

The most important characteristic of GAIM is the fact that the pressure drop in the gas core is negligibly small compared to the pressure drop in an equivalent molten polymer core, because the viscosity of the gas is roughly  $10^8$  times smaller than that of the polymer. Consequently, the gas pressure can be considered constant throughout the gas core, and this accounts for most of the advantages of GAIM, which will be discussed later.

One should realise, that the fact that a layer of polymer is left behind at the mould walls after gas penetration, is only partly accounted for by the solidification of the polymer. Actually, when gas penetrates into an isothermal liquid, there would still be a liquid layer residing at the mould walls, as depicted in Figure 1.1. This is inherent to the physics of a fluid displacing another, more viscous liquid. A review of this phenomenon will be given in Section 1.3 of this thesis.

For this moment, we will consider a simple gas-leading channel with cross-sectional area  $A$ , partially filled with a polymer melt that is penetrated by gas. If we neglect compressibility effects, and define  $\phi$  as the fraction of polymer left behind after the gas front has passed, the mass balance for the polymer domain downstream of the gas front yields:

$$(1 - \phi)A\langle u_{gas\ front} \rangle = A\langle u_{polymer\ front} \rangle, \quad (1.1)$$

in which  $\langle u \rangle$  denotes the average front velocity. Since  $\phi$  is by definition a number between 0 and 1, the average gas front velocity is always larger than the average polymer front velocity. Hence, the amount of polymer melt ahead of the gas front decreases during gas injection, causing both the gas and the polymer front to be continuously accelerated due to the ever diminishing viscous flow resistance. If the initial amount of polymer in the mould is insufficient, this may even lead to the gas front overtaking the polymer front, resulting in what is known as *gas breakthrough*. It is obvious that such a breakthrough prohibits the complete filling of the mould, and should therefore be prevented by injecting a sufficient amount of polymer before the gas is injected. Evidently, in order to know what exactly is 'a sufficient amount', one needs to know the fraction  $\phi$  of polymer left behind at the mould walls.

The injected gas typically penetrates along the path of least flow resistance. This has two consequences: first, any thick-walled part of a mould offers a significantly lower flow resistance than the thin-walled parts that usually make up a major part of the product. The gas is, therefore, inclined to penetrate inside the thick-walled parts, such as ribs and bosses. GAIM product and mould designers should account for this fact, either by properly incorporating ribs to lead the gas flow, or by supplying designated gas-leading channels (Barton and Turng, 1994; Rennefeld, 1996). If, for some reason, the gas enters a thin-walled part, the gas flow front is likely to become unstable, upon which it will proceed as irregularly shaped fingers into the part. This is known as the *fingering effect*,

and should be avoided in GAIM. Although the gas will generally penetrate through the thick parts, it may flow into thinner parts as soon as the thick part is completely filled.

The second consequence of the gas following the path of least flow resistance, is the inherent instability of the gas front advancement at — apparently symmetric — bifurcations in the mould (Turng, 1995; Yang and Huang, 1995a). In conventional injection moulding, symmetric bifurcations (or at least bifurcations yielding downstream branches of equal flow resistance) are often used to balance runner systems for multiple-cavity moulds: if in any runner the polymer front starts to run slightly ahead, the flow resistance in that particular runner will increase, leading to a smaller flow that enables the flow fronts in the other runners to catch up (see Figure 1.2(a)). However, in GAIM the opposite effect occurs. As the pressure drop  $\Delta p$  between gas front and polymer front is constant everywhere, *i.e.*:

$$\Delta p = p_{\text{gas}} - p_{\text{ambient}}, \quad (1.2)$$

the flow  $\Phi$  is determined by the flow resistance  $R$ :

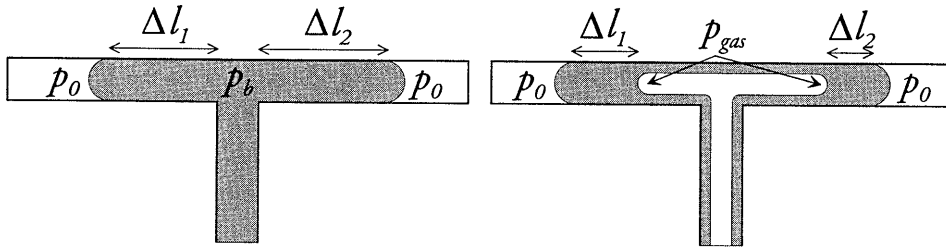
$$\Phi = \frac{1}{R} \Delta p. \quad (1.3)$$

The flow resistance is proportional to the distance  $\Delta l$  between the gas front and the polymer front. In case of a geometrically symmetric bifurcation, any minor disturbance that causes the gas front in one of the downstream branches to (slightly) run ahead, will result in a lower flow resistance in that branch (see Figure 1.2(b)). Consequently, any perturbation of the symmetry of the gas penetration will cause one of the fronts to increasingly run ahead. At that point the gas flow cannot be controlled any more. Therefore bifurcations that split the advancing gas flow should be avoided. Instead, one may consider to inject the gas through several injection points in such a way, that multiple (separated) gas cores are obtained that are not affected by each other's flow field.

Furthermore, in curved gas-leading channels the path of least flow resistance lies closer to the inner wall of the bend than to the outer wall, causing the gas front to penetrate accordingly. This effect is usually enhanced by the fact that mould cooling is more effective at the outer wall than at the inner wall, leading to a higher temperature — and thus to a lower viscosity — at the inner wall. Therefore, also sharp corners and transitions in gas-leading channels are to be avoided, as they may lead to weak spots.

### 1.2.2 Advantages

Provided the pitfalls mentioned in the previous section are avoided, gas-assisted injection moulding offers a number of advantages over conventional injection moulding. These will be discussed here, and it will become clear that they mainly originate from the negligible pressure drop in the gas core.



(a) Conventional injection moulding.

(b) Gas-assisted injection moulding.

**Figure 1.2:** Flow bifurcation in injection moulding. The flow resistance in each branch  $i$  is proportional to the flow length  $\Delta l_i$ . If in conventional injection moulding  $\Delta l_2 > \Delta l_1$ , the flow resistance in the right branch will increase, having a balancing effect. In gas-assisted injection moulding, a minor instability causing  $\Delta l_2 < \Delta l_1$  will evolve into asymmetric gas penetration, since  $\Delta l_2$  will continue to decrease faster than  $\Delta l_1$ .

### Reduced clamp force

For a given product geometry, the machine clamp force is determined by the maximum pressure, which is usually the packing pressure. In conventional injection moulding, this pressure has to be very high to overcome the large pressure drop between the injection point and the mould extremities, because of the polymer's high viscosity (see Figure 1.3). In GAIM, a major part of the distance between injection point and mould extremities is covered by the gas channel. Consequently, the packing pressure is determined by the pressure drop between the mould extremities and the gas core, which is considerably smaller than the pressure drop in conventional injection moulding. As a result, the maximum pressure can be reduced to a few hundred bar, and the required machine clamp force can be decreased accordingly.

### Reduced sink marks

Sink marks are caused by shrinkage and are therefore most likely to occur at relatively thick mould parts, such as ribs and bosses. These just happen to be the parts along which the gas penetrates in GAIM. As the gas channels are used to transmit the packing pressure to the polymer, the shrinkage in such parts manifests itself as a local enlargement of the gas core, instead of a sink mark at the outer surface.

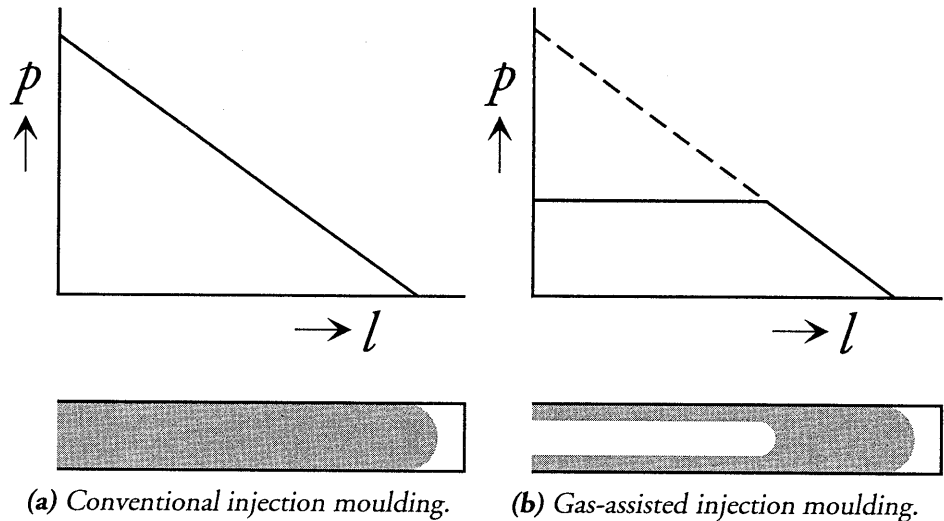


**Figure 1.3:** The principle of injection pressure reduction (for a thick-walled part) by gas-assisted injection moulding compared to conventional injection moulding.

### Reduced residual stresses

Residual stresses fall into two categories: thermally and pressure-induced stresses, and flow-induced stresses. The first are caused by inhomogeneous cooling under pressure: different material elements solidify (*i.e.*, cool below the glass transition temperature) at different pressure conditions and different cooling rates. This leads to density differences in the final product, which give rise to residual stresses. The packing pressure in GAIM is both lower and more uniform than in conventional injection moulding, thus reducing the density differences and, ultimately, the thermally and pressure-induced residual stresses.

Flow-induced stresses are caused by orientation of polymer molecular segments during flow, and characterised by  $\dot{\epsilon}\tau$ , which is the product of strain rate and relaxation time. Orientation will appear in the final product if the following three conditions are met:

- the strain rate must be sufficiently high to outgrow the relaxation ( $\dot{\epsilon}\tau > 1$ );
- the total strain must be large enough ( $\epsilon = \dot{\epsilon}t > 1$ );
- the orientated polymer must vitrify almost immediately (which requires fast cooling).

In conventional injection moulding, the largest flow-induced stresses can develop during the packing stage, when the polymer in the product core flows slowly, but the relaxation

time is very long because of the relatively low temperatures. This kind of flow hardly occurs in GAIM, since the mould core is usually a gas channel. Therefore, flow-induced residual stresses can be significantly reduced.

The reduction of residual stresses in GAIM products may well be used to avoid warpage problems. However, one should be aware that if the injection of gas leads to large differences in the polymer layer thickness, warpage may even be increased.

### Enhanced design possibilities

Formally, the demand for thick mould parts along which the gas is to penetrate, constitutes an extra constraint in the design process. But as ribs and bosses are present in most injection moulded products — usually being potential sources for product imperfections — the necessity for thick-walled parts can now be exploited. For instance, hollow ribs in GAIM products provide structural rigidity without adding much weight and without causing sink marks (see *e.g.*, Woods *et al.* (1995) and Yang *et al.* (1996)). Thus, with GAIM new product designs become possible, and are generally necessary.

### Shorter cycle times

For some applications, GAIM may reduce the injection moulding cycle times: the actual gas injection occurs at high speeds, and the dominating cooling times for thick-walled parts are reduced since these parts are partially filled with gas. However, shorter cycle times cannot always be achieved: the (extra) gas-leading channels and ribs may bring along an extra amount of polymer to be cooled.

### 1.2.3 Practical aspects

Since the first patents on gas-assisted injection moulding appeared in the early 70's, different types of GAIM processes have been developed, partly due to attempts to circumvent patent rights (see Pearson, 1986; Eckardt and Ehrirt, 1989; Eyerer *et al.*, 1993). Nowadays, the major part of GAIM processes is commonly divided into two categories. In the Cinpres (Controlled internal pressure) process, patented by Peerless Cinpres Ltd in the UK, the gas is injected through the machine nozzle in a volume-controlled manner (hence the name of the process is somewhat misleading!). The German moulding machine manufacturer Battenfeld developed the Airmould process, which uses pressure-controlled gas injection.

A process variant of minor importance is the blow-out technique, in which the gas is injected after the mould has been filled *completely* with polymer. The gas then forces part of the molten polymer out of the mould, either back into the injection unit or into a separate cavity. Finally, in the retracting core process, a mould containing a movable core part is completely filled with polymer. Then the core part is withdrawn while gas

is injected, filling up the space that is left by the retracting core. A similar procedure is followed when the mould is enlarged by means of a moving mould wall.

All these techniques require a GAIM unit, consisting of a gas pressure generator, a gas injection unit, and an injection control unit, to be attached to a conventional injection moulding machine. Up to 95% of the pressurised gas in the gas core can be regained when the gas pressure is released after the packing stage. To re-use this gas, a gas filtering system is needed as well.

GAIM can be done with virtually any polymer, including reinforced, thermosetting, and semi-crystalline plastics (Anders and Sauer, 1991; Eyerer *et al.*, 1993; Rennefeld, 1996). In spite of this, there are some pitfalls in the practical application of the process. For instance, gas and polymer cannot be injected simultaneously: being (necessarily) injected at equal pressures, the gas would flow much faster than the polymer, which would soon result in breakthrough. (White and Lee (1975) did a similar observation when they simultaneously injected two polymers of different viscosities.) Thus, the gas can only be supplied after the polymer injection has been stopped. Consequently, the polymer melt front will halt momentarily at the switch-over from polymer to gas injection, which may result in so-called *hesitation marks* at the product surface. The above-mentioned blow-out technique avoids these hesitation marks. Also, the thick-walled part where the gas is supposed to flow into, may well have a significant lower flow resistance, giving rise to the *race-track effect*: the polymer front in the thick-walled part runs far ahead of the fronts in the adjacent thin-walled sections. This may cause the gas-leading channel to be filled prematurely, causing the gas to flow into the thin-walled sections, where fingering occurs.

Although gas-assisted injection moulding has been practised commercially for more than a decade, the understanding of the characteristics of the process, particularly with respect to the typical flow phenomena, is still lagging behind. Years of practical GAIM experience, mostly gained from trial-and-error, have led to design guidelines for GAIM moulds and products, which, however, do not always have an explicit connection to the physics of the process. Consequently, several researchers who have investigated the effect of some ten-odd parameters on the process and final product, sometimes report contradictory conclusions (Eyerer *et al.*, 1993). A more thorough understanding of the process is expected to establish a clear connection between these process parameters and the process physics, and may hence reveal which parameters are important and which are not. Therefore, the next sections will review two subjects: the phenomenon of gas penetrating into a fluid, and the modelling of gas-assisted injection moulding that has been reported so far. The conclusions from these reviews will then lead to a formulation of the objective of this thesis.

### 1.3 Gas penetration into a viscous fluid

When Fairbrother and Stubbs (1935) tried to determine the volume flow rate of a liquid in a capillary tube by measuring the velocity of large air bubbles in this liquid, they found that the air bubbles did not displace the liquid entirely, but left behind a certain fraction of liquid sticking at the tube walls. They found this fraction  $\phi$  — defined as the ratio of the cross-sectional area of the liquid that is left behind, and the cross-sectional area of the tube — to be given approximately by:

$$\phi = 1.0\sqrt{Ca}, \quad (1.4)$$

in which the Capillary number  $Ca$  expresses the ratio of viscous stresses and interfacial (or surface) tension, defined by:

$$Ca = \frac{\eta U}{\gamma}, \quad (1.5)$$

where  $\eta$  is the liquid viscosity,  $U$  is the characteristic velocity, and  $\gamma$  is the interfacial tension. The highest Capillary number in the experiments of Fairbrother and Stubbs was 0.014, indicating that the interfacial tension was far more important than the viscous forces.

The subject of a fluid — whether it be a gas or a liquid — displacing a liquid of higher viscosity again drew attention in the early 60's, particularly since the phenomenon was observed when water was pumped into nearly exhausted oil fields, in an attempt to have the water push up the lighter oil still present in the porous rock. In a model experiment, Taylor (1961) used air to drive out either glycerine or Golden Syrup (a strong sucrose solution) from a tube. With these fluids, he was able to extend the Capillary number in his experiments to nearly 2.0. For small Capillary numbers, up to 0.09, his experimental results are in good agreement with equation (1.4). Above this value, the fraction  $\phi$  was found to increase more slowly with  $Ca$ , yielding  $\phi = 0.55$  at  $Ca = 1.9$ . From extrapolation of his  $\phi$ - $Ca$  curve, Taylor expected  $\phi$  to reach an asymptotic value of at least 0.56 for large  $Ca$  numbers. Furthermore, he suggested a streamline pattern as depicted in Figure 1.4 for  $\phi > 0.5$ . It is obvious from these streamlines that velocities in the radial direction cannot be neglected near the penetrating gas front.

Cox (1962) further increased the Capillary number in his experiments to  $Ca > 10$  having tetrachloromethane penetrate into Golden Syrup. The residual liquid fraction  $\phi$  reached a value of 0.60 for such large Capillary numbers, and a constant residual wall thickness of the liquid was already present after  $1\frac{1}{2}$  tube diameters from the nose of the penetrating front.

Cox also attempted to derive a (semi-)analytical expression for the shape of the penetrating front, by assuming that the radius of this front can be approximated by:

$$r = r_{\infty} - \delta, \quad (1.6)$$

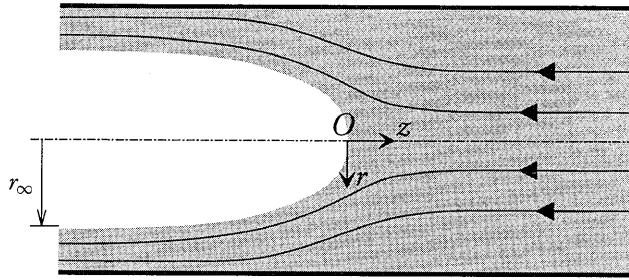


**Figure 1.4:** Characteristic streamlines in a liquid (grey) with respect to the penetrating fluid (white) according to Taylor (1961).

in which  $r_\infty$  is the (constant) radius of the penetrating fluid bubble behind the front region, and  $\delta$  is a small disturbance on  $r_\infty$  given by:

$$\delta = \delta_0 e^{kz}, \quad (1.7)$$

in which  $z$  is the axial distance from the front nose (see Figure 1.4). Since in Cox's approximation  $\delta$  is supposed to be small with respect to  $r$ , and  $\frac{\partial z}{\partial r} \neq 0$  at the nose (*i.e.*, at  $z = 0$ ), this approach is invalid close to the front nose. Moreover, it does not yield an expression for  $r_\infty$ , which is a measure for the amount of fluid left behind.

However, Cox was the first to describe the boundary conditions that have generally been considered correct for this problem:

- Both the normal and the tangential velocities of the liquid at the wall are zero (*i.e.*, impermeable wall and no-slip boundary conditions).
- The tangential stresses at the fluid-liquid interface are negligibly small.
- The difference in normal stress over the fluid-liquid interface is equal to the interfacial stress.
- The diffusion over the interface can be neglected.

In another paper, Cox (1964) experimentally visualised the streamline pattern suggested by Taylor.

Almost parallel to the investigations described above, the interest in the penetration of a fluid into a more viscous liquid in a Hele-Shaw cell — as a physical model for a porous medium — was aroused by a classical paper of Saffman and Taylor (1958). Neglecting effects in the thickness direction, they found that the interface between the



two fluids became unstable under certain conditions, and they tried to set up a mathematical description for the interface. This problem, which has become known as the Saffman–Taylor problem, has continued to receive considerable attention, as it turned out that such an apparently simple physical phenomenon involved many mathematical problems. These mainly concern the stability of the penetrating fluid finger (Bensimon *et al.*, 1986; Saffman, 1991).

The Saffman–Taylor problem can play a role in GAIM, but only in the undesired case of gas penetrating into thin-walled mould parts, which is bound to lead to the fingering effect that has been described in section 1.2.1. Without going into the quantitative details of viscous fingering in Hele-Shaw cells, a stability analysis will be employed in appendix C in an attempt to elucidate the fingering effect in GAIM.

Fluid penetration in a viscous liquid in a tube did not attract further attention until the mid-80's, when Reinelt and Saffman employed the finite difference method to predict the residual fluid fraction  $\phi$  (Reinelt and Saffman, 1985). In their method, they used two coupled meshes: one to describe the flow, and another one to describe the fluid-liquid interface, taking into account the interfacial tension. To solve this problem, they discarded the normal stress (jump) boundary condition at the interface, made an initial guess for the interface shape, and determined its actual shape by modifying the interface as to minimise the error in the normal stress boundary condition. For Capillary numbers between 0 and 2, the results of this method were in good agreement with the experimental results of Taylor (1961).

Being interested in the coating process of capillary tubes, which is, for instance, used in the production of automotive catalysts, Kolb and Cerro (1991) studied the problem of fluid penetration into tubes of *square* cross section. They observed that air penetrating into silicone oil forms a bubble that more or less follows the square shape of the tube for small Capillary numbers. However, for  $Ca > 0.1$  the gas bubble cross section becomes circular, yielding a liquid fraction  $\phi$  of 0.64 for large Capillary numbers, whereas for circular tubes they measured  $\phi = 0.60$ . The conclusions of Cox (1962), that the final liquid wall thickness is already obtained at a few tube diameters behind the bubble nose and that the bubble shape is very stable, were confirmed. Kolb and Cerro (1993a,b) also derived an analytical solution for the residual liquid fraction, based on series of harmonic functions, that agrees well with their experimental results for  $0.1 < Ca < 1.2$ , but fails for larger Capillary numbers.

A large range of Capillary numbers ( $0.05 \leq Ca \leq 10^4$ ) is covered by the simulations of Halpern and Gaver III (1994), who employ a Boundary Element Method (BEM) to simulate gas penetration into a Newtonian fluid between two parallel plates. This seems to resemble the Saffman–Taylor problem at first sight, but Halpern and Gaver III focus on the effects in *thickness* direction, whereas Saffman and Taylor considered the *width* direction of a Hele-Shaw cell (assuming that the gas would expel the liquid completely over the cell thickness). Consequently, the case studied by Halpern and Gaver III is

more closely related to gas penetration in a tube. It is remarkable that they find the same residual fluid fraction  $\phi = 0.58$  that has been reported earlier for the tube geometry. This asymptotic value was found for  $Ca > 20$ , above which value the gas front shape does not change any more. Moreover, the actual gas front region (which contains the flow phenomena yielding a certain gas front shape and residual wall thickness) is found to be approximately  $-3 \leq x/h \leq 1$ , with  $x$  being the axial distance from the gas front nose in flow direction, and  $h$  the distance between the parallel plates.

Poslinski *et al.* (1995) were the first to connect the above-mentioned work on fluid penetration in a liquid-filled tube to gas-assisted injection moulding. In order to decouple the thermal and the viscous effects on gas penetration, they performed both isothermal gas injection experiments and an isothermal analysis of the problem. From their dimensional analysis, they concluded that the inertial and gravity effects can be neglected, leaving the Capillary number as the sole factor characterising the flow. As  $Ca$  is at least of order  $10^3$  for the primary gas injection stage of GAIM — the secondary stage is not considered — they also neglect interfacial tension effects.

Their experiments on primary gas penetration in a Newtonian liquid show that the *residual wall thickness*  $\varepsilon$ , which is defined as the ratio of the residual skin layer of liquid and the tube radius, approaches a value of 0.35 — corresponding to a cross-sectional residual liquid fraction  $\phi = 0.58$  — for sufficiently large Capillary numbers ( $Ca > 10^2$ ). From finite element computations, they conclude that  $\varepsilon$  decreases with increasing power-law exponent for generalised Newtonian fluids (see Figure 1.5).

The main contributions of Poslinski and co-workers are summarised in the following conclusions:

- The residual polymer wall thickness in GAIM is determined by two phenomena: the penetration of a gas into a viscous liquid, and the growth of a solid layer.
- As the solid layer growth *during* the primary gas injection stage is negligibly small, the contribution of thermal and viscous effects to the residual wall thickness can be decoupled; the final residual wall thickness is the sum of the solid layer thickness at the beginning of gas injection and the liquid polymer layer left behind by the penetrating gas.
- For Newtonian fluids in isothermal flows, the residual wall thickness is only a function of the Capillary number.
- The residual wall thickness is further affected by non-uniform viscosity, caused by temperature and shear rate gradients.

Although the work of Poslinski and co-workers has elucidated the underlying GAIM principles, they are still not able to offer anything more than the following phenomeno-

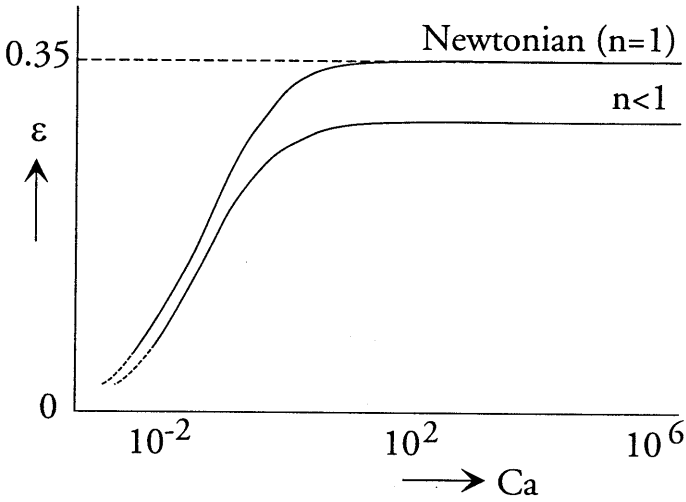


**Figure 1.5:** Residual wall thickness as a function of the Capillary number for Newtonian and power-law fluids ( $\eta = \eta_0 \dot{\gamma}^{n-1}$ ). (After Poslinski *et al.* (1995).)

logical description of the residual wall thickness:

$$\varepsilon = \varepsilon_\infty \frac{(Ca/c_\infty)^q}{1 + (Ca/c_\infty)^q}, \quad (1.8)$$

in which the parameters  $\varepsilon_\infty$ ,  $c_\infty$ , and  $q$  still have to be determined for each material separately.

Recently, Huzyak and Koelling (1997) investigated the penetration of gas into a viscoelastic fluid in a tube. In their experiments, they used two types of Boger fluids, which are highly elastic fluids with a Newtonian viscosity behaviour. They define the Deborah number, representing the ratio of material and process time scale, as:

$$De = \theta \dot{\gamma}_w \quad (1.9)$$

where  $\dot{\gamma}_w$  is the wall shear rate, and  $\theta$  is the material's characteristic relaxation time given by:

$$\theta = \frac{\Psi_1(\dot{\gamma}_w)}{2\eta}, \quad (1.10)$$

in which  $\Psi_1$  is the first normal stress difference coefficient. For small Deborah numbers ( $De < 1$ ), the residual wall thickness for the viscoelastic fluids is equal to that for Newtonian fluids reported by Taylor (1961). However, for  $De > 1$  the residual wall thickness

increases with increasing Deborah number, and reaches a value of 0.48 for  $De \approx 5$ . This is remarkable, since such an increase has never been reported in the literature on GAIM experiments. On the contrary: Chen *et al.* (1995b,c) have done GAIM experiments with polystyrene under practical (non-isothermal) moulding conditions, but still found residual wall thickness close to the Newtonian values reported by Poslinski *et al.* (1995).

However, Huzyak and Koelling motivate their investigations by claiming that: 'none of the published studies have considered the effect of viscoelasticity on the penetration of a long gas bubble through a tube.' This claim is not entirely correct: Poslinski and co-workers did consider the effect of shear-thinning on the residual wall thickness, which is in fact a viscoelastic effect (see, *e.g.*, Macosko (1993) and Baaijens (1991)). Huzyak and Koelling want to isolate the effects of fluid elasticity from shear-thinning phenomena by choosing the above-mentioned Boger fluids, which exhibit a rather artificial type of rheological behaviour. However, by excluding the important effects of shear-thinning on gas penetration in favour of the less important elastic effects, their investigations have little practical relevance to gas-assisted injection moulding.

#### 1.4 A review of gas-assisted injection moulding modelling

As mentioned earlier, optimisation of moulds and products by trial-and-error methods, *i.e.*, by modifying the mould and changing the process parameters in a series of test mouldings, is both expensive and time-consuming. To avoid this, injection moulding simulation codes have been developed that enable the optimisation of the injection moulding process. Commercial injection moulding simulation packages, such as Moldflow and C-MOLD, cover a wide range of injection moulding processes (such as conventional injection moulding, reaction injection moulding, resin transfer moulding, and multi-component injection moulding) for which they have proven to be useful tools in process optimisation. Most of these packages are based on the so-called *thin-film* or *Hele-Shaw approximation* developed by Hieber and Shen (1980), in which the fact that most injection parts are thin-walled is used to decouple flow and thermal effects in mid-plane and thickness directions; this has led to what is known as the  $2\frac{1}{2}$ - $D$  approach (see Figure 1.6). This approach has become the state-of-the-art for the simulation of injection moulding processes (see Shen (1992) for a detailed review).

In the simulation of gas-assisted injection moulding, first of all the distribution of the gas inside the product has to be predicted. In this respect, it is important to realise that during the gas injection stage, four flow regions can be distinguished (Poslinski *et al.*, 1995):

1. The polymer flow front region, which is characterised by the fountain flow phenomenon.
2. The polymer melt flow, where the velocity field is quasi-parabolic.

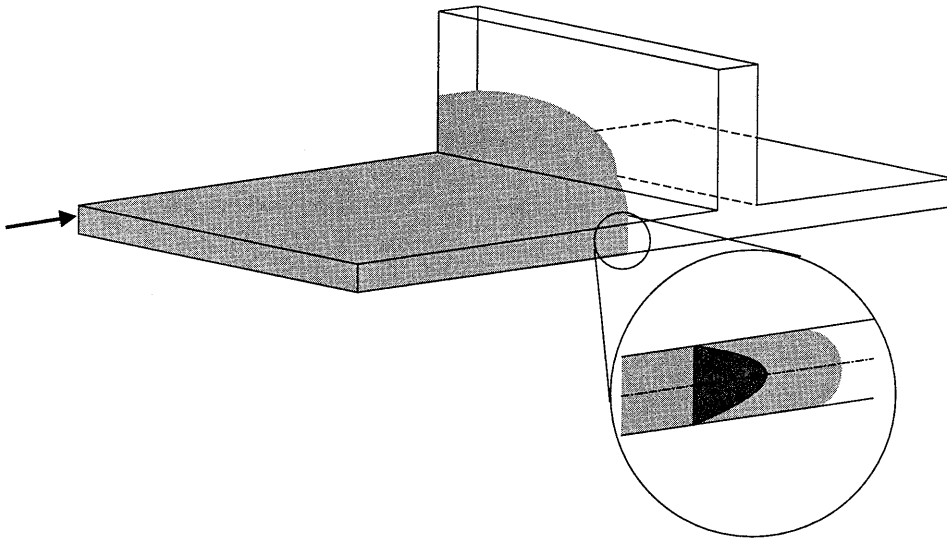


**Figure 1.6:** The  $2\frac{1}{2}$ -D approach: moulds are considered to consist of thin-walled parts. Pressure gradients and velocities are all parallel to the midplane direction of each part. The dark-grey parabola in the thickness direction illustrates a velocity profile over the part thickness.

3. The region around the advancing gas front, where the velocity distribution is different from parabolic, in the sense that velocity components perpendicular to the main flow direction become important.
4. And the gas core region, where the shear forces exerted by the gas on the polymer skin layer are too small to induce any polymer flow.

The distinction between these flow regions is clearly based on the polymer flow characteristics, since from a modelling perspective the velocity distribution in the gas is irrelevant: the gas is merely a medium to impose a uniform pressure boundary condition on the gas/polymer interface.

The first and second flow regions mentioned above can also be distinguished in conventional injection moulding. It is the third and the fourth region that are characteristic for GAIM. Our attention will especially be focused on the advancing gas front, as it determines the thickness of the polymer skin layer that is left behind on the mould walls. In this respect, it is important to realise that the residual wall thickness consists of two contributions, as has already been pointed out by Poslinski *et al.* (1995):

1. The solidified layer that is already present at the mould walls at the time the gas front passes; this is governed entirely by the thermal conditions of the process.

2. The polymer melt layer that is deposited on the mould walls (actually: on the solidified layer) by the penetrating gas. This is governed by the viscous behaviour of the melt (see Figure 1.5), and is therefore affected indirectly by the thermal conditions.

From the qualitative analysis exercised so far, we can already conclude that both the geometrical conditions (*i.e.*, the gas penetrating into *thick-walled* parts) and the flow phenomena around the gas front are three-dimensional. Hence, the fluid (and thermal) flow phenomena in different directions cannot be simply decoupled, implying that the standard  $2\frac{1}{2}$ -D approach for the modelling of injection moulding cannot be adopted straightforwardly for GAIM simulations. Instead, there are two options to model and simulate the GAIM process:

- find a good analytical or phenomenological description of three-dimensional gas penetration, and incorporate it into the  $2\frac{1}{2}$ -D approach, or
- develop a three-dimensional model for gas penetration that intrinsically captures the three-dimensional phenomena.

Developers of existing injection moulding simulation codes have attempted to incorporate GAIM into their programs without abandoning the Hele-Shaw approach these codes are based on. For instance, Turng and Wang (1991), IKV (1994), Gao *et al.* (1995, 1997), and Chen *et al.* (1996) take the modelling of co-injection moulding (*or*: multi-component injection moulding) as the starting point for the modelling of GAIM, since both processes involve the injection of two components. To keep track of the different components (in GAIM: polymer and gas), the particle tracking concept of multi-component injection moulding simulation is adopted: each material particle entering the mould is assigned a label defining its material identity. This label is also used to determine the particle's material properties; for instance, the gas particles are given a negligibly small viscosity. By tracking these labels throughout the mould, the distribution of both components can be determined (see also Zoetelief (1995) and Zoetelief *et al.* (1997)).

However, in multi-component injection moulding the components have comparable viscosities, whereas in GAIM the viscosities differ by a factor of order  $10^8$ . This has major consequences for the flow characteristics: in multi-component injection moulding, the velocity fields in both the first and the second components are still quasi-parabolic, whereas in GAIM the gas (*i.e.*, the second component) penetrates into the polymer melt, leaving part of the polymer behind at the mould wall. Zuidema (1995) showed that incorporating a large viscosity difference in a multi-component injection moulding simulation employing the  $2\frac{1}{2}$ -D approach alone did not reveal the typical gas penetration of the GAIM process. His subsequent attempt to overrule the (quasi-)parabolic flow by

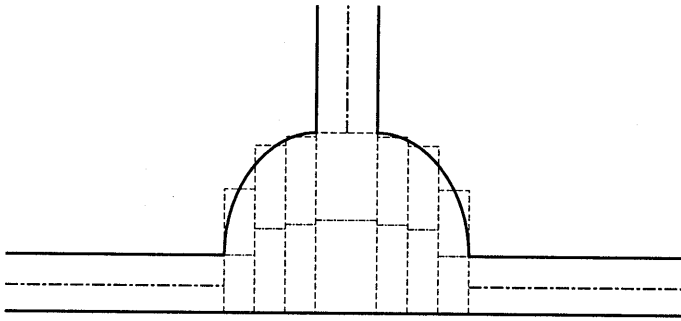


**Figure 1.7:** Attempt by Potente and Hansen (1993) to model a rib (shown here in cross-sectional view) with  $2\frac{1}{2}$ -D slices (represented by dashed lines) for gas-assisted injection moulding simulation. Midplanes are indicated by dash-dotted lines. It is obvious that these slices are not able to capture the three-dimensional flow and temperature phenomena in the rib.

prescribing a block velocity distribution near the gas front did yield the gas penetration in a qualitative sense, but the results were far from accurate.

Since the advancement of the gas front is intrinsically accompanied by three-dimensional flow, a GAIM model based on the  $2\frac{1}{2}$ -D approach requires a more sophisticated approximation for the penetrating gas front. Chen *et al.* (1996) therefore incorporate an empirical relation for the residual wall thickness into their model. For instance, in their comparison between experimental and simulated GAIM of a spiral tube, they use the *measured* value (sic!) for the residual wall thickness (being 0.36 times the tube radius) as input for their simulation. As one would rather like to predict than measure the residual wall thickness, this does not seem a desirable procedure (as Chen *et al.* (1995a) already remarked).

Another shortcoming of the Hele-Shaw-based codes is demonstrated (unintentionally) by Potente and Hansen (1993) when they tried to model a rib for GAIM simulations with C-MOLD/C-GASFLOW: they approximate the rib by meshing it as a series of  $2\frac{1}{2}$ -D slices of varying thickness (see Figure 1.7). Although the result may represent the rib's geometry, it does certainly not take into account the three-dimensional nature of the flow and temperature fields in the rib.

Consequently, to avoid having to put any (material-dependent) information on the residual wall thickness *a priori* into the simulation code, one has to resort to full three-dimensional simulations. This has also been recognised by Khayat *et al.* (1995) and Costa *et al.* (1995, 1996), who both employed a boundary element method to model GAIM. Khayat *et al.* (1995) use a three-dimensional boundary element method to simulate the primary penetration of gas into a three-dimensional cavity that is partially filled

with polymer. This 'polymer' is assumed to be isothermal, incompressible and Newtonian. To track the moving gas front, the gas core boundary is moved at every time step according to the local velocity. The use of a coarse mesh, due to computing time and storage restrictions, make their results for three-dimensional flow in a rectangular cavity inaccurate. Although their technique has the potential to predict the residual wall thickness, the results of Khayat *et al.* show two remarkably unrealistic features: the penetrating gas front seems to affect the shape of the melt front (which is strongly deformed when the gas enters), and the gas seems to penetrate in lateral directions after the gas front has passed.

Costa *et al.* (1995, 1996) use a similar method, starting with a two-dimensional example of gas injection into a non-Newtonian (shear-thinning) fluid. The non-Newtonian fluid behaviour gives rise to domain integrals in their boundary element method, which requires an additional mesh over the entire polymer domain. Their results on gas penetration through a contraction, an expansion, and in bent parts show a qualitative agreement with practical GAIM situations. However, no quantitative results for the residual wall thickness are given. Moreover, the use of a mesh over the polymer domain to account for non-Newtonian effects implies the need for remeshing, which will become very expensive in three-dimensional simulations.

## 1.5 Objective

Although gas-assisted injection moulding has established itself as a successful injection moulding technique for specific applications, there is still no complete understanding of the physics of the process. Consequently, mould design still involves a lot of experience and trial-and-error methods. A simulation tool can not only predict the gas distribution in a product and the resulting product properties; it may also help to understand the process features and thereby contribute to moulding experience. A model that pretends to elucidate the features of the process should therefore be based on the underlying physics, not on a sheer description of the phenomena that are observed; the model should reveal these phenomena, not merely describe them.

As there is no such thing as an analytical solution for gas penetrating into a liquid in a confined cavity, one has to resort to a numerical technique. Moreover, the recognition that gas injection is governed by three-dimensional flow inevitably leads to the conclusion that the computational model for gas-assisted injection moulding has to be based on a three-dimensional approach. The argument that

'although a complete three-dimensional analysis may be the final solution, the computational cost is too expensive to be implemented at the present stage for engineering design purposes' (Chen *et al.*, 1996)

may currently be valid from an engineering point-of-view, but should not keep us from



investigating the potential of such analyses. The continuous improvement of computing hardware and software (*e.g.*, faster computers, faster solvers, parallel computing), pushed by the demand for faster computations of increasingly complex (three-dimensional) phenomena, gradually lifts the restrictions on the use of three-dimensional simulation software.

From the experience with the finite-element-based injection simulation program *VIp*, which has been developed at the Eindhoven University of Technology and which employs the  $2\frac{1}{2}$ -D approach (Caspers, 1995; Zoetelief, 1995), the finite element method will be chosen as the computational foundation of the GAIM simulation code. Not only is the finite element method a versatile tool, *e.g.*, in its capability to deal with complex geometries and material behaviour; also the three-dimensional finite element modelling of the Reaction Injection Moulding process by Reijniere (1995) proved to be a good starting point for GAIM simulations.

The objective of this thesis is therefore to develop a simulation tool for the gas-assisted injection moulding process. At first instance, such a tool should enable the prediction of the gas distribution in GAIM products (usually expressed in terms of residual wall thickness and gas penetration length), as it yields information on the ratio of polymer and gas to be injected. Figure 1.8 gives some typical examples of cases that the simulation model should be able to deal with.

Once the gas distribution in a GAIM product can be simulated successfully, the next important step will be the prediction of product properties. Since it has been advocated that the reduction of sink marks and of residual stresses are the main advantages of GAIM over conventional injection moulding, it will be obvious that these are the product properties to be focused on.

Thus, a model has to be developed that is based on the process physics, and that employs the finite element method. Simulation results obtained with this model will be shown, starting with simple conditions (*i.e.*, isothermal Newtonian flow in a two-dimensional geometry) and gradually extending to more complex situations, in order to demonstrate the model's capabilities. The numerical results will also be compared with experimental results for relatively simple, but yet characteristic gas injection conditions. Finally, simulations will be presented that demonstrate the effects of gas injection on residual stresses in a typical GAIM product geometry.

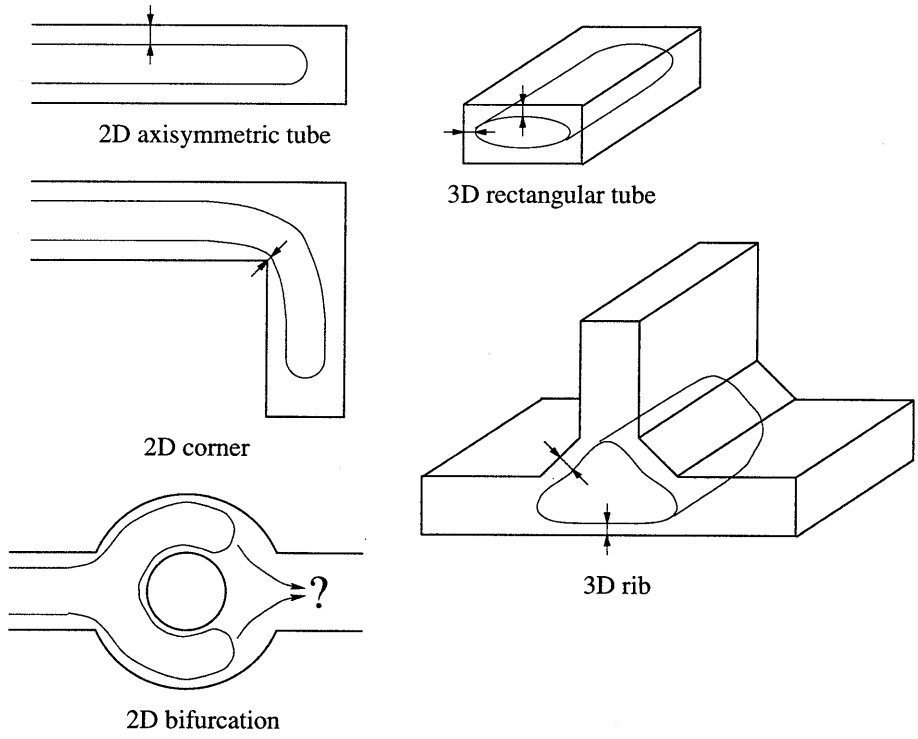


**Figure 1.8:** Typical test problems for a GAIM simulation code.

## Chapter 2

# Modelling

In this chapter, a model for three-dimensional gas-assisted injection moulding simulations will be presented. It is based on a pseudo-concentration method of Thompson (1986), which is related to the Volume of Fluid (VOF) method (Hirt and Nichols, 1981). With this method, the flow problem is solved on a fixed grid that covers the entire mould, so that elaborate three-dimensional remeshing can be avoided. A fictitious fluid is introduced to represent both the air downstream of the polymer flow front and the injected gas. The main property of this fictitious fluid is that it should not contribute to the pressure build-up in the mould during filling. Therefore, its viscosity is set to a value at least  $10^3$  times smaller than the viscosity of the filling fluid. However, the viscosity of the fictitious fluid exceeds the real value for air by several orders of magnitude in order to keep the Reynolds number small, so that inertia terms do not have to be taken into account. Furthermore, the fictitious fluid is allowed to leave the mould at some specified boundaries.

The essence of our pseudo-concentration model is that the distinction between filling fluid and fictitious fluid is made by labelling fluid particles with a material label  $c$  (being the pseudo-concentration), which is given the value  $c = 1$  for the filling fluid, and  $c = 0$  for the fictitious fluid. Near the flow front,  $c$  is a continuous function between 1 and 0; the flow front itself is determined by the iso-value line for  $c = 0.5$ . This interface is kept track of by convecting the material labels with the fluid velocity.

Actually, the use of a pseudo-concentration method makes gas-assisted injection moulding nothing more than a special case of conventional injection moulding: beside the fictitious fluid domain representing the air downstream of the polymer flow front, GAIM simulations involve a second fictitious fluid domain for the injected gas. As there is no fundamental difference between these two fictitious fluid domains (also because the injected gas is usually nitrogen, which has nearly the same physical properties as air), we will present our model as a general model for mould filling simulations, and refer only

to gas-assisted injection moulding if necessary. Consequently, as far as the modelling is concerned, the words 'air' and 'gas' in the sequel of this chapter can be interchanged.

## 2.1 Mould filling simulation: a moving boundary problem

The main problems in the simulation of mould filling processes are related to the modelling of the flow front. This flow front is a moving free surface, of which the position is to be determined as part of the solution procedure. The contact lines of the free surface at the mould walls are moving as well, giving rise to extra complications, such as a stress singularity at the contact line in case of a no-slip boundary condition for the filling fluid (Huh and Scriven, 1971).

Several methods have been developed to solve problems of viscous flows with moving boundaries (see Floryan and Rasmussen (1989) for a review). Adaptive grid methods (involving remeshing) have been commonly used in codes for two-dimensional simulation of moulding processes: the mesh covers the fluid area and is extended every time step.

In viscous flows, the region immediately upstream of the flow front is characterised by the fountain flow phenomenon (Rose, 1961): fluid particles that approach the front from the (upstream) core of the flow, are diverted towards the wall. In the past, approximate solutions were developed for fountain flow in an axisymmetric cylinder (Bhattacharji and Savic, 1965) and between two parallel plates (Castro and Macosko, 1982). These analytical relations are commonly used to evaluate the effects of fountain flow in simulation codes that employ the  $2\frac{1}{2}$ -D approach. However, no such expressions for fountain flow in three-dimensional moulds are available.

The pseudo-concentration method has also been used in the context of mould filling by others, who all use different boundary conditions at the mould walls. Thompson (1986) imposes a no-slip condition at the mould wall parts that are wetted by the filling fluid, but he is not clear about the boundary condition in the fictitious fluid. His mould filling example shows a moving contact line that is considerably lagging behind with respect to the flow front. His pseudo-concentration function is a continuously decreasing function that has to be smoothed regularly because it is severely distorted by the convection algorithm. Moreover, he reports a mass loss of 10%. Lewis and co-workers (Usmani *et al.*, 1992; Lewis *et al.*, 1995) adopt the method for the two-dimensional simulation of metal casting. However, they approach the turbulent metal flow as a laminar flow with a free slip boundary condition at the entire mould wall. Hence the fountain flow effect, which is irrelevant to their case, does not occur. Fortin *et al.* (1995) also use the pseudo-concentration method for two-dimensional (polymer) injection moulding. Prescribing no-slip for the filling fluid, and free stress in both normal and tangential direction for the fictitious fluid, they are able to capture the fountain flow effect. Their attempts to impose a zero normal velocity for the fictitious fluid along the mould walls (except at

specified air vents) failed, as it turned out that this resulted in a thin layer of fictitious fluid remaining at the wall after the flow front had passed (Fortin, 1997). Hétu *et al.* (1995) use the same boundary conditions as Fortin *et al.* (1995). Their flow front results seem rather inaccurate — with material appearing at locations in the mould that have not been reached by the flow front yet — and they do not show any fountain flow results. Finally, Medale and Jaeger (1997) solve the pseudo-concentration convection equation only in a limited domain surrounding the interface. They then correct for mass losses by slightly changing the value of the material label  $c_{interface}$  that determines the interface position. At the mould walls, the following slip condition is imposed:

$$\tau_{wall} = -f u_t, \quad (2.1)$$

in which  $\tau_{wall}$  is the wall shear stress,  $u_t$  is the velocity tangential to the wall, and  $f$  is a friction coefficient which is set to 0.01.

Because we treat the simulation of gas-assisted injection moulding as a special case of mould filling simulation, the results to be presented in Chapter 4 will first focus on some characteristic aspects of mould filling in general (such as fountain flow and flow bifurcations), before the actual GAIM simulation results will be dealt with.

In this section we will derive the model for three-dimensional mould filling simulations from the equations governing the process. It will be shown that the boundary and interface conditions require special attention.

## 2.2 Governing equations

Our modelling starts with the conservation equations for mass, momentum, and internal energy\*:

$$\frac{\partial \rho}{\partial t} + (\nabla \cdot \rho \mathbf{u}) = 0 \quad (2.2)$$

$$\rho \frac{\partial \mathbf{u}}{\partial t} + \rho \mathbf{u} \cdot \nabla \mathbf{u} = \nabla \cdot \boldsymbol{\sigma} + \rho \mathbf{g} \quad (2.3)$$

$$\rho \dot{e} = \boldsymbol{\sigma} : \mathbf{D} - \nabla \cdot \mathbf{h} + \rho r + \rho h_r R_c. \quad (2.4)$$

Formally, the conservation of moment of momentum, which requires that the stress tensor is symmetric, has to be added to this set of equations. Moreover, the use of a pseudo-concentration method demands for an equation of ‘conservation of identity’:

$$\dot{c} = 0, \quad (2.5)$$

which states that each material particle (actually: each infinitesimal material volume element) in the mould is labelled with a value  $c$  that does not change.

---

\*For an explanation of the symbols used in these and following equations, the reader is referred to the Notation section on page xv.

**Table 2.1:** Process variables expressed as products of dimensionless variables (marked with an asterisk: \*) and characteristic values. (The rate-of-deformation tensor  $\mathbf{D}$  has been scaled with the largest components of  $\nabla \mathbf{u}$  for  $\epsilon \leq 1$ , which are  $\frac{\partial u}{\partial y}$  and  $\frac{\partial u}{\partial z}$ .)

$x = x^*L$	$y = y^*H = y^*\epsilon L$	$z = z^*H = z^*\epsilon L$
$u = u^*U$	$v = v^*V = v^*\epsilon U$	$w = w^*V = w^*\epsilon U$
$\mathbf{D} = \mathbf{D}^*\frac{U}{H}$	$\epsilon = \frac{H}{L}$	$p = p^*p_{ref}$
$t = t^*\tau$	$T = T^*(\Delta T)_0$	$\mathbf{g} = \mathbf{g}^*g_0$
$\eta = \eta^*\eta_0$	$\rho = \rho^*\rho_0$	$\kappa = \kappa^*\kappa_0$
$c_p = c_p^*c_{p0}$	$\lambda = \lambda^*\lambda_0$	$\alpha = \alpha^*\alpha_0$

Each variable in equations (2.2) to (2.4) can be written as a product of a dimensionless variable and a characteristic value (see Table 2.1). At this point, we will not specify the characteristic value  $p_{ref}$  for the pressure yet.

The ratio  $\epsilon$  determines the type of mould geometry; here we focus on cube-like ( $\epsilon \approx 1$ ) and oblong ( $\epsilon < 1$ ) geometries, as these exhibit three-dimensional flow. (The reader may note that since  $y$  is rather unconventionally scaled with  $H$  instead of  $L$ , thin-walled geometries are characterised by  $\epsilon > 1$ .) Furthermore, the coupling of the characteristic values for the velocity components  $v$  and  $w$  to the characteristic value  $U$  through the ratio  $\epsilon$  in Table 2.1 will, strictly speaking, only be valid if the flow is incompressible. It is shown in Appendix A that the density variations are very small, so that the coupling between  $U$  and  $V$  can be maintained.

Using the dimensionless variables, the equations that govern the fluid flow, the material label convection, and the temperature will now be derived. Solving these equations with the appropriate initial and boundary conditions suffices to simulate an injection moulding process. The prediction of residual stresses can — in principle — be decoupled from this simulation (as shown by Baaijens (1991) and Douven (1991)) and will be treated as a post-processing step.

### 2.3 Flow problem

Usually, polymer flow is assumed to be incompressible. However, we will retain the original continuity equation (2.2) in order to be able to compute the polymer shrinkage. Thus, we consider the polymer density to be a given function of pressure and temperature:

$$\rho = \rho(p, T). \quad (2.6)$$

The constitutive equation for the Cauchy stress tensor  $\boldsymbol{\sigma}$  is given by:

$$\boldsymbol{\sigma} = -p\mathbf{I} + \boldsymbol{\tau} \quad (2.7a)$$

$$p = p_0 - \mu \text{tr}(\mathbf{D}) \quad (2.7b)$$

$$\boldsymbol{\tau} = 2\eta\mathbf{D} - \frac{2}{3}\eta \text{tr}(\mathbf{D})\mathbf{I} = 2\eta\mathbf{D}^d, \quad (2.7c)$$

whereas for the shear viscosity, generalised Newtonian behaviour is assumed:

$$\eta = \eta(p, T, \mathbf{D}). \quad (2.8)$$

The bulk viscosity  $\mu$  expresses the difference between the real (thermodynamic) pressure  $p$  in a flowing fluid (which is not in equilibrium) and the equilibrium (hydrodynamic) pressure  $p_0$ . Batchelor (1967) describes the bulk viscosity  $\mu$  as an 'expansion damping' coefficient which accounts for the pressure lag in a system with continuously changing state variables  $\rho$  and internal energy  $e$ . Usually, the term  $\mu \text{tr}(\mathbf{D})$  can be neglected for compressible fluids, except in cases where the rates of expansion approach the order of magnitude of the shear rates, such as in shock waves and the damping of high frequency sound waves. Furthermore, it is shown in Appendix A that the influence of compressibility on the equation of conservation of momentum can be neglected, *i.e.*,

$$\mathcal{O}(\text{tr}(\mathbf{D})\mathbf{I}) \ll \mathcal{O}(\mathbf{D}), \quad (2.9)$$

in equation (2.7c).

Introducing the dimensionless variables given in Table 2.1 in the continuity equation (2.2) and the momentum equation (2.3), and substituting the constitutive equations for the Cauchy stress tensor into the latter, yields the dimensionless Navier-Stokes equations<sup>†</sup>:

$$Sr \frac{\partial \rho}{\partial t} + (\nabla \cdot \rho \mathbf{u}) = 0 \quad (2.10)$$

$$Sr \rho \frac{\partial \mathbf{u}}{\partial t} + \rho \mathbf{u} \cdot \nabla \mathbf{u} = -\frac{p_{ref}}{\rho_0 U^2} \nabla p + \frac{1}{Re} \nabla (2\eta \mathbf{D}) + \frac{1}{Fr} \rho \mathbf{g}, \quad (2.11)$$

from which the asterisk (\*), indicating dimensionless variables, has been removed. The dimensionless numbers  $Re$ ,  $Sr$ , and  $Fr$  are the Reynolds, Strouhal, and Froude number, respectively; they are given by:

$$Re = \frac{\rho_0 U H}{\eta_0}, \quad Sr = \frac{L}{\tau U}, \quad Fr = \frac{U^2}{g_0 L}. \quad (2.12)$$

<sup>†</sup>Strictly speaking, the term 'Navier-Stokes equations' has been reserved for the flow of incompressible fluids with constant viscosity.

**Table 2.2:** Characteristic values of the process variables for thermoplastic injection moulding.

variable	unit	characteristic value	
		polymer	air
$\rho_0$	$\text{kg m}^{-3}$	$10^3$	1
$\eta_0$	Pa s	$10^4$	$10^{-5}$
$c_{p0}$	$\text{J kg}^{-1} \text{K}^{-1}$	$10^3$	$10^3$
$\lambda_0$	$\text{W m}^{-1} \text{K}^{-1}$	$10^{-1}$	$10^{-2}$
$\alpha_0$	$\text{K}^{-1}$	$10^{-5}$	$10^{-3}$
$\kappa_0$	$\text{Pa}^{-1}$	$10^{-9}$	$10^{-5}$
$L$	m	$10^{-1}$	
$H$	m	$10^{-2}$	
$U$	$\text{m s}^{-1}$	$10^{-1}$	
$g_0$	$\text{m s}^{-2}$	10	
$\gamma_0$	$\text{N m}^{-1}$	$10^{-2}$	
$(\Delta T)_0$	K	$10^2$	

Characteristic values for injection moulding of polymers are given in Table 2.2. The value  $\eta_0 = 10^4$  Pa s is characteristic for *non-isothermal* flow of polymer melts in injection moulding, *i.e.*, when the polymer cooling is taken into account. (In a previous publication, Haagh *et al.* (1997) limited themselves to *isothermal* polymer flow, for which a characteristic viscosity of  $10^3$  Pa s was considered more appropriate.) The characteristic time  $\tau$  is related to the time scale upon which velocity fluctuations of order  $U$  occur. In injection moulding, such a fluctuation will only occur immediately after starting the process. As we are not interested in start-up phenomena,  $\tau$  is very large with respect to  $\frac{L}{H}$ , and consequently the Strouhal number  $Sr$  is very small. The other dimensionless numbers can be determined as:

$$Re = \begin{cases} 10^{-4} & \text{for polymer} \\ 10^2 & \text{for air} \end{cases} \quad (2.13)$$

$$Fr = 10^{-2}. \quad (2.14)$$

### 2.3.1 Polymer domain

For the polymer melt domain, the Reynolds number indicates that the stationary inertia terms can be neglected. The conservation of momentum equation is now re-scaled with



respect to the viscous stress term:

$$\frac{p_{ref}H}{\eta_0 U} \nabla p = \nabla(2\eta\mathbf{D}) + \frac{Re}{Fr} \rho \mathbf{g}. \quad (2.15)$$

Since the pressure in the polymer is determined by the viscous stresses, we define the characteristic value for the pressure as  $p_{ref} = \frac{\eta_0 U}{H}$ , which yields a stationary Stokes equation:

$$\nabla p = \nabla(2\eta\mathbf{D}) + \frac{Re}{Fr} \rho \mathbf{g}. \quad (2.16)$$

Whether or not the gravity forces have to be taken into account, is determined by:

$$\frac{Re}{Fr} = \frac{\rho_0 g_0 H L}{\eta_0 U} = \frac{10^3 10^1 H 10^{-1}}{10^4 10^{-1}} = \mathcal{O}(H). \quad (2.17)$$

Since usually  $H \leq 10^{-1}$  m, the gravity forces can be neglected and equation (2.16) reduces to:

$$\nabla p = \nabla(2\eta\mathbf{D}). \quad (2.18)$$

Conforming to injection moulding practice, we choose  $H$  to be of order  $10^{-2}$  m, thus further limiting ourselves to oblong geometries (of which ribs and other gas-leading channels are typical examples).

Conforming to the pseudo-concentration method, any solidified polymer is modelled as a highly viscous (Newtonian) fluid: as soon as the polymer solidifies, its viscosity is set to  $10^6$  Pas, which exceeds the melt viscosity by approximately a factor  $10^2$ – $10^3$ .

### 2.3.2 Air domain

For the air domain, we can neglect the viscous forces and maintain the scaling of equation (2.11). In this case, we define the characteristic pressure as  $p_{ref} = \rho_0 U^2$ , yielding:

$$\rho \mathbf{u} \cdot \nabla \mathbf{u} = -\nabla p + \frac{1}{Fr} \rho \mathbf{g}. \quad (2.19)$$

This implies that we would have to solve a non-linear (Euler) equation, which, however, would yield a pressure drop in the air domain that is considerably smaller than in the polymer domain (which can be seen from a comparison of the pressure scaling for both materials). By replacing the air with a fictitious fluid, of which the viscosity is of order  $10^{-3}$  of the polymer viscosity and which has the same mass density as the air, the Reynolds number for the fictitious fluid domain would reduce to  $Re = 10^{-4}$ . Hence the inertia and gravity terms in the fictitious fluid domain can be neglected, while the pressure drop is still negligibly small compared to the pressure drop in the polymer domain. As a result, we can apply the stationary Stokes equation (equation 2.18) for the entire computational domain.

### 2.3.3 Boundary conditions

We define a domain  $\Omega$  covering the mould, with boundaries  $\Gamma_e$ ,  $\Gamma_w$ , and  $\Gamma_v$  designating the mould entrance, the mould walls, and the air vents. At the mould entrance, either the injection flow rate or the normal stress (*i.e.*, the injection pressure) is prescribed. Wherever the mould wall is covered with polymer, a no-slip condition is imposed. The physically correct boundary conditions near the moving contact line, however, cannot be uniquely determined, since the physics of this phenomenon are still not completely understood (Dussan V., 1979; de Gennes, 1985), and will demand modelling at scales much smaller than any mesh size that is manageable for mould filling simulations (van der Zanden, 1993). As a no-slip boundary condition in the air would prevent the polymer from contacting the mould wall, we have chosen to prescribe a free slip condition downstream of the flow front, thus enabling the contact point to move freely. Hence, the boundary condition along the mould walls is a function of the type of material, which is indicated by the material label  $c$ . This has been implemented by using an adjustable Robin boundary condition for the (dimensionless) velocity and stress components  $\mathbf{u}_t$  and  $\sigma_t$  in tangential direction:

$$a\mathbf{u}_t + \sigma_t = \mathbf{0} \quad \forall \mathbf{x} \in \Gamma_w \cup \Gamma_v, \quad (2.20)$$

in which the dimensionless 'Robin penalty parameter'  $a$  is defined as

$$a = a(c) = \begin{cases} \text{large } (\geq 10^4) & \text{if } c \geq 0.5 \text{ no slip} \\ 0 & \text{if } c < 0.5 \text{ free slip} \end{cases} \quad (2.21)$$

(From equation (2.20) it can be derived that  $a$  scales with  $\frac{\eta_0}{H}$ .)

The mould walls are impermeable, except at the air vents  $\Gamma_v$  where the air is allowed to leave the mould, yielding the following boundary conditions for the velocity and stress component  $u_n$  and  $\sigma_n$  in normal direction:

$$u_n = 0 \quad \forall \mathbf{x} \in \Gamma_w \quad (2.22a)$$

$$a u_n + \sigma_n = 0 \quad \forall \mathbf{x} \in \Gamma_v, \quad (2.22b)$$

in which  $a$  is again given by equation (2.21).

### 2.3.4 Interfacial conditions

From a physical point of view, two more boundary conditions hold for the flow front, namely immiscibility and conservation of momentum. The immiscibility condition is already implied by the 'conservation of identity' (equation 2.5). The conservation of momentum at the interface is expressed as (Batchelor, 1967):

$$(\sigma_2 - \sigma_1) \cdot \mathbf{n}_{12} = \gamma_{12} \kappa \mathbf{n}_{12}, \quad (2.23)$$

in which the subscripts 1 and 2 denote the polymer and the fictitious fluid, and  $\gamma_{12}$ ,  $\kappa$ , and  $\mathbf{n}_{12}$  denote the interfacial tension, the interface curvature, and the normal vector to the interface, respectively. Using equation (2.7a) and introducing dimensionless variables, equation (2.23) can be written as:

$$(\sigma_2^* - \sigma_1^*) \cdot \mathbf{n}_{12}^* = \frac{1}{Ca} \gamma_{12}^* \kappa^* \mathbf{n}_{12}^*, \quad (2.24)$$

in which the Capillary number  $Ca$  has been defined by equation (1.5). For injection moulding of polymers, the Capillary number is of order  $10^4$ , indicating that interfacial forces can be neglected. Thus equation (2.23) reduces to (when omitting the asterisk from the dimensionless variables):

$$\sigma_2 - \sigma_1 = \mathbf{0}, \quad (2.25)$$

which is already taken care of by the overall conservation of momentum equation (equation 2.11), since the material properties are continuous functions of  $c$  at the interface. As a result, the phenomena at the flow front have already been taken into account in our model.

## 2.4 Material label convection problem

The material labels that are used to distinguish polymer from air, are convected through the mould with velocity  $\mathbf{u}$ , while maintaining their 'identity' according to equation (2.5). Hence, in a Eulerian coordinate system, a pure (passive scalar) convection equation describes the evolution of the material label distribution; in its dimensionless form, it reads:

$$Sr \frac{\partial c}{\partial t} + \mathbf{u} \cdot \nabla c = 0. \quad (2.26)$$

As mentioned earlier, this can be regarded as a conservation equation of particle identity. Initially,  $c$  is set to zero in the entire domain  $\Omega$ , and only boundary conditions at the flow entrance are needed:

$$c = 0 \quad \forall \mathbf{x} \in \Omega, t = 0 \quad (2.27a)$$

$$c = 1 \quad \forall \mathbf{x} \in \Gamma_e, 0 < t < t_{gas} \quad (2.27b)$$

$$c = 0 \quad \forall \mathbf{x} \in \Gamma_e, t \geq t_{gas}, \quad (2.27c)$$

in which  $t_{gas}$  is the time when gas is injected.

The boundary condition for the convection equation can also be the time of entrance (injection time) or one of the entrance coordinates. Equation (2.26) can then be used to perform particle tracking to visualise the flow (Zoetelief *et al.*, 1997). Some examples will be shown in Chapter 4.

The material properties, as they appear in the Stokes equation, can now be determined locally as a function of the material label. The mould filling problem can thus be simulated by solving equations (2.16) and (2.26), and updating the material properties at every time step.

## 2.5 Temperature problem

Assuming that neither the thermal radiation  $r$  nor the reaction heat  $h_r$  plays a role in injection moulding of thermoplastics, equation (2.4) can be reduced to:

$$\rho \dot{e} = \boldsymbol{\sigma} : \mathbf{D} - \nabla \cdot \mathbf{h}. \quad (2.28)$$

For the rate of change of internal energy, the following equation can be obtained from thermodynamics (Batchelor, 1967):

$$\rho \dot{e} = \rho c_p \dot{T} - \alpha T \dot{p}, \quad (2.29)$$

in which the thermal expansion coefficient  $\alpha$  is given by:

$$\alpha = \frac{1}{v} \left( \frac{\partial v}{\partial T} \right)_p = -\frac{1}{\rho} \left( \frac{\partial \rho}{\partial T} \right)_p. \quad (2.30)$$

Hence, the last term in equation (2.29) is due to compressibility.

The constitutive equations for the Cauchy stress tensor and the viscosity have already been given by equations (2.7a) to (2.9). The heat capacity coefficient  $c_p$  is given as:

$$c_p = c_p(p, T), \quad (2.31)$$

and Fourier's law is used to describe the (isotropic) heat flux:

$$\mathbf{h} = -\lambda \nabla T, \quad (2.32)$$

in which the heat conduction coefficient  $\lambda$  is given by:

$$\lambda = \lambda(p, T). \quad (2.33)$$

Substitution of equation (2.29) and the appropriate constitutive equations in equation (2.28) yields:

$$\rho c_p \dot{T} = 2\eta \mathbf{D} : \mathbf{D} + \lambda \nabla^2 T + \alpha T \dot{p}. \quad (2.34)$$

Introducing the dimensionless variables given in Table 2.1 into this equation yields the dimensionless temperature equation:

$$\frac{1}{Fo} \rho c_p \frac{\partial T}{\partial t} + \epsilon Pe \rho c_p \mathbf{u} \cdot \nabla T = 2Br \mathbf{D} : \mathbf{D} + \lambda \nabla^2 T + \frac{\epsilon Br Sr}{Gc} \alpha T \frac{\partial p_0}{\partial t} + \frac{\epsilon Br}{Gc} \alpha T \mathbf{u} \cdot \nabla p_0, \quad (2.35)$$

in which all variables are dimensionless, and the dimensionless numbers are defined as:

$$Fo = \frac{\lambda_0 \tau}{\rho_0 c_{p0} H^2} \quad \text{Fourier number} \quad (2.36a)$$

$$Pe = \frac{\rho_0 c_{p0} U H}{\lambda_0} \quad \text{Péclet number} \quad (2.36b)$$

$$Br = \frac{\eta_0 U^2}{\lambda_0 (\Delta T)_0} \quad \text{Brinkman number} \quad (2.36c)$$

$$Sr = \frac{L}{\tau U} \quad \text{Strouhal number} \quad (2.36d)$$

$$Gc = \frac{1}{\alpha_0 (\Delta T)_0} \quad \text{Gay-Lussac number.} \quad (2.36e)$$

The characteristic time  $\tau$  in the temperature equation is typically the time in which either the temperature or the pressure changes in the order of its magnitude. For the injection stage, the cooling down of hot polymer melt contacting a cold mould wall is roughly estimated to take about 1 second, so that  $\tau = 1$  s for this stage. The packing stage is characterised by a fast increase of the pressure, for which  $\tau$  is of the order of 0.1 s. The temperature decreases rather slowly in the cooling stage, so  $\tau$  is estimated to be 10 s.

As for the flow problem, a distinction between the polymer and the air domain has to be made, in order to determine which terms of the temperature equation are important in each domain.

### 2.5.1 Polymer domain

Determining the dimensionless numbers defined in (2.36) from the characteristic values for the polymer as given in Table 2.2, and substituting these into the dimensionless temperature equation (2.35) yields the orders of magnitude of the different terms:

$$\underbrace{\frac{1}{Fo} \rho c_p \frac{\partial T}{\partial t}}_{10^3 \tau^{-1}} + \underbrace{\epsilon Pe \rho c_p \mathbf{u} \cdot \nabla T}_{?} = \underbrace{2Br \mathbf{D} : \mathbf{D}}_{10} + \underbrace{\lambda \nabla^2 T}_{1} + \underbrace{\frac{\epsilon Br Sr}{Gc} \alpha T \frac{\partial p_0}{\partial t}}_{10^{-3} \tau^{-1}} + \underbrace{\frac{\epsilon Br}{Gc} \alpha T \mathbf{u} \cdot \nabla p_0}_{10^{-3}}. \quad (2.37)$$

The order of magnitude of the convective term (the second term on the left hand side) is difficult to estimate because of the inner product of the velocity  $\mathbf{u}$  and the temperature gradient  $\nabla T$ : the largest temperature gradient is found near the wall in a temperature boundary layer of a limited thickness  $\delta < H$ , in which the velocity will be very small.

With the given estimates for the characteristic time for the different moulding stages, the last two terms of equation (2.37) can be neglected for all injection stages, leaving the following temperature problem to be solved for the polymer domain:

$$\frac{1}{Fo} \rho c_p \frac{\partial T}{\partial t} + \epsilon Pe \rho c_p \mathbf{u} \cdot \nabla T = 2Br \mathbf{D} : \mathbf{D} + \lambda \nabla^2 T, \quad (2.38)$$

which is an ordinary convection-diffusion equation. As a matter of fact, the second (convection) and third (dissipation) term can be neglected as well in the cooling stage, since  $U \approx 0$  for that stage.

### 2.5.2 Air domain

A similar exercise yields the order of magnitude of the temperature equation terms for the air domain:

$$\underbrace{\frac{1}{Fo} \rho c_p \frac{\partial T}{\partial t}}_{10^{-1}} + \underbrace{\epsilon Pe \rho c_p \mathbf{u} \cdot \nabla T}_{?} = \underbrace{2Br \mathbf{D} : \mathbf{D}}_{10^{-6}} + \underbrace{\lambda \nabla^2 T}_1 + \underbrace{\frac{\epsilon Br Sr}{Gc} \alpha T \frac{\partial p_0}{\partial t}}_{10^{-6} \tau^{-1}} + \underbrace{\frac{\epsilon Br}{Gc} \alpha T \mathbf{u} \cdot \nabla p_0}_{10^{-6}}. \quad (2.39)$$

Discarding the irrelevant terms results in:

$$\frac{1}{Fo} \rho c_p \frac{\partial T}{\partial t} + \epsilon Pe \rho c_p \mathbf{u} \cdot \nabla T = \lambda \nabla^2 T, \quad (2.40)$$

which is identical to the resulting equation for the polymer domain, except for the missing viscous dissipation term. However, this term needs careful re-examination, since we artificially increased the air viscosity when we introduced the fictitious fluid. Thus, for the fictitious fluid, the Brinkman number is of order  $10^{-2}$ , indicating that the use of a fictitious fluid will hardly affect the temperature solution.

Consequently, applying equation (2.38) on the entire computational domain would yield a sufficiently accurate temperature solution. However, the viscous dissipation term will be set to zero for the air domain, since the computed velocity field in the fictitious fluid does not represent the actual air velocity distribution.

### 2.5.3 Initial and boundary conditions

As an initial condition for the temperature problem, a temperature field over the entire domain is imposed:

$$T = T_0(\mathbf{x}) \quad \forall \mathbf{x} \in \Omega, t = 0. \quad (2.41)$$

At the injection gate  $\Gamma_e$ , the injection temperature is prescribed:

$$T = T_e(t) \quad \forall \mathbf{x} \in \Gamma_e, t > 0. \quad (2.42)$$

The boundary conditions at the mould walls and air vents can either be a constant temperature (Dirichlet boundary condition):

$$T = T_w(t) \quad \forall \mathbf{x} \in \Gamma_w \cup \Gamma_v, t > 0, \quad (2.43)$$

or a heat flux (Biot or Robin boundary condition):

$$\lambda \frac{\partial T}{\partial \mathbf{n}} = h_w(T - T_w) \quad \forall \mathbf{x} \in \Gamma_w \cup \Gamma_v, t > 0, \quad (2.44)$$

in which  $\mathbf{n}$  is the normal vector on the mould wall,  $h_w$  is the effective heat transfer coefficient from the polymer to the cooling medium, and  $T_w$  is the wall temperature.

Since the actual temperatures at the mould wall are rarely known accurately, a complete thermal analysis of the mould (including the cooling channels *etc.*) would yield a more reliable moulding simulation. However, such an extension of the analysis is beyond the scope of this thesis.

At the air/polymer interface(s), the temperature is continuous. Solving the temperature equation (2.38) on a fixed grid will inherently satisfy this condition.

## 2.6 Residual stresses

The three-dimensional modelling of residual stresses in injection moulding products is treated in this section, initially following the approach of Baaijens (1991) and Douven (1991). These authors applied the modelling to conventional, thin-walled injection moulding products, for which the Hele-Shaw approach is used. The computational aspects involved in our three-dimensional approach will be different.

Since the kinematics of the flow during mould filling are dominated by in-elastic viscous (shear) effects (see, *e.g.*, Macosko, 1993), we can decouple the residual stress computations from the actual moulding simulation. For the moulding simulation, a generalised Newtonian viscosity model (equation 2.8) is used. The flow kinematics resulting from these types of simulation, together with the temperature and pressure history, serve as input for the residual stress computations, in which a viscoelastic constitutive equation should be employed.

### 2.6.1 The compressible Leonov model

Baaijens (1991) pointed out that compressibility effects are important in the post-filling stage, and that the Leonov model could in principle give a reasonably good description of the mechanical behaviour in injection moulding, provided that compressibility is taken into account. Therefore, he introduced a compressible version of the Leonov model. His modelling will, to a large extent, be followed below.

The Cauchy stress tensor  $\sigma$  is first split into a viscoelastic part  $\sigma_{ve}$  and a viscous part  $\sigma_v$ :

$$\sigma = \sigma_{ve} + \sigma_v. \quad (2.45)$$

The viscous part of the stress tensor is defined as:

$$\sigma_v = 2\eta_v(p, T)\mathbf{D}^d. \quad (2.46)$$

The viscosity  $\eta_v$  can be interpreted as the infinite-shear-rate limit of the polymer melt viscosity. For polymer melts, the viscous part of the stress is usually negligibly small compared to the viscoelastic part.

The viscoelastic stresses are once more split into a hydrostatic and a deviatoric part:

$$\sigma_{ve} = -p\mathbf{I} + \tau_{ve}, \quad (2.47)$$

in which  $\tau_{ve}$  is the viscoelastic extra stress tensor. The thermodynamic pressure  $p$  can be obtained from the relation between density, temperature, and pressure (equation 2.6).

The deformation gradient tensor  $\mathbf{F} = \nabla_0\mathbf{x}$  is split into an elastic part  $\mathbf{F}_e$  and a plastic part  $\mathbf{F}_p$ , such that:

$$\mathbf{F} = \mathbf{F}_e \cdot \mathbf{F}_p. \quad (2.48)$$

Moreover, any volume change  $J$  is assumed to be elastic, so that  $J = \det(\mathbf{F}) = \det(\mathbf{F}_e)$  and  $\det(\mathbf{F}_p) = 1$ . Subsequently, the volumetric effects are separated from the deviatoric effects:

$$\bar{\mathbf{F}}_e = J^{-\frac{1}{3}}\mathbf{F}_e, \quad (2.49)$$

for which the associated Finger (or left Cauchy-Green) strain tensor is given by:

$$\bar{\mathbf{B}}_e = \bar{\mathbf{F}}_e \cdot \bar{\mathbf{F}}_e^c. \quad (2.50)$$

The velocity gradient tensor  $\mathbf{L}$  is decomposed into an elastic and a plastic part:

$$\mathbf{L} = (\nabla\mathbf{u})^c = \mathbf{L}_e + \mathbf{L}_p; \quad \mathbf{L}_e = \dot{\bar{\mathbf{F}}}_e \cdot \bar{\mathbf{F}}_e^{-1}; \quad \mathbf{L}_p = \mathbf{F}_e \cdot \dot{\mathbf{F}}_p \cdot \mathbf{F}_p^{-1} \cdot \mathbf{F}_e^{-1}, \quad (2.51)$$



and can be split into a symmetric part  $\mathbf{D}$  (the deformation rate tensor) and an anti-symmetric part  $\mathbf{W}$  called the spin tensor:

$$\mathbf{L} = \mathbf{D} + \mathbf{W} = (\mathbf{D}_e + \mathbf{W}_e) + (\mathbf{D}_p + \mathbf{W}_p). \quad (2.52)$$

For a single relaxation mode, the constitutive equation for the deviatoric part of the (visco)elastic stress,  $\tau_{ve}$ , is given by:

$$\tau_{ve} = \tau_e = \frac{\eta}{\theta} \bar{\mathbf{B}}_e^d, \quad (2.53)$$

which can be extended for the general multi-mode case (with  $m$  relaxation modes) to:

$$\tau_e = \sum_{j=1}^m \frac{\eta_j}{\theta_j} \bar{\mathbf{B}}_{ej}^d. \quad (2.54)$$

Leonov (1976) assumed (rather arbitrarily) that  $\mathbf{W}_p = \mathbf{0}$ , which yields the following relation for (the material time derivative of) the elastic Finger strain tensor  $\bar{\mathbf{B}}_e$ :

$$\dot{\bar{\mathbf{B}}}_e = (\mathbf{L}^d - \mathbf{D}_p) \cdot \bar{\mathbf{B}}_e + \bar{\mathbf{B}}_e \cdot (\mathbf{L}^{dc} - \mathbf{D}_p). \quad (2.55)$$

Furthermore, he introduced the following relation for the plastic deformation rate  $\mathbf{D}_p$ :

$$\mathbf{D}_p = \frac{1}{4\theta} (\bar{\mathbf{B}}_e^d - \bar{\mathbf{B}}_e^{-d}). \quad (2.56)$$

The essential feature of this proposal for  $\mathbf{D}_p$  is, that it turns out to follow the (empirical) Cox-Merz rule, which states that the shear rate dependence of the steady-state viscosity  $\eta$  is equal to the frequency dependence of the dynamic viscosity  $\eta_d$ :

$$\eta(\dot{\gamma}) = |\eta_d(\omega)| \quad \text{for } \dot{\gamma} = \omega. \quad (2.57)$$

Using equation (2.56), equation (2.55) can be rewritten as:

$$\dot{\bar{\mathbf{B}}}_e = \mathbf{L}^d \cdot \bar{\mathbf{B}}_e + \bar{\mathbf{B}}_e \cdot \mathbf{L}^{dc} - \frac{1}{2\theta} \left( \bar{\mathbf{B}}_e \cdot \bar{\mathbf{B}}_e - \mathbf{I} - \frac{1}{3} (\text{tr}(\bar{\mathbf{B}}_e) - \text{tr}(\bar{\mathbf{B}}_e^{-1})) \bar{\mathbf{B}}_e \right). \quad (2.58)$$

Assuming thermo-rheologically simple behaviour, it follows that

$$\eta_j = a_T(T) \eta_{j0} \quad \text{and} \quad \theta_j = a_T(T) \theta_{j0}, \quad (2.59)$$

hence

$$\frac{\eta_j}{\theta_j} = \frac{\eta_{j0}}{\theta_{j0}}. \quad (2.60)$$

The compressible Leonov model can in principle be used to compute both the flow-induced stresses and the thermally and pressure-induced stresses.

### 2.6.2 Flow-induced stresses

Flow-induced stresses develop during flow, above the glass transition (or melting) temperature. Neglecting the viscous part, these stresses are given by:

$$\boldsymbol{\sigma} = -p\mathbf{I} + \boldsymbol{\tau}_e, \quad (2.61)$$

in which  $\boldsymbol{\tau}_e$  has to be computed from equations (2.58) and (2.54). The hydrostatic fluid pressure can be obtained directly from the mould filling simulation, and so can the deviatoric part of the velocity gradient tensor  $\mathbf{L}$  that is required for equation (2.58). Hence, the largest computational effort is concerned in solving this equation through numerical time integration for each relaxation mode.

### 2.6.3 Thermally and pressure-induced stresses

The thermally and pressure-induced stresses develop below the glass transition (or melting) temperature, *i.e.*, in the solidifying material where the deformations are small. Consequently, Baaijens (1991) and Douven (1991) linearised the Leonov model. The resulting linear Maxwell model was then used to determine these stresses. We will, however, continue with three-dimensional residual stress computations that do not need any additional assumptions as used by, *e.g.*, Baaijens and Douven, related to their  $2\frac{1}{2}$ -D approach.

The thermally and pressure-induced stresses are given by:

$$\boldsymbol{\sigma} = -p_s\mathbf{I} + \boldsymbol{\tau}_e, \quad (2.62)$$

in which the elastic extra stress tensor  $\boldsymbol{\tau}_e$  is, in principle, defined by equations (2.58) and (2.54). The hydrostatic pressure  $p_s$  in the solid state, as opposed to the hydrostatic pressure  $p$  in the fluid, is defined as:

$$p_s = \int_{t_g}^t \left( \frac{\alpha}{\kappa} \dot{T} - \frac{1}{\kappa} \text{tr}(\mathbf{D}) \right) dt' + p(t_g) \quad \text{for } t > t_g. \quad (2.63)$$

$\alpha$  is the thermal expansion coefficient (equation 2.30),  $\kappa$  is the compressibility coefficient defined as:

$$\kappa = \frac{1}{\rho} \left( \frac{\partial \rho}{\partial p} \right)_T, \quad (2.64)$$

and  $t_g$  is the time when a material element solidifies. Obviously,  $t_g = t_g(\mathbf{x})$ . Note that also  $p_s = p_s(\mathbf{x})$ , since  $\dot{T}$ ,  $\text{tr}(\mathbf{D})$ , and  $p(t_g)$  are functions of the coordinates  $\mathbf{x}$ .

Both the temperature rate  $\dot{T}$  and the volumetric rate of change  $\text{tr}(\mathbf{D})$  can be obtained from the preceding (decoupled) mould filling simulation (*i.e.*, from the solutions of equations (2.10) and (2.38), respectively). This does require that the appropriate  $p\nu T$ -behaviour for both the melt and the solid is taken into account in the mould simulation.

The deviatoric part of the thermally and pressure-induced stresses is determined by the flow kinematics through the (deviatoric) part of the velocity gradient tensor,  $\mathbf{L}^d$  (see equation (2.58)). Neglecting the viscous parts of these stresses, the balance of stresses at the solid-melt 'interface' demands that:

$$-p_s \mathbf{I} + \boldsymbol{\tau}_{e,s} = -p \mathbf{I} + \boldsymbol{\tau}_{e,m}, \quad (2.65)$$

which, after substitution of equation (2.63) for  $t = t_g$ , reduces to:

$$\boldsymbol{\tau}_{e,s} = \boldsymbol{\tau}_{e,m}. \quad (2.66)$$

Hence, the thermally and pressure-induced extra stresses balance the flow-induced stresses at the glass transition (or melting) temperature.

Now we can compare the orders of magnitude of the two terms in equation (2.62) that determine the thermally and pressure-induced stresses. From equation (2.63), the pressure contribution can be estimated as:

$$\mathcal{O}(p_s) = \left( \frac{\alpha_0 (\Delta T)_0}{\kappa_0 \tau} - \frac{1}{\kappa_0} \mathcal{O}(\text{tr}(\mathbf{D})) \right) \tau + p_{ref}, \quad (2.67)$$

in which the order of magnitude of  $\text{tr}(\mathbf{D})$  can be obtained from:

$$\mathcal{O}(\text{tr}(\mathbf{D}) = \frac{\dot{\rho}}{\rho}) = \mathcal{O}\left(\frac{1}{\rho} \frac{\partial \rho}{\partial t}\right) = \frac{\Delta \rho_0}{\rho_0 \tau}. \quad (2.68)$$

The relative density change  $\frac{\Delta \rho_0}{\rho_0}$  in the solid polymer is approximately 1% in a characteristic cooling time  $\tau$  of 10 s. Using the characteristic values from Table 2.2, with  $p_{ref} = \frac{\eta_0 U}{L}$ , the order of magnitude of the pressure contribution becomes:

$$\mathcal{O}(p_s) = \left( \frac{10^{-5} 10^2}{10^{-9} 10^1} - \frac{10^{-2}}{10^{-9} 10^1} \right) \cdot 10^1 + \frac{10^4 10^{-1}}{10^{-2}} = 10^7 \text{ Pa}. \quad (2.69)$$

Equation (2.66) implies that the deviatoric part of the elastic stress can be estimated from the deviatoric ('shear') stress exerted by the fluid on the solidified layer. Hence:

$$\mathcal{O}(\boldsymbol{\tau}_{e,s}) = \mathcal{O}(2\eta \mathbf{D}) = \frac{\eta_0 U}{H} = \frac{10^4 10^{-1}}{10^{-2}} = 10^5 \text{ Pa}. \quad (2.70)$$

Consequently, the deviatoric contribution to the thermally and pressure-induced residual stresses can be neglected compared to the pressure contribution. The question whether the modelling of the solidified polymer as a highly viscous fluid during the mould filling simulation yields the appropriate flow kinematics for the thermally and pressure-induced stresses is, apparently, not relevant.

In conclusion, both the governing equations for the flow-induced and the thermally and pressure-induced residual stresses constitute an evolution problem, analogous to the material label convection and temperature problems defined above. For the flow-induced stresses, the evolution of  $\bar{\mathbf{B}}_e$  is computed using the compressible Leonov model, for which  $\mathbf{L}^d$  is obtained from the (compressible) flow problem. In the solid,  $\mathbf{L}^d$  is set to zero, hence  $\bar{\mathbf{B}}_e$  is not calculated. The thermally and pressure-induced stresses are calculated using  $\text{tr}(\mathbf{D})$  from the *compressible* flow problem and  $\dot{T}$  from the temperature problem.

The complexity of the residual stress computation is constituted in the non-linear character of the right hand side of equation (2.58), and in the fact that the six stress components can give rise to a huge amount of degrees of freedom.

#### 2.6.4 Initial and boundary conditions

We assume that any material (*i.e.*, polymer and air) that is initially present in the mould, has not deformed elastically. This yields the initial condition

$$\bar{\mathbf{B}}_e = \mathbf{I} \quad \forall \mathbf{x} \in \Omega, t = 0, \quad (2.71)$$

and

$$\boldsymbol{\sigma} = -p(t)\mathbf{I} \quad \forall \mathbf{x} \in \Omega, t = 0. \quad (2.72)$$

Also, all material that is injected into the mould is assumed to have no deformation history upon entering the mould:

$$\bar{\mathbf{B}}_e = \mathbf{I} \quad \forall \mathbf{x} \in \Gamma_e, t \geq 0. \quad (2.73)$$

Actually, this boundary condition is based on the assumption that any deformation history will relax quickly, since the polymer melt is generally injected at a high temperature.

Strictly speaking, the initial conditions given above apply to the flow-induced residual stresses (assuming that there is initially no solidified material present in the mould). For the thermally and pressure-induced residual stresses, which start to develop at the solidification time  $t_g$ , a separate set of initial conditions has to be defined. The initial conditions for the thermally and pressure-induced stresses read:

$$\boldsymbol{\sigma} = -p(t_g)\mathbf{I} \quad \{\forall \mathbf{x} \in \Omega \mid T(\mathbf{x}) = T_g \text{ (or } T_m)\}, t_g = t_g(\mathbf{x}). \quad (2.74)$$

In fact, these are the (solid/melt interface) boundary conditions given by equation (2.65) in which the deviatoric effects are neglected.

Finally, we will obviously not allow residual stresses to build up in the air and gas domains. Throughout the residual stress computations, we will therefore prescribe

$$\boldsymbol{\sigma} = -p(t)\mathbf{I} \quad \{\forall \mathbf{x} \in \Omega \mid c(\mathbf{x}) < 0.5\}, t > 0. \quad (2.75)$$

This can be realised by setting all viscosities  $\eta_j$  in equation (2.54) to zero in the air and gas domains.

## 2.7 Conclusions

In this chapter, we have given the mathematical framework for a gas-assisted injection moulding simulation program. By making the general equations that govern the process dimensionless, the contributions of the different terms have been quantified, and the equations have been simplified by neglecting the irrelevant terms. The pseudo-concentration method, which involves a pure convection equation to be solved, has been introduced to solve the system equations on a fixed grid. Also, the appropriate initial and boundary conditions have been identified. Special attention has been given to the boundary conditions near the moving contact line of the flow front. The model that has been developed, enables a full three-dimensional simulation of the GAIM process.

The computation of the residual stresses has been decoupled from the mould filling simulations, and can be carried out as a 'post-processing step.' The flow-induced stresses have been modelled using the compressible Leonov model. The deviatoric contribution to the thermally and pressure-induced stresses can be neglected, and only an evolution equation for the pressure contribution has to be solved.

Now that this framework has been established, we will treat the numerical methods and some details of the solution procedure in the first part of the next chapter. In the second part, a description of the experimental methods that have been used for the validation of the simulation code, will be given.



## Chapter 3

# Methods

### 3.1 Numerical methods

The model has been implemented in the finite element package SEPRAN. This section gives a short description of the implementation.

#### 3.1.1 Stokes equation

A standard Galerkin finite element method is used to solve the continuity equation (2.10) and the Stokes equation (2.16), which can be written after spatial discretisation as:

$$K\underline{u} = \underline{f} \quad (3.1)$$

$$S\underline{u} + L\underline{p} = \underline{g}, \quad (3.2)$$

in which  $\underline{g}$  is the right hand side vector containing the essential boundary conditions and any volume forces, and:

$$K_{ij} = - \int_{\Omega} \psi_i \nabla (\rho \phi_j) d\Omega \quad (3.3a)$$

$$L_{ij} = - \int_{\Omega} \psi_j \nabla \phi_i d\Omega \quad (3.3b)$$

$$S_{ij} = \frac{1}{Re} \int_{\Omega} \eta \nabla \phi_i \cdot \nabla \phi_j d\Omega, \quad (3.3c)$$

and  $\phi_i$  and  $\psi_i$  are the shape functions for the velocity and the pressure respectively. The right hand side vector  $\underline{f}$  will be explained below.

The elements used are so-called Crouzeix-Raviart ( $Q_2$ - $Q_1$ ) rectangular (2-D) or brick (3-D) elements, that employ a quadratic approximation for the velocity and a piece-wise linear approximation, which is discontinuous at the element boundaries, for

the pressure. These elements have the velocity components as degrees of freedom in all nodal points, plus the pressure and pressure gradients added as degrees of freedom to the central nodal point. The integration on the element level is carried out using a 9-point (2-D) or 27-point (3-D) Gauss rule. At the boundary elements that are required for the Robin boundary condition given by equation (2.20), however, a 2-point or 4-point Newton-Cotes integration scheme (for 1-D and 2-D boundary elements, respectively) turns out to yield the best results with respect to the moving contact line.

The right hand side vector  $\tilde{f}$  contains the partial time derivative of the density in the following manner: let us consider equation (3.1) for a single element:

$$K_{ij}^{(e)} u_j^{(e)} = f_i^{(e)} \quad \text{for } i = 1, \dots, m^{(e)} \text{ and } j = 1, \dots, n^{(e)}, \quad (3.4)$$

in which  $n^{(e)}$  and  $m^{(e)}$  are the number of degrees of freedom per elements for the velocity and the pressure (gradient), respectively. Suppose that  $i = 1$  corresponds to the pressure unknown, and  $i = 2, \dots, m^{(e)}$  to the pressure gradient unknowns. Then  $f^{(e)} = [f_1^{(e)} \dots f_m^{(e)}]^c$  is given by:

$$f_i^{(e)} = \begin{cases} -\frac{1}{Sr} \int_e \psi_i \frac{\rho^n - \rho^{n-1}}{\Delta t} de & \text{for } i = 1 \\ 0 & \text{for } i = 2, \dots, m^{(e)} \end{cases}, \quad (3.5)$$

in which the superscripts  $n$  and  $n-1$  indicate subsequent time levels. Hence, the partial time derivative of the density,  $\frac{\partial \rho}{\partial t}$ , is taken into account by a first order approximation in time, and a piece-wise constant approximation in space.

The system of equations is solved by an integrated method, employing both velocities and pressures as unknowns, in combination with an iterative (Conjugate Gradient Squared — CGS) solver in order to avoid excessive CPU time and memory usage (Shewchuk, 1994; Segal and Vuik, 1995). However, for 2-D problems involving incompressible flow, a penalty function method in combination with a direct solver will often suffice. A general description of these solution methods is given by Cuvelier *et al.* (1986) and Pittman (1989).

The material parameters are initially defined as discontinuous functions of the material labels, *e.g.*, for viscosity:

$$\eta = \eta(c) = \begin{cases} \eta_{polymer} & \text{if } c \geq 0.5 \\ \eta_{fictitious} & \text{if } c < 0.5 \end{cases} \quad (3.6)$$

The use of quadratic shape functions may then lead to negative values of the material property at the elements' integration points (see Figure 3.1). This is avoided by piece-wise linear interpolation of the material parameter at the midpoints of elements containing the flow front (see also Fortin *et al.*, 1995).



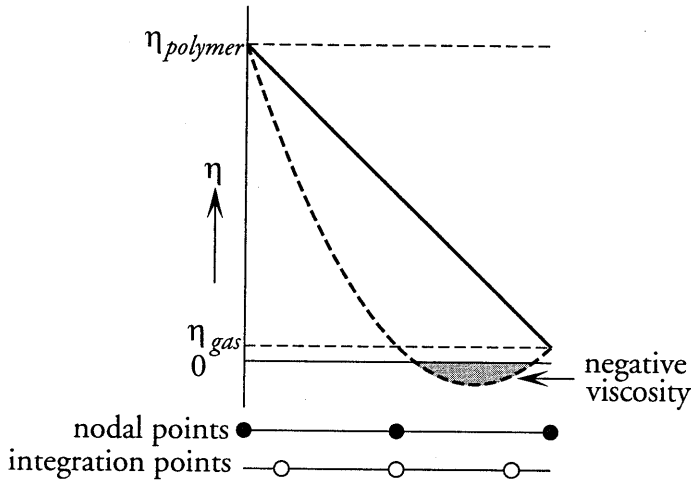


**Figure 3.1:** Piece-wise linear interpolation of viscosity on a quadratic element to avoid negative values: - - - = original (quadratic) function, — = interpolated (linear) function.

### 3.1.2 Convection equation

The convection equation for the material labels is solved with the finite element method using an Streamline-Upwind Petrov-Galerkin (SUPG) scheme (Brooks and Hughes, 1982). In the SUPG method, a discontinuous streamline upwind function  $\pi$  is added to the continuous weighing function  $\phi$  used in the Galerkin formulation to yield the modified weighing function  $\tilde{\phi}$ :

$$\tilde{\phi} = \phi + \pi, \quad (3.7)$$

in which  $\pi$  is generally of the form:

$$\pi = k\mathbf{u} \cdot \nabla\phi. \quad (3.8)$$

The SUPG formulation can actually be interpreted as compensating for the negative artificial diffusion that is often present in Galerkin formulations.

There are several options to specify  $k$ ; we have obtained the best results (*i.e.*, which suffer least from diffusion) for the material label convection problem by employing the streamline upwind function suggested by Shakib (1989) for time-dependent problems (see Segal, 1993):

$$\pi = \left( \left( \frac{2}{\Delta t} \right)^2 + \left( \frac{2|\mathbf{u}|}{h} \right)^2 + \left( \frac{4\zeta}{h} \right)^2 \right)^{\frac{1}{2}} \mathbf{u} \cdot \nabla\phi, \quad (3.9)$$

in which  $\Delta t$  is the time step size,  $b$  is a characteristic dimension of the element, and  $\zeta$  is defined by:

$$\zeta = \underline{u}^c \lambda \underline{u}. \quad (3.10)$$

with  $\lambda$  the diffusion tensor (which is the null tensor in the pure convection case).

Applying spatial discretisation, the convection equation can be written in the form:

$$M\dot{\underline{c}} + N(\mathbf{u})\underline{c} = 0, \quad (3.11)$$

in which the mass matrix  $M$  and the convection matrix  $N(\mathbf{u})$  are given by:

$$M_{ij} = Sr \int_{\Omega} \tilde{\phi}_i \phi_j d\Omega \quad (3.12a)$$

$$N_{ij}(\mathbf{u}) = - \int_{\Omega} \phi_j \mathbf{u} \cdot \nabla \tilde{\phi}_i d\Omega. \quad (3.12b)$$

(Because the weighing functions  $\tilde{\phi}$  are not equal to the approximation functions  $\phi$ , the mass matrix is not symmetric as it would be in a Galerkin formulation.)

Temporal discretisation with a finite difference  $\vartheta$ -method yields:

$$M \frac{\underline{c}^{n+1} - \underline{c}^n}{\Delta t} + \vartheta N(\mathbf{u}^{n+1}) \underline{c}^{n+1} + (1 - \vartheta) N(\mathbf{u}^n) \underline{c}^n = 0, \quad (3.13)$$

in which the superscripts  $n + 1$  and  $n$  indicate consecutive time steps. This can be approximated by a two-step procedure, yielding a set of equations that can be solved more efficiently:

$$\left( \frac{M}{\vartheta \Delta t} + N(\mathbf{u}^{n+\vartheta}) \right) \underline{c}^{n+\vartheta} = \frac{M}{\vartheta \Delta t} \underline{c}^n \quad (3.14a)$$

$$\underline{c}^{n+1} = \frac{1}{\vartheta} \left( \underline{c}^{n+\vartheta} - (1 - \vartheta) \underline{c}^n \right). \quad (3.14b)$$

For the time discretisation, a modified version of the Crank-Nicolson scheme ( $\vartheta = 0.5$ ) is used:  $\vartheta$  is set to  $0.5 + \alpha \Delta t$ , in which  $\alpha$  is a small positive real number. This suppresses oscillations in  $c$  without affecting the order of accuracy.

After every time step, the material labels are rounded off to either unity or zero everywhere, except in the elements containing an interface, where the original values of the material labels are retained (see Figure 3.2). Hence, possible oscillations in the material label field are suppressed.

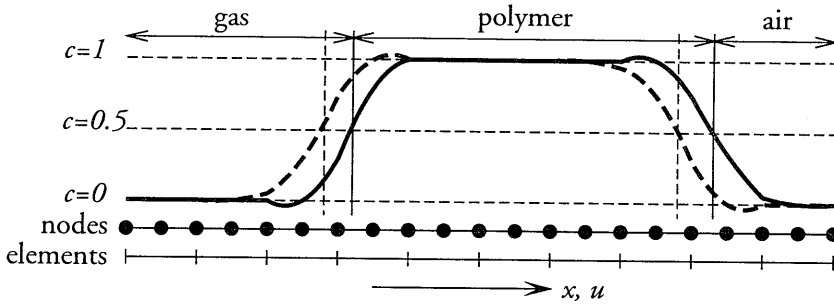


**Figure 3.2:** Convection of material labels: - - - time step  $n - 1$ , — time step  $n$ .

### 3.1.3 Temperature equation

The temperature equation is a convection-diffusion equation, of which the convection equation treated above was just a special (zero diffusion) case. Thus, the temperature equation is dealt with similarly — this time with a non-zero diffusion term and a non-zero right-hand-side to be included. Applying spatial discretisation employing the SUPG method then yields:

$$\mathbf{M}\dot{\underline{T}} + \mathbf{N}(\mathbf{u})\underline{T} + \mathbf{D}\underline{T} = \underline{f}. \quad (3.15)$$

The mass matrix  $\mathbf{M}$ , the convection matrix  $\mathbf{N}(\mathbf{u})$ , the diffusion matrix  $\mathbf{D}$ , and the right-hand-side vector  $\underline{f}$  are given by:

$$\mathbf{M}_{ij} = \frac{1}{Fo} \int_{\Omega} \rho c_p \tilde{\phi}_i \phi_j d\Omega \quad (3.16a)$$

$$\mathbf{N}_{ij}(\mathbf{u}) = \epsilon Pe \int_{\Omega} \rho c_p (\underline{u} \cdot \nabla \tilde{\phi}_i) \phi_j d\Omega \quad (3.16b)$$

$$\mathbf{D}_{ij} = \int_{\Omega} \lambda \nabla \tilde{\phi}_i \cdot \nabla \phi_j d\Omega \quad (3.16c)$$

$$\underline{f}_i = 2Br \int_{\Omega} \tilde{\phi}_i \mathbf{D}^d : \mathbf{D}^d d\Omega. \quad (3.16d)$$

The finite difference  $\vartheta$ -method as used for the convection equation (equations 3.13 and 3.14) is applied here.

**Note:** In simulations of injection moulding processes where a relatively large solidified polymer layer develops directly behind the advancing melt front, small amounts of air may be found at the walls that are supposed to be wetted by the polymer. To avoid such air enclosures (which usually occupy only a single node each, and which do not

affect the flow kinematics), a little diffusion may be added to material label convection equation (3.11), yielding:

$$M\dot{\underline{\zeta}} + \mathbf{N}(\mathbf{u})\underline{\zeta} + D\underline{\zeta} = \underline{0}. \quad (3.17)$$

For reasons of consistency, the diffusion coefficient for the material label convection  $\lambda_c$  is defined as:

$$\lambda_c = \lambda_{c0} \Delta t, \quad (3.18)$$

so that the diffusion would disappear if  $\Delta t$  approached zero. Hence, the diffusion matrix  $D$  is given by:

$$D_{ij} = \frac{1}{Pe_c} \Delta t \int_{\Omega} \nabla \tilde{\phi}_i \cdot \nabla \phi_j \, d\Omega, \quad (3.19)$$

in which the 'Péclet number for material label transfer' is defined as  $Pe_c = \frac{U}{L\lambda_{c0}}$ . Usually, a value for  $\lambda_{c0}$  such that  $Pe_c = 10$  suffices to make the air enclosures disappear.

### 3.1.4 Residual stresses

The largest computational effort required to compute the residual stresses concerns solving the elastic Finger tensor  $\bar{\mathbf{B}}_e$  from equation (2.58) on every time step and for all relaxation modes. Once  $\bar{\mathbf{B}}_e$  is known, the calculation of the flow-induced stresses is rather straightforward: solving equation (2.53) is actually a matter of solving equation (2.58) for each mode  $j$  and substituting the results in equation (2.54). The material derivative in equation (2.58) is split into a local time derivative and a convective part, yielding:

$$\begin{aligned} \frac{\partial \bar{\mathbf{B}}_{ej}}{\partial t} = & -(\mathbf{u} \cdot \nabla) \bar{\mathbf{B}}_{ej} + \mathbf{L}^d \cdot \bar{\mathbf{B}}_{ej} + \bar{\mathbf{B}}_{ej} \cdot \mathbf{L}^{dc} + \\ & - \frac{1}{2\theta_j} \left( \bar{\mathbf{B}}_{ej} \cdot \bar{\mathbf{B}}_{ej} - \mathbf{I} - \frac{1}{3} \left( \text{tr}(\bar{\mathbf{B}}_{ej}^{-1}) - \text{tr}(\bar{\mathbf{B}}_{ej}^{-1}) \right) \bar{\mathbf{B}}_{ej} \right). \end{aligned} \quad (3.20)$$

As the number of degrees of freedom will be very large, particularly for three-dimensional stress computations, we choose to solve equation (3.20) explicitly. Therefore, a fourth-order Runge-Kutta Cash-Karp algorithm with adaptive step-size control (Press *et al.*, 1992) has been adopted to deal with this equation in a finite element environment. Additionally, a similar algorithm can be employed to solve the thermally and pressure-induced stresses (see equation 2.62). Hence, equation (2.63) is written in its differential form:

$$\dot{p}_s = \frac{\partial p_s}{\partial t} = \frac{\alpha}{\kappa} \dot{T} - \frac{1}{\kappa} \text{tr}(\mathbf{D}). \quad (3.21)$$

The residual stresses are calculated using a finite element mesh (actually: a mesh consisting of second-order spectral elements) that is not necessarily identical to the mesh that was used for the mould filling simulation, since the solutions from that simulation are interpolated onto the new mesh. To avoid spurious solutions for the elastic Finger tensor components near the advancing melt front — which are caused by the (artificial) high deformation rates near the moving contact line — the velocity gradient tensor  $\mathbf{L}$  is set to zero in all elements that contain air. Moreover, the stability of the Runge-Kutta Cash-Karp algorithm can be improved by discarding the convective term  $\mathbf{u} \cdot \nabla \bar{\mathbf{B}}_e$  from equation (3.20). This has only limited consequences for the stress solutions: the velocity vector  $\mathbf{u}$  and the Finger tensor gradient  $\nabla \bar{\mathbf{B}}_e$  are directed almost perpendicular to each other in fully developed, (quasi-)stationary flow, which is generally present in the major part of the mould. Hence, the contribution of  $\mathbf{u} \cdot \nabla \bar{\mathbf{B}}_e$  may be neglected.

## 3.2 Implementation

The model, as it has been described in the previous sections, has been implemented in a program called *VIp3D*, which uses subroutines from the libraries of the SEPRAN finite element package. The structure of this program is similar to that of its predecessor *VIp* that employed the  $2\frac{1}{2}$ -D-approach (Sitters, 1988; Zoetelief, 1995; Caspers, 1995). An outline of this structure is given below:

### Structure of the *VIp3D* program

- Start the program.
- Read the input file and construct the mesh.
- Scale all variables with their characteristic values.
- Build the finite element systems for:
  - the flow problem;
  - the material label convection problem;
  - the injection time label convection problem (*optional*);
  - the temperature problem (*optional*).
- Apply the boundary conditions.
- Initialise the velocity, pressure, material and injection time label, and temperature fields.
- **Start the time loop:**
  - Determine the process stage.
  - Write the results from the latest time step to output.
  - Update the boundary conditions at the mould walls for the flow problem as a function of the material labels.

- **Start the iteration loop:**
    - \* Compute the viscosity and density using the latest velocity, pressure, temperature, and material label fields.
    - \* Solve the (quasi-stationary Stokes) flow problem.
    - \* Compute the viscous dissipation, thermal capacity, and thermal conductivity using the latest velocity, pressure, temperature, and material label fields.
    - \* Solve the temperature problem.
    - \* If the velocity, pressure and temperature fields have not converged sufficiently, do another iteration step.
  - Solve the convection problem(s) using the newly obtained velocity field.
  - Reset the material label field *outside* the interface regions to either 1 or 0.
  - If not at the end of the process, do another time step.
- Write the final results to output.
  - Stop the program.

The optional injection time label convection is similar to the material label convection: each particle entering the mould is labelled with its time of injection. These labels are convected through the mould analogously to the material labels; they will be used in Chapter 4 to visualise the fountain flow effect.

### 3.3 Experimental methods

To validate the computational model for gas-assisted injection moulding, a number of gas injection experiments were set up. As argued in Section 1.4, the residual thickness consists of a solidified layer (governed by thermal effects) and a melt layer (governed by viscous behaviour). Although the solid layer contribution is of major importance in practical GAIM conditions, it is not of interest in our validation experiments: Poslinski *et al.* (1995) argued that the solidification at the mould walls prior to gas injection merely adds up a constant to the residual wall thickness. Hence, we will isolate the viscous contribution by performing two types of experiments: isothermal experiments, in which the temperature effects are disregarded; and non-isothermal experiments, in which the thermal conditions are used to affect the viscosity behaviour.

Consequently, we decided not to use a real moulding machine for our experiments (since it is not suitable for isothermal experiments). Instead, we built two experimental set-ups for our validation experiments: one for gas injection experiments in a axisymmetric cylinder (in the tradition of Cox (1962) and Poslinski *et al.* (1995)), and another one for gas injection in a plaque with a rib.

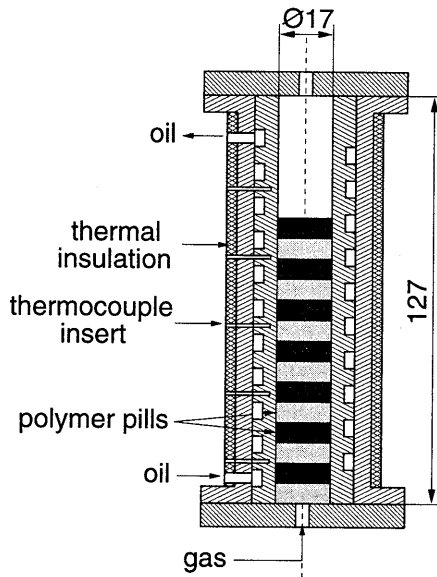


**Figure 3.3:** Experimental set-up for GAIM experiments in an axisymmetric cylinder.

### 3.3.1 Cylinder set-up

The experimental set-up for gas injection experiments consists of two hollow coaxial cylinders separated by a spiral groove (Figure 3.3). The actual cavity is a cylinder of 127 mm long and 17 mm in diameter, closed by a bottom lid through which gas can be injected and a top lid containing an air vent. Initially, the cavity is filled with 4 mm thick tablets of polystyrene to a height that is sufficient to prevent gas breakthrough (usually 70–80% of the cylinder height). Then the cylinder is heated by pumping hot oil through the spiral groove. We can cool the cylinder by switching to cold oil. By stacking alternately black and yellow polystyrene tablets into the cylinder, the flow patterns can be visualised.

Five small holes were drilled into the cylinder mantle at equidistant (15 mm) intervals to facilitate temperature measurements. Type J thermocouples were inserted into these holes to monitor the temperature at approximately 3 mm from the inner mould wall. In spite of the cylinder being insulated with glass fibre matting, temperature differences of 5°C at an average cylinder temperature of 180°C were measured along the cylinder length, with the lower temperatures towards both ends.

In each experiment, the cylinder is heated long enough for the polystyrene to obtain a ‘homogeneous’ temperature. Nitrogen gas can be injected through a pressure valve either before cooling (isothermal gas injection) or after we have allowed for a stagnant polymer layer to develop (non-isothermal gas injection). The gas pressure is in the order of a few

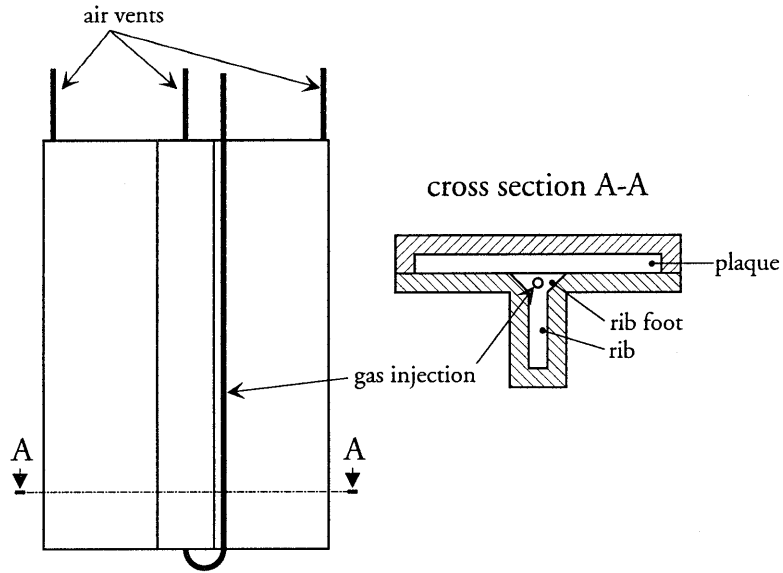


**Figure 3.4:** Experimental set-up for GAIM experiments in a plaque with a rib.

bar, and gas injection may take from a few seconds to a few minutes to fill the entire cylinder. One might object that the pressures used in these experiments are much lower than the gas injection pressures that are common in GAIM practice. However, it was advocated in Chapter 1 that the residual wall thickness is only a function of the viscosity behaviour and the Capillary number, and not (at least not directly) of the pressure.

After the mould has cooled sufficiently, the sample is pressed out of the cylinder and cut in half. In this way, the gas distribution and melt deformation can be visualised and the residual wall thickness can be determined.

### 3.3.2 Plaque-with-rib set-up

The plaque-with-rib set-up, which is depicted in Figure 3.4, represents a commonly used GAIM geometry, as ribs often serve as gas-leading channels. Yang and Huang (1995b), and Rennefeld (1996) review several rib geometries and their effect on the gas core size, whereas Woods *et al.* (1995) investigated the effect on product strength and stiffness. The rib geometry in our set-up has been designed in accordance with the guidelines given by Rennefeld.

The principle of the plaque-with-rib set-up is similar to the cylinder set-up: pre-moulded polystyrene inserts (in three parts: plaque, rib foot, and rib) are put inside the mould. The mould is closed and submerged into a hot oil bath, in order to melt the



polystyrene inserts. After the mould has attained a homogeneous temperature (which is measured as the oil temperature), gas can be injected. Once the process is completed, the mould is cooled in a cold oil bath (*i.e.*, at room temperature), after which the specimen can be removed from the mould. For non-isothermal experiments, the gas is injected after the mould has been submerged into the cold bath for a specified time. The specimen is cut into slices perpendicular to its length direction, and the residual wall thicknesses are measured.

Although our set-up enables isothermal gas injection experiments, it does lack one particular feature of a real injection moulding machine: the polymer melt inside the mould cannot be pressurised before the actual gas injection. It appeared that, as a result of this, the gas did not always penetrate into the molten polystyrene, but often found its way towards the mould walls, along which it escaped to the air vents. In particular, when the mould was submerged into the cold oil bath (for non-isothermal experiments), the polymer shrinkage definitely provided such a 'short circuit' from injection gate to air vents. As a consequence, non-isothermal gas injection experiments turned out to be impossible with this set-up, and the gas penetration was hard to control in the isothermal experiments.

### 3.3.3 Material properties

The polystyrene used in the experiments is Styron 678E from DOW Chemical. The shear viscosity of this polystyrene is described by a 7-constant Cross model (Zoetelief, 1995):

$$\eta(p, T, \mathbf{D}) = \frac{\eta_0}{1 + (\eta_0 |II_{2\mathbf{D}}| / \tau^*)^{1-n}}, \quad (3.22a)$$

in which  $II_{2\mathbf{D}}$  is the second invariant of (twice) the rate-of-deformation tensor, and  $\eta_0$  is the zero shear rate viscosity given by:

$$\eta_0(T) = \eta_0(T^*) e^{\frac{-c_1(T-T^*)}{c_2+T-T^*}} \quad (3.22b)$$

$$T^* = T_0 + s \cdot p \quad (3.22c)$$

$$c_2^* = c_2 + s \cdot p. \quad (3.22d)$$

The  $p\nu T$ -behaviour of the polystyrene can be described by a so-called double-domain

Tait equation (Chiang *et al.*, 1991):

$$v(p, T) = \begin{cases} (a_{0s} + a_{1s}(T - T_{g0})) \left(1 - 0.0894 \ln \left(1 + \frac{p}{B_s}\right)\right) & \text{if } T \leq T_g \\ (a_{0m} + a_{1m}(T - T_{g0})) \left(1 - 0.0894 \ln \left(1 + \frac{p}{B_m}\right)\right) & \text{if } T > T_g \end{cases} \quad (3.23a)$$

$$T_g = T_{g0} + s \cdot p \quad (3.23b)$$

$$B_s = B_{0s} e^{-B_{1s}(T-273)} \quad (3.23c)$$

$$B_m = B_{0m} e^{-B_{1m}(T-273)} \quad (3.23d)$$

The thermal conductivity and thermal capacity are assumed constant for each phase. For the nitrogen gas that is injected, we assume the relevant properties to be constant within the window of processing conditions; these properties are given in Table 3.1.

The parameters for the Cross model and the Tait equation, as well as the thermal properties, are given in Table 3.2; the shear viscosity and the  $pvT$ -behaviour of Styron 678E are presented in Figures 3.5 and 3.6, respectively. Figure 3.5 clearly shows that increasing the pressure from 0 to 50 MPa has a similar effect on the viscosity as decreasing the temperature from 473 K to 423 K. Finally, the parameters for the compressible Leonov model are given in Table 3.3. The associated time-temperature shift function  $a_T$  is defined as:

$$a_T = \begin{cases} e^{\frac{-c_1(T-T_0)}{c_2+T-T_0}} & \text{if } T_g < T < T_g + 100 \text{ K} \\ e^{-c_3(T-T_0)} & \text{if } T < T_g \end{cases} \quad (3.24)$$

**Table 3.1:** Material parameters for nitrogen gas (at  $T = 273$  K and  $p = 0$  MPa; from Dubbel (1995)).

$v$	$\text{m}^3\text{kg}^{-1}$	0.8
$\lambda$	$\text{Wm}^{-1}\text{K}^{-1}$	25
$c_p$	$\text{Jkg}^{-1}\text{K}^{-1}$	$1.04 \cdot 10^3$

**Table 3.2:** Material parameters for polystyrene Styron 678E from DOW Chemical (after Zoetelief (1995)).

(a) Viscosity parameters.			(b) Specific volume parameters.			
$n$		0.2520			melt	glass
$\tau^*$	Pa	$3.080 \cdot 10^4$	$a_0$	$\text{m}^3\text{kg}^{-1}$	$9.72 \cdot 10^{-4}$	$9.72 \cdot 10^{-4}$
$\eta_0(T^*)$	Pas	$4.76 \cdot 10^{10}$	$a_1$	$\text{m}^3\text{kg}^{-1}\text{K}^{-1}$	$5.44 \cdot 10^{-7}$	$2.24 \cdot 10^{-7}$
$T_0$	K	373	$B_0$	Pa	$2.53 \cdot 10^8$	$3.53 \cdot 10^8$
$c_1$		25.74	$B_1$	$\text{K}^{-1}$	$4.08 \cdot 10^{-3}$	$3.00 \cdot 10^{-3}$
$c_2$	K	61.06	$T_{g0}$	K	373	
$s$	$\text{KPa}^{-1}$	$5.1 \cdot 10^{-7}$	$s$	$\text{KPa}^{-1}$	$5.1 \cdot 10^{-7}$	

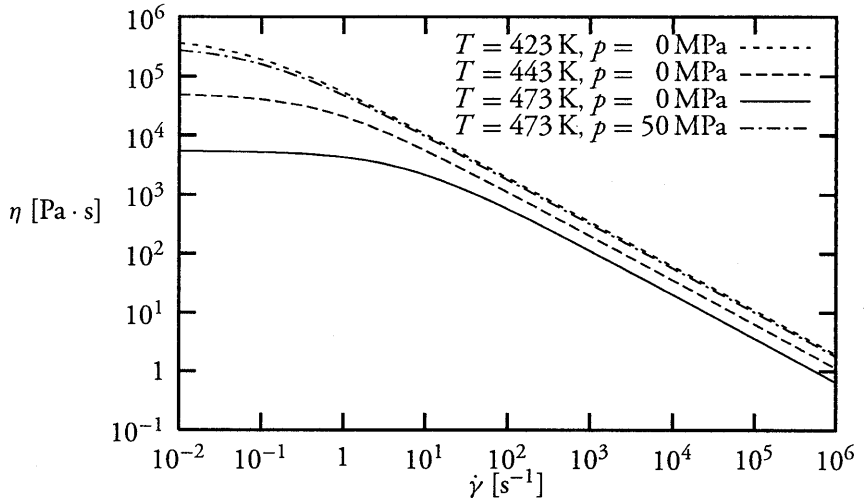
(c) Thermal properties.			
		melt	glass
$\lambda$	$\text{Wm}^{-1}\text{K}^{-1}$	0.17	0.17
$c_p$	$\text{Jkg}^{-1}\text{K}^{-1}$	2289	1785

**Table 3.3:** Viscoelastic parameters (Leonov model) for polystyrene Styron 678E from DOW Chemical (after Douven (1991)).

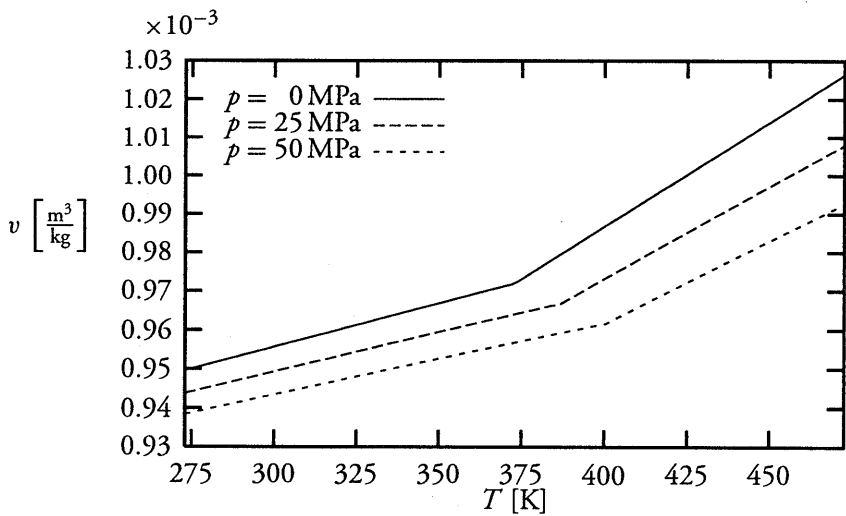
mode	melt			glass	
$j$	$\theta_{j0}$ [s]	$\eta_{j0}$ [Pas]	$\theta_{j0}$ [s]	$\eta_{j0}$ [Pas]	
1	2.250	$6.011 \cdot 10^3$	4.996	$4.564 \cdot 10^8$	
2	$1.965 \cdot 10^{-1}$	$5.639 \cdot 10^3$	$3.000 \cdot 10^{-1}$	$1.030 \cdot 10^8$	
3	$1.175 \cdot 10^{-2}$	$7.402 \cdot 10^2$	$6.660 \cdot 10^{-3}$	$1.479 \cdot 10^6$	
4	$7.872 \cdot 10^{-4}$	$6.499 \cdot 10^1$	$1.178 \cdot 10^{-4}$	$1.417 \cdot 10^4$	
5	$5.472 \cdot 10^{-5}$	8.616	$2.498 \cdot 10^{-6}$	$1.488 \cdot 10^3$	
6	$4.140 \cdot 10^{-6}$	2.335	$4.769 \cdot 10^{-8}$	3.300	
$\eta_{\infty,0} = 2.05 \text{ Pas}$					

		melt	glass
$T_0$	[K]	462	363
$c_1$	[-]	10.45	
$c_2$	[K]	150.36	
$c_3$	$[\text{K}^{-1}]$		0.6242



**Figure 3.5:** Shear viscosity  $\eta$  of polystyrene Styron 678E from DOW Chemical as a function of shear rate  $\dot{\gamma}$ , temperature  $T$ , and pressure  $p$  according to equation (3.22a) and Table 3.2.



**Figure 3.6:** Specific volume  $v$  of polystyrene Styron 678E from DOW Chemical as a function of temperature  $T$ , and pressure  $p$  according to equation (3.23) and Table 3.2.

## Chapter 4

# Results

In the previous two chapters, it is described how a three-dimensional model for the gas-assisted injection moulding process has been developed and implemented into a finite element code. In this chapter, we will determine whether this model is able to simulate this process, and how well it predicts the resulting product properties. Therefore, the model is applied to a number of moulding situations with increasing complexity.

The testing and validation of the code has been split into three parts. First, three benchmark problems will be presented that focus on typical phenomena occurring in general (conventional) mould filling processes. Accordingly, the simulations will be extended to typical gas-assisted injection moulding situations. Finally, the code will be experimentally validated, by comparing the results of a number of simulations with experimental gas injection results. Eventually, a computation of the residual stresses will be presented and discussed to show the potential of the model with respect to the prediction of product properties.

### 4.1 Simulation of general mould filling phenomena

To demonstrate that the pseudo-concentration method, as it has been described in Chapters 2 and 3, is suitable to simulate moulding processes, we will present three simulation results:

1. The filling of an axisymmetric cylinder with a liquid.
2. The filling of a T-shaped mould, with particular attention to the flow front advancement in the (two-dimensional) bifurcation.
3. The filling of a three-dimensional rectangular cavity.

**Table 4.1:** Process parameters for the mould filling simulations.

mould type	axisymmetric cylinder	T-shaped bifurcation	3-D box
viscosity ratio	$10^3$	$10^3$	$10^3$
filling time [s]	1.0	1.0	1.0
# elements	$40 \times 10$	1710	$20 \times 7 \times 7$
# degrees of freedom*	3 402	14 102	31 595
time step [s]	$1 \cdot 10^{-2}$	$5 \cdot 10^{-3}$	$1 \cdot 10^{-2}$

\* This is the number of degrees of freedom for the flow problem, which dominates the computing time.

At this point, thermal effects are irrelevant to the performance test of the method itself, since the temperature is just a parameter that alters the viscosity behaviour. Therefore, we limit ourselves to isothermal flows of Newtonian liquids in this section. Furthermore, a constant parabolic velocity profile at the entrance is prescribed in all three simulations. Table 4.1 presents the process parameters for the mould filling simulations that will be discussed below.

#### 4.1.1 Filling of an axisymmetric cylinder

As an initial test for the model, we simulated the injection of a highly viscous fluid into an axisymmetric cylinder, with geometry and parameters given in Figure 4.1(a) and Table 4.1. A parabolic velocity profile is prescribed at the flow entrance, causing the cylinder to be filled in 1.0 s. An air vent has been defined opposite to the entrance. A mesh of  $40 \times 10$  quadrilateral, axisymmetric elements (along the length and radius, respectively) was used.

To visualise the flow, we introduce time labels: particles entering the mould are given their injection times as labels (see Section 2.4). These are convected through the mould analogously to the material labels. The air that is initially present in the mould is given a negative injection time label.

The injection time label distribution after 70% filling, as depicted in Figure 4.1(b), clearly shows the fountain flow effect: polymer material has approached the flow front from the centre and has been diverted towards the wall. This results in the typical 'V'-shaped injection time label field near the mould wall that also has been encountered in experiments (Schmidt, 1974; Beris, 1987; Coyle *et al.*, 1987). It can be seen from the pressure contours in Figure 4.1(c), that the fictitious fluid does not contribute significantly to the pressure drop. The polymer mass loss due to inaccuracies of the pseudo-concentration method was less than 2%.

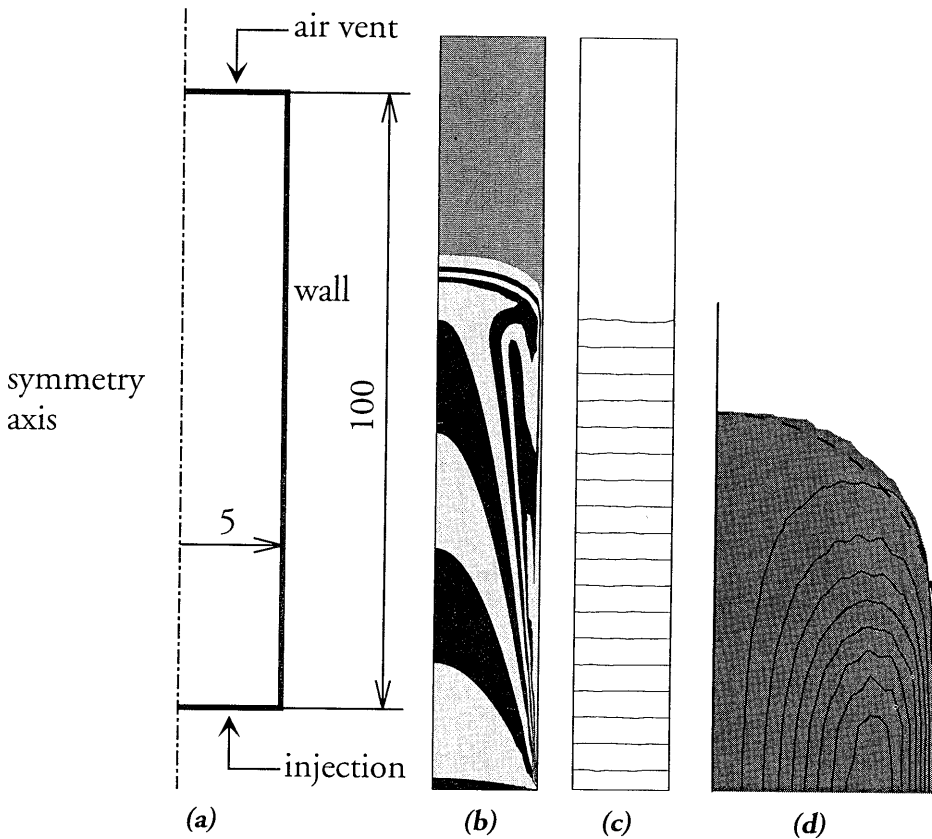
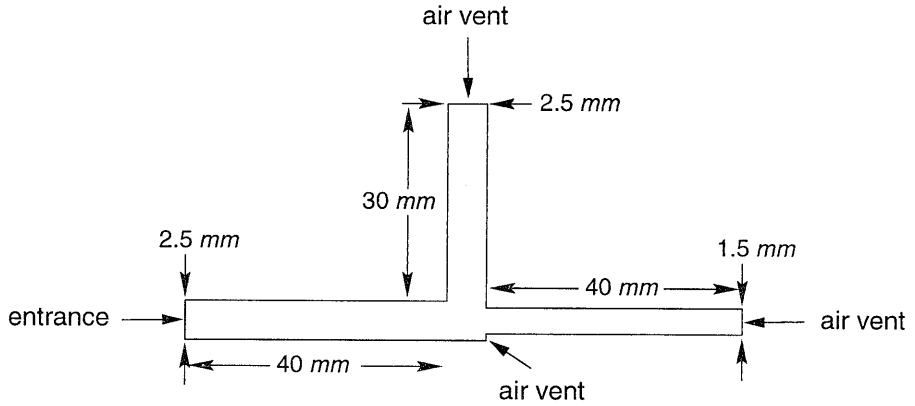


**Figure 4.1:** Simulation of the filling of an axisymmetric cylinder (results shown for 70% filling). **(a):** Geometry. **(b):** Time label distribution (black and light grey = polymer, dark grey = air). **(c):** Pressure contour lines at equal pressure intervals. **(d):** Detail of the flow front area: material labels (grey = polymer, white = air), and streamlines relative to the flow front velocity. The dashed line corresponds to a semi-spherical flow front. (Note that scaling of the width-to-length ratio of the cylinder has distorted the semi-spherical shape of the flow front in Figure **(b)**.)

A detail of the flow front and the streamlines relative to the moving flow front are shown in Figure 4.1(d). These streamlines clearly exhibit the 'fountain flow'. Hoffman (1975) found that the flow front of an advancing Newtonian liquid in a cylinder is semi-spherical, which is represented in Figure 4.1(d) by a dashed arc. The computed interface appears to approximate this semi-spherical shape fairly well.



(a) Geometry.

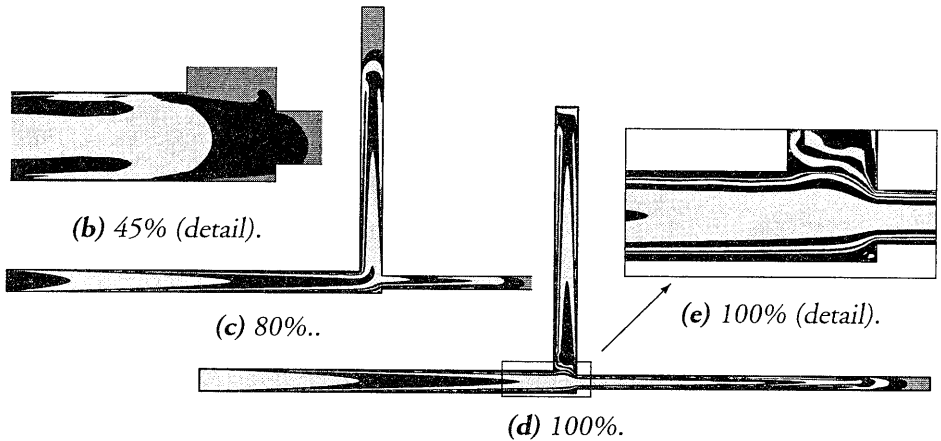


**Figure 4.2:** Simulation of flow in a two-dimensional bifurcation. (b)–(e): Time label distributions at several filling percentages (black and white = polymer, grey = air).

#### 4.1.2 Flow in a bifurcation

Flow bifurcations are common in mould filling processes, especially in polymer injection moulding. Therefore, we have tested whether our model is able to deal with the bifurcation that is present in the T-shaped two-dimensional mould shown in Figure 4.2(a), which is taken from Zoetelief *et al.* (1997). Of the two downstream branches, the top branch has a lower flow resistance than the right branch, since it is both wider and shorter. An extra air vent at the bifurcation is necessary to prevent air entrapment. The process and material parameters are similar to the previous case (see Table 4.1).



Figures 4.2(b) to 4.2(e) show the time label fields at three different filling stages. In Figure 4.2(b) the flow front has just started to split between the two downstream branches. Due to the lower flow resistance, the flow front in the top branch runs ahead, as shown in Figure 4.2(c). After the top branch has been filled, all material will flow into the right branch (Figure 4.2(d)). It can even be seen in Figure 4.2(e) that material originally present in the entrance of the top branch is eventually dragged into the right branch. Due to a mass loss of 2.8%, the mould is not entirely filled at  $t = 1.0$  s.

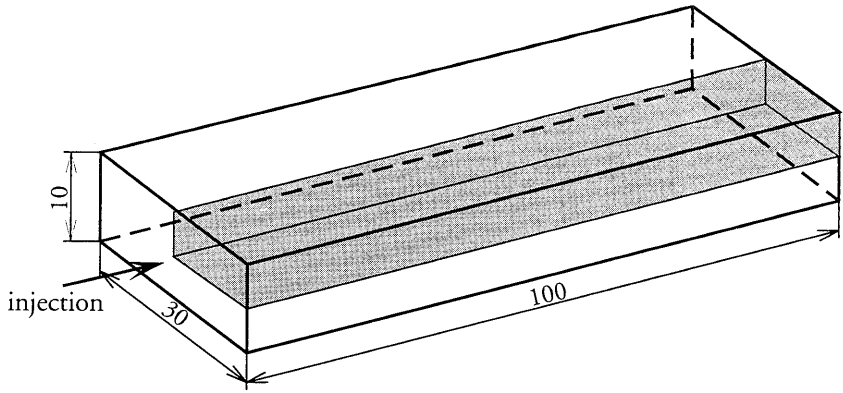
### 4.1.3 Filling of a three-dimensional rectangular cavity

Since the modelling described in Chapters 2 and 3 did not contain any restriction to two-dimensional flows only, the method should be directly applicable to three-dimensional mould filling simulations. Figure 4.3(a) shows a three-dimensional rectangular cavity, of which only one quarter is meshed given the two-fold symmetry (see Figure 4.3(b)). Due to the increase in computing time and memory usage, this mesh is somewhat coarser than in the two-dimensional situations presented above. To (partly) compensate for this coarseness, the mesh is refined towards to mould walls, where both the velocity gradients and the injection time label gradients are large. With process and material parameters similar to the previous cases (see Table 4.1), the simulation for this mesh of  $20 \times 7 \times 7$  elements took nearly 6 hours of CPU-time on a Silicon Graphics Power Challenge R10000.

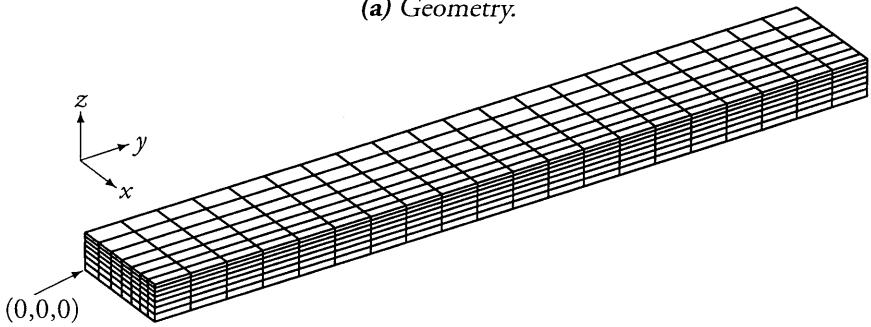
Figure 4.3(c) shows the three-dimensional fountain flow effect in both planes of symmetry. The relatively coarse mesh in  $x$ - and  $z$ -direction together with the large time label gradients near the mould walls give rise to minor oscillations in the injection time label field, as can be seen in cross-sectional plots made at  $y = 0.3L$  and  $y = 0.7L$  (Figure 4.3(d)). Such oscillations do not occur in the material label distribution, because all material labels are continuously updated by setting them to either zero or one outside the interface regions. The mass loss of polymer is 3.5%, which is nearly twice as much as in the axisymmetric cylinder case.

### 4.1.4 Discussion

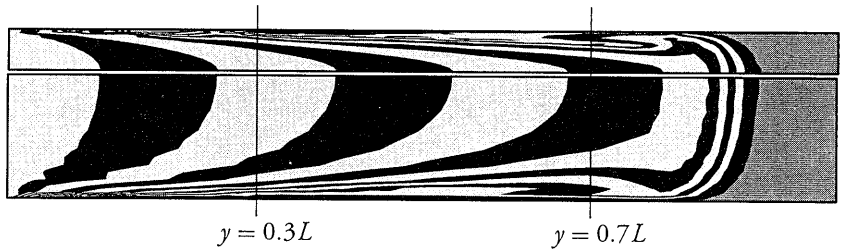
The three simulations presented in this section have clearly demonstrated the model's ability, at least in a qualitative sense, to simulate mould filling processes governed by viscous effects. In particular, the approximation of the moving contact line problem by a rather coarse transition from a no-slip to a free slip boundary condition (*i.e.*, coarse compared to the actual length scale of the physical phenomena involved) appears to be successful: not only do the semi-spherical shape of the flow front and the fountain flow effect emerge from these simulations, but also bifurcations can be dealt with without any modifications of the model. The mass loss for the simulations presented in this section was in the order of a few percent; it is believed that this figure can be further decreased



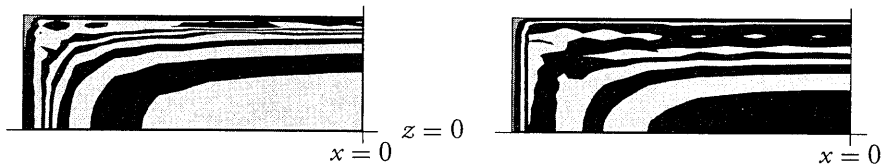
(a) Geometry.



(b) Mesh (corresponding to grey quarter of geometry shown above).



(c) Cross sections at planes of symmetry  $x = 0$  (above) and  $z = 0$  (below).



(d) Cross sections at  $y = 0.3L$  (left) and  $y = 0.7L$  (right).

**Figure 4.3:** Filling simulation for a three-dimensional rectangular cavity (results shown for 90% filling). (c) and (d): Injection time labels (black and light grey = polymer, dark grey = air).

by using smaller time steps. Finally, the model is directly applicable to three-dimensional flows, although these do require considerably more computing time.

## 4.2 Simulation of gas-assisted injection moulding phenomena

With the pseudo-concentration method, the transition from the simulation of (conventional) mould filling processes to the simulation of gas-assisted injection moulding is straightforward: it is just a matter of adjusting the inflow boundary condition for the material label convection (equation 2.27c) at the appropriate time, so that gas instead of polymer is injected into the mould. Consequently, a second (polymer/gas) interface will develop. As a matter of fact, if one had reversed 'polymer' and 'air' (by reversing the material labels) in the mould filling simulation presented in Section 4.1.1, a simulation of gas penetration in a liquid-filled tube would have resulted, which has been demonstrated elsewhere (see Haagh and van de Vosse, 1997).

In order to investigate whether the model captures the characteristics of the gas penetration in the GAIM process, four simulations that represent typical GAIM situations will be dealt with:

1. an axisymmetric cylinder;
2. a mould containing a sharp corner (two-dimensional flow);
3. a two-dimensional bifurcation;
4. a three-dimensional rectangular cavity.

A convergence test for the code, based on the problem of gas injection into a partially filled axisymmetric cylinder, was carried out separately to yield the minimum number of elements and time steps that are required to obtain a converged solution; this is described in Appendix B. The meshes and time steps that have been used in the simulations presented in this section are in accordance with the conclusions of the convergence test. Once again, these simulations involve isothermal flow of Newtonian liquids, unless stated otherwise. Furthermore, the injection of polymer is immediately followed by gas injection, without any delay time. The process parameters for the different simulations are given in Table 4.2.

### 4.2.1 GAIM of an axisymmetric cylinder

As an initial test for the model, we simulated the GAIM process of an axisymmetric cylinder, for which results are available in the literature (Taylor, 1961; Poslinski *et al.*,

**Table 4.2:** Process parameters for the gas-assisted injection moulding simulations.

mould type	axisymmetric cylinder	sharp corner	ring bifurcation	3-D box
viscosity ratio	$10^3$	$10^3$	*	$10^3$
filling time [s]	1.0	2.1	1.4	1.0
gas injection time [s]	0.625	1.0	1.4	0.4
time step size [s]				
polymer injection	$2.5 \cdot 10^{-3}$	$5 \cdot 10^{-3}$	†	$1 \cdot 10^{-2}$
gas injection	$1.25 \cdot 10^{-3}$	$1.25 \cdot 10^{-3}$	$5 \cdot 10^{-3}$	$1 \cdot 10^{-2}$
# elements	$40 \times 10$	1221	1424	$24 \times 10 \times 8$
# degrees of freedom‡	3 402	10 138	16 028	60 159

\* The polymer viscosity is given by power-law model (equation 4.1), whereas the gas viscosity has a constant value of  $1 \cdot 10^{-1}$  [Pa.s].

† Initially filled entirely with polymer.

‡ This is the number of degrees of freedom for the flow problem, which dominates the CPU time and memory usage.

1995). The test geometry and the parameters are presented in Figure 4.1(a) and Table 4.2. A parabolic velocity profile is prescribed at the flow entrance; the polymer is injected over the entire radius, whereas the gas is injected over 40% of the radius at the same flow rate. An air vent has been defined opposite to the entrance.

Figures 4.4(a) to 4.4(e) show the injection time labels at five stages of the process, similar to Figure 4.1(b). After a sufficient amount of polymer has been injected, gas penetrates into the polymer, leaving a polymer layer at the mould wall. The material label distribution at the end of the gas injection stage is shown in Figure 4.4(f). The relative polymer skin thickness resulting from this simulation is 36% of the tube radius, which agrees well with the results of Taylor (1961) and Poslinski *et al.* (1995). The fact that gas seems to be present over the entire entrance is due to the fact that the material label boundary condition (equation 2.27c) has been defined over the entire entrance boundary; it does not affect the residual wall thickness. Apparently, it takes approximately one tube radius for the penetrating gas bubble to establish the final polymer skin layer thickness. A detailed view of the gas front region (Figure 4.5) shows that the computed streamlines (which have been depicted relative to the gas front velocity) agree well with the streamline pattern suggested by Taylor (1961) (see Figure 1.4) and visualised by Cox (1964).

This simulation also shows that the gas front moves faster than the polymer front, which is simply the consequence of mass conservation. This is related to another typical GAIM phenomenon: if the gas is injected too early, the gas will break through the

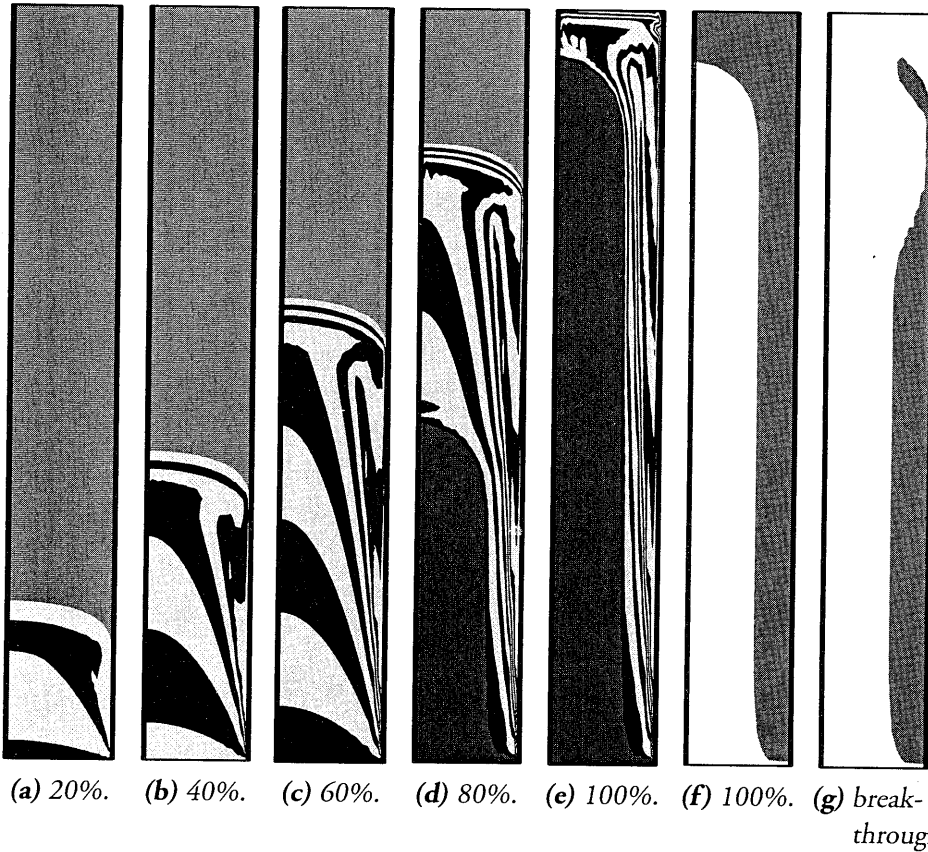


**Figure 4.4:** Simulation results for an axisymmetric cylinder at several filling percentages; (a)–(e): injection time labels (medium grey = air, black and light grey = polymer, dark grey = gas); (f)–(g): material labels (grey = polymer, white = gas). In (g) gas breakthrough was enforced by injecting gas already after 0.45 s. (Note that these plots are extended in radial direction by a factor 3, and that only one half of the cylinder cross section is shown.)

polymer front. Figure 4.4(g) shows that our model is capable of predicting breakthrough.

The requirement for polymer mass conservation (which, in this case, is equivalent to polymer volume conservation because of assumed incompressibility) can also be used to determine the accuracy of the convection algorithm. At the switch-over from polymer to gas injection, the theoretical polymer volume fraction should be 0.625 of the entire mould volume, and this fraction should obviously remain constant during gas injection. In our simulation, the relative error in this polymer volume fraction is merely 0.15% at

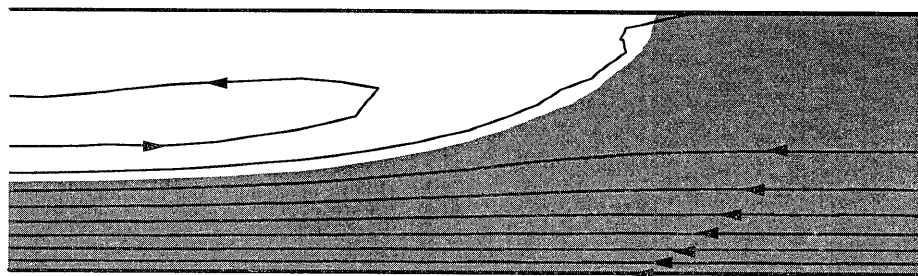


**Figure 4.5:** Gas injection into an axisymmetric tube: detail of the gas front area, with streamlines relative to the gas front velocity. (Compare with Figure 1.4.)

the end of the polymer injection stage. During the gas injection stage, no relative errors larger than 0.6% occurred. Although pseudo-concentration methods have been reported to cause mass losses in the order of 10% (Thompson, 1986; Chang *et al.*, 1996), the use of an SUPG method, together with an algorithm to set the material labels to either zero or one in all elements not containing an interface, apparently suffices to keep the mass loss fairly low.

#### 4.2.2 Gas flow around a sharp corner

From common GAIM experience, it has become clear that sharp corners in gas leading channels are to be avoided: the polymer skin usually becomes very thin at the inner corner, and the gas may even break through the skin. This is inherent to the nature of the gas flow, which advances in the direction of least flow resistance. Figure 4.6(a) and Table 4.2 give the geometry and the parameters for a two-dimensional simulation of gas flow around a sharp corner. Note that an extra air vent at the corner had to be defined in order to avoid air entrapment.

The results of this simulation are shown in Figure 4.6. The initially symmetrical flow patterns behind the polymer flow front are disturbed by the sharp corner, but the semi-spherical front shape is restored (see Figure 4.6(c)). The gas clearly takes a 'short-cut' around the corner, after which it returns to the centre of the channel (see Figure 4.6(f)). This demonstrates that the cross-sectional gas distribution eventually becomes insensitive to the gas injection location. The fact that the mould is not entirely filled after 2.1 s is due to a slight mass loss of 0.9%.

#### 4.2.3 Bifurcation of the gas flow

As explained in Section 1.2.1, a bifurcation of the gas flow will lead to an asymmetric gas core, even if the mould is symmetric. A clear demonstration of this effect can be seen on

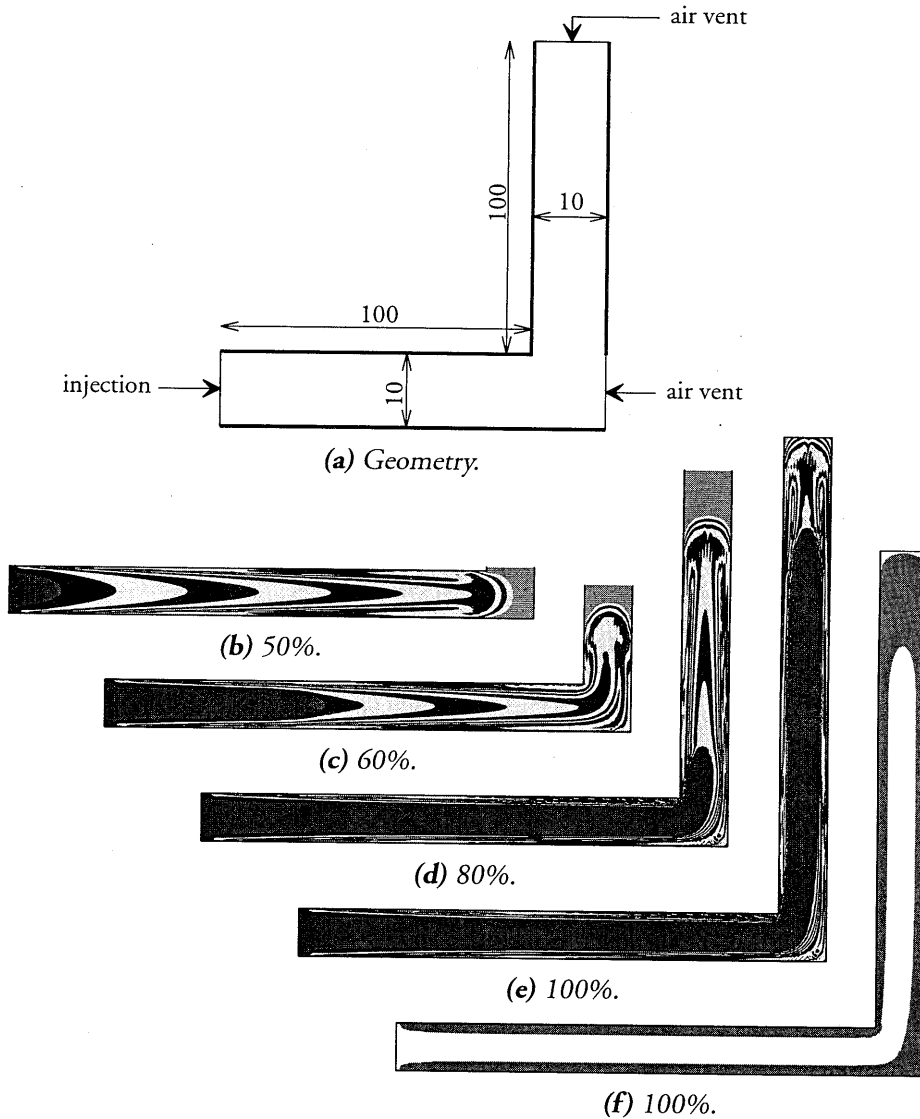


**Figure 4.6:** Simulation results for 2-D gas flow around a sharp corner; (c)–(f): injection time labels (medium grey = air, black and light grey = polymer, dark grey = gas); (g): material labels (grey = polymer, white = gas).

the IKV videotape on gas-assisted injection moulding (Findeisen *et al.*, 1991). To test whether our model is able to deal with this phenomenon, the experiment from the IKV

videotape is taken as the starting point for a simulation on a geometrically symmetric bifurcation (Figure 4.7(a)). Previously, Zuidema (1996) induced a slight initial disturbance in this bifurcation through a very small geometrical asymmetry (see also Haagh *et al.* (1997)). Here, only the mesh is made slightly asymmetric by defining 20 elements in flow direction along the left branch, and 23 elements along the right one, as shown in Figure 4.7(b). At the start of the simulation, the mould is completely filled with polymer, and only the gas injection stage is simulated. The polymer is represented by a power-law fluid (instead of a Newtonian fluid) to enhance its sensitivity to pressure variations; its viscosity is given by:

$$\eta = 1000 \dot{\gamma}^{0.5} [\text{Pa s}]. \quad (4.1)$$

Both polymer and gas are allowed to leave the mould at the exit.

Figure 4.7 shows that, after an initially symmetric gas penetration, the mesh asymmetry is sufficient to cause one of the gas fronts to run ahead (which happens to be the gas front in the right branch). As explained in Section 1.2.1, such a disturbance — once it has been initiated — will grow continuously. In a qualitative sense, these results compare well to the observations recorded on the IKV videotape.

#### 4.2.4 GAIM of a three-dimensional rectangular cavity

Since GAIM is governed by three-dimensional phenomena, our ultimate aim is to perform simulations on three-dimensional moulds. Once again, the three-dimensional rectangular cavity presented in Figure 4.3(a) will be used. However, this time the geometry is meshed as shown in Figure 4.8(a). The finite element mesh for this simulation (shown in Figure 4.8(a)) does not contain mesh refinement towards the mould walls (contrary to the mesh for the 'conventional' three-dimensional moulding simulation, as depicted in Figure 4.3(b)), since we are now interested in predicting the gas/polymer interface, of which the location is formally not known *a priori*. The parameters for this simulation are given in Table 4.2.

Although the geometry is not exactly the same, we can compare our results in Figure 4.8 to a certain extent with the experimental results of Kolb and Cerro (1991), who injected air into a square capillary filled with (Newtonian) silicone oil. They found that the residual wall thicknesses at the centres of the tube walls (compare with planes  $x = 0$  and  $z = 0$  in Figure 4.8(b)) were smaller than for the circular (axisymmetric) tube; our simulation for the rectangular tube yields a similar result, as is shown in Table 4.3.

#### 4.2.5 Discussion

The simulations of isothermal test cases described above have demonstrated that the developed model captures the important aspects of gas-assisted injection moulding: the



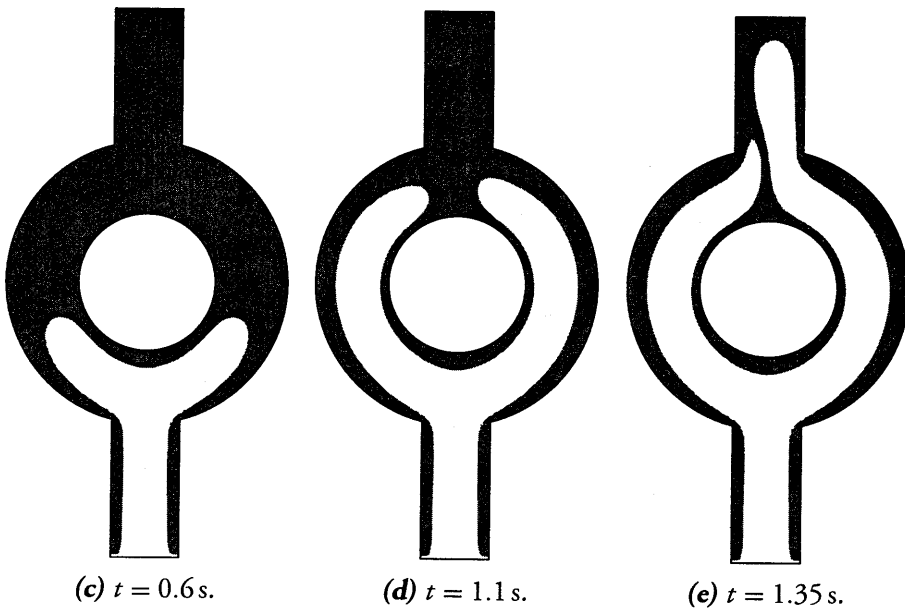
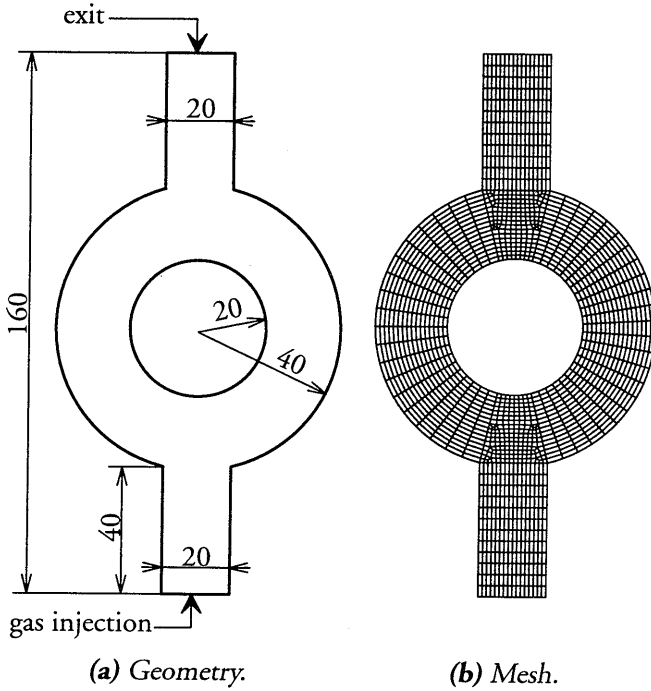


**Figure 4.7:** Ring-shaped bifurcation: the left ring branch contains 20 elements in flow direction, whereas the right branch has 23. (c)–(e): Development of the gas core in a flow bifurcation; material labels (grey = polymer, white = gas).

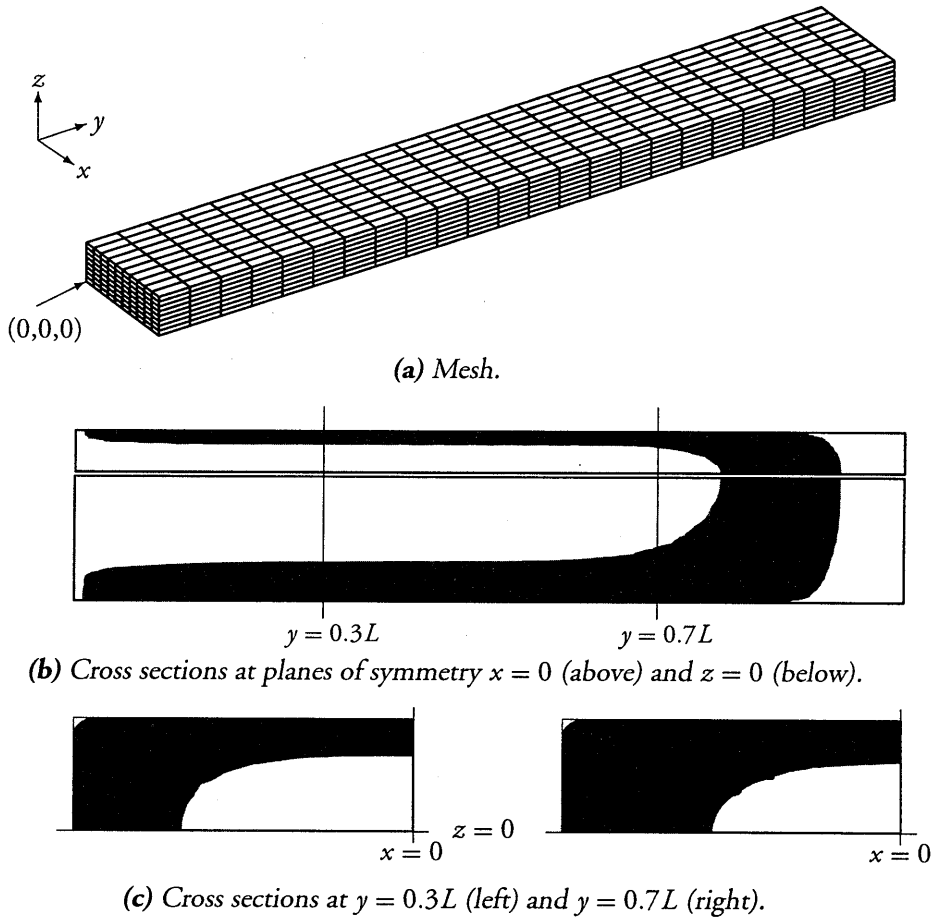


**Figure 4.8:** Gas-assisted injection moulding simulation for a three-dimensional rectangular cavity (results shown for 90% filling). (b) and (c): Material labels (grey = polymer, white = air). Note that a small amount of the initially present air remains in the mould corners (upper left corners in Figure (c)).

residual wall thickness for the case of gas penetration into a Newtonian fluid is predicted accurately, and typical GAIM phenomena such as gas breakthrough, a decreased skin thickness at the inner side of a sharp corner, and asymmetric gas penetration in a symmetric bifurcation have been predicted, at least qualitatively. Furthermore, a three-dimensional simulation has shown the model's ability to deal with three-dimensional geometries, which is a prerequisite for successful gas-assisted injection moulding simulations.

**Table 4.3:** Comparison of residual liquid fractions for circular, square, and rectangular tube;  $\varepsilon$  = residual liquid layer thickness as a fraction of the tube radius (or half the cavity thickness, respectively), and  $\phi$  = residual liquid layer cross-sectional area as a fraction of the tube or cavity cross-sectional area. (Data for square tube from experiments for  $Ca=10$  by Kolb and Cerro (1991).)

	$\varepsilon_{x=0}$	$\varepsilon_{z=0}$	$\phi$
circular tube	0.36		0.59
square cavity	0.32		0.64
rectangular cavity	0.32	0.33	0.61

### 4.3 Experimental validation

Having shown that our model for gas-assisted injection moulding simulations is able to predict the process characteristics in a qualitative sense, we will have to validate it by comparing simulation results with experimental data. Therefore, gas injection experiments have been carried out with the cylinder and the plaque-with-rib set-ups that were introduced in Section 3.3. As explained, the cylinder set-up allowed for both isothermal and non-isothermal experiments. Moreover, the maximum shear rate in the isothermal experiments could be varied through the process conditions. Thus, we could force the polystyrene to act either as a Newtonian or a shear-thinning liquid. For the plaque-with-rib mould, only isothermal gas injection experiments were carried out.

For a comparison of experimental and numerical results, we will focus on the residual wall thickness as the most important quantity. Furthermore, the stacking of alternately black and yellow polymer in the cylinder mould (see Figure 3.3) enables us to visualise the polymer flow patterns through experimental particle tracking, which can be compared directly to the numerical particle tracking results.

The incompressibility assumption underlying the results presented so far is abandoned in the remainder of this chapter.

#### 4.3.1 Axisymmetric cylinder

With the axisymmetric cylinder set-up, three different experiments have been carried out under the conditions that are given in Table 4.4. When gas is injected at a pressure of 1.0 bar into the cylinder filled with polystyrene that has a uniform temperature of 171°C, the shear rate is low enough for the polymer viscosity to be on the Newtonian plateau (which can be derived from the material parameters given in Section 3.3.3). Hence, if shrinkage were to be neglected, a residual wall thickness of approximately 36% would be expected. The shrinkage of the polymer will cause this fraction to be somewhat

**Table 4.4:** Experimental conditions for the gas injection experiments in an axisymmetric cylinder.

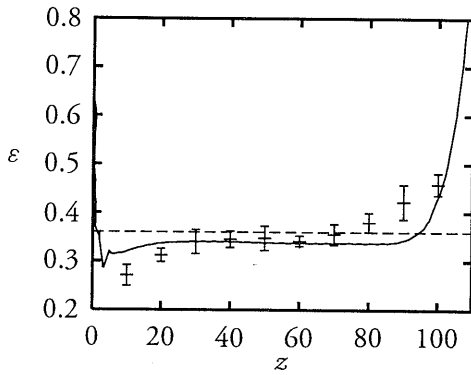
case	temperature [°C]	pressure [10 <sup>5</sup> Pa]	initial filling	$t_{delay}$ [s]
isothermal, Newtonian	171	1.0	67%	–
isothermal, shear-thinning	179	5.8	67%	–
non-isothermal	170	5.8	81%	75

smaller. Isothermal shear-thinning conditions are obtained when the gas is injected at 5.8 bar into polystyrene of 179°C. According to Poslinski *et al.* (1995), shear-thinning will cause the residual wall thickness to decrease (see Figure 1.5). In the non-isothermal experiment, the polymer is cooled down for 75 seconds from an initial homogeneous temperature of 170°C before the gas is injected. At that time, the wall temperature has decreased to approximately 150°C, which causes a ten-fold increase in the (zero shear-rate) viscosity near the mould wall compared to the viscosity in the centre (see Figure 3.5). Consequently, the residual wall thickness is expected to be larger than in the isothermal cases. The temperatures given in Table 4.4 are average values over the cylinder length, since both the temperatures at the top and bottom of the cylinder were about 5°C lower than at the central part. Simulations showed that these temperature differences did not have a significant effect on the results.

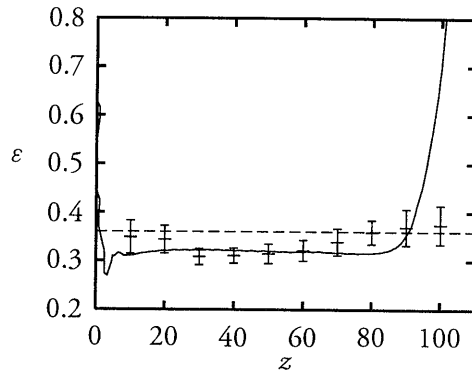
Five experiments were carried out for each case of experimental conditions. The specimens were cut in half, after which the residual wall thickness was measured with a micrometer at 10 mm intervals along the cylinder length at both sides of the gas core. Whenever necessary, these measurements were corrected for errors caused by cutting asymmetrically.

The simulation results for the residual wall thickness fraction  $\varepsilon$  and the filling time are compared with the experimental results in Figures 4.9 and 4.10, and in Table 4.5. Apart from some minor entrance effects, the agreement for the residual wall thicknesses in the isothermal cases is good. Also the filling time is predicted well. The slight deviation of the results for the Newtonian case from the value of  $\varepsilon = 0.36$  can be accounted for by the shrinkage of the polystyrene. Shear-thinning does indeed cause a slight decrease in the residual wall thickness, which is in accordance with the conclusions of Poslinski *et al.* (1995). The filling time for this case is much shorter due to the higher pressure, and some discrepancy between the experimental and the computed value is found.

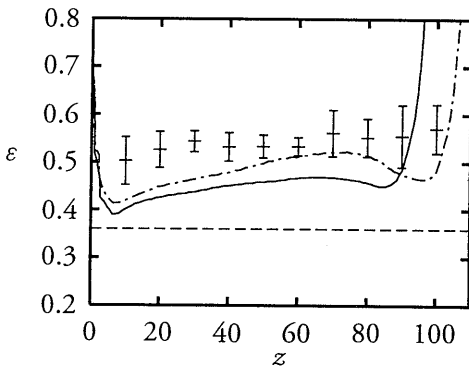
The difference between experiment and simulation is somewhat larger for the non-isothermal case, although the general trend is predicted well (see the solid line in Figure 4.9(c)). If this discrepancy between measured and computed residual wall thickness were due to a lag between the measured and the actual mould wall temperatures, then



(a) Isothermal, Newtonian.



(b) Isothermal, shear-thinning.



(c) Non-isothermal.

**Figure 4.9:** Comparison of experimental and numerical results for gas injection into an axisymmetric cylinder: relative residual wall thickness  $\varepsilon$  along the axial distance  $z$  from the gas injection point (error bars = experimental results; solid line = numerical result; dashed line: Newtonian 36% limit). The dash-dot line in (c) has been obtained by assuming a  $5^\circ\text{C}$  lower wall temperature.

Figure 4.9(c) would suggest that the actual wall temperature should be lower. Simulation shows that a  $5^\circ\text{C}$  decrease in wall temperature does indeed yield a larger residual wall thickness, although it covers only half the original gap between numerical and experimental values. Prescribing an actual wall temperature that is about  $10^\circ\text{C}$  lower than the measured temperature might yield coinciding experimental and numerical results, but such a large temperature difference is very unlikely to occur in the actual experiment. Moreover, the  $5^\circ\text{C}$  decrease in wall temperature doubles the calculated filling

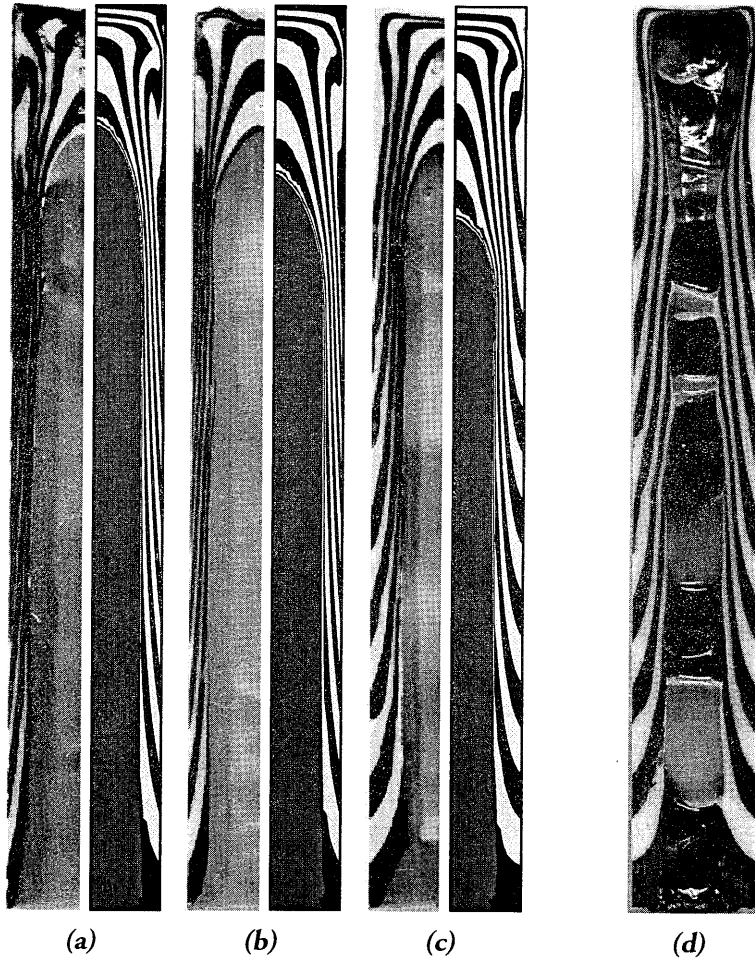


**Figure 4.10:** Comparison of experimental (left) and numerical (right) flow patterns for gas injection into an axisymmetric cylinder; (a): isothermal Newtonian case, (b): isothermal shear-thinning case, (c): non-isothermal case, (d): a specimen exhibiting severe 'local breakthrough' of polymer pills (non-isothermal case).

time, which was already twice as long as the experimental filling time.

Closer examination of the specimens from the non-isothermal experiments revealed that the experimental gas contours sometimes were highly irregular, with polymer indentations protruding into the gas core; this causes the experimental error in the non-isothermal case to be larger than in the isothermal cases (compare the error bars in Fig-

**Table 4.5:** Experimental and numerical results for gas injection in the cylinder mould. The residual wall thickness is averaged over the domain  $30 \text{ mm} \leq z \leq 70 \text{ mm}$ , where  $z$  is the axial distance from the gas injection point.

case	residual wall thickness [%]		filling time [s]	
	experiment	simulation	experiment	simulation
isoth., Newtonian	$34.6 \pm 0.8$	33.8	$92 \pm 15$	98
isoth., shear-thinning	$31.8 \pm 0.9$	32.0	$3.2 \pm 0.5$	4.7
non-isothermal	$54.0 \pm 1.2$	45.8	$13.1 \pm 5.1$	29

ure 4.9(c) to those in Figures 4.9(a) and 4.9(b)). To explain this, we recall that the cylinder had been initially filled with a stack of polystyrene pills. Stacking these pills is believed to give rise to contaminations and small air gaps at the interfaces between these pills. It seems that under high shear deformation such as shown in Figure 4.10(c), the material (partly) loses its coherence at the interface between two pills. The gas then supposedly breaks through the polymer pill that covers the gas front. Consequently, the number of polymer layers downstream of the gas front decreases, which can be seen in the left half of Figure 4.10(c): of the original 16 coloured layers, only ten are found between the gas core and the top of the specimen. The remaining six layers are visible as alternating light and dark shades of grey ‘behind’ the gas core. This ‘local breakthrough’ effect is accompanied by local increases in wall thickness at the transitions between pills, which is shown for an extreme case in Figure 4.10(d). In this respect, we suggest that the experimental values in Figure 4.9(c) be regarded as an ‘upper bound’ for the residual wall thickness. Apparently, the breakthrough of polymer layers decreases the flow resistance, and hence decreases the experimental filling time, which is less than half the computed filling time. Local breakthrough of polymer layers has also been found in the isothermal experiments, but to a much lesser extent, and usually for  $z > 90 \text{ mm}$ , so that the influence on the residual wall thickness is very small.

### 4.3.2 Plaque-with-rib

In the plaque-with-rib experiment, nitrogen gas was injected at a pressure of 3.0 bar into polystyrene having a homogeneous temperature of  $180^\circ\text{C}$ . This gas pressure was maintained during the cooling of the mould. Eventually, four specimens were obtained from the isothermal experiments. These specimens were cut into ten slices along the length direction, after which the residual wall thicknesses at the centre of the rib bottom and the rib flanks (indicated by Figure 4.11) were measured with a micrometer. The set-up did not allow the filling times to be measured accurately; roughly, they were of the order of 30 seconds.

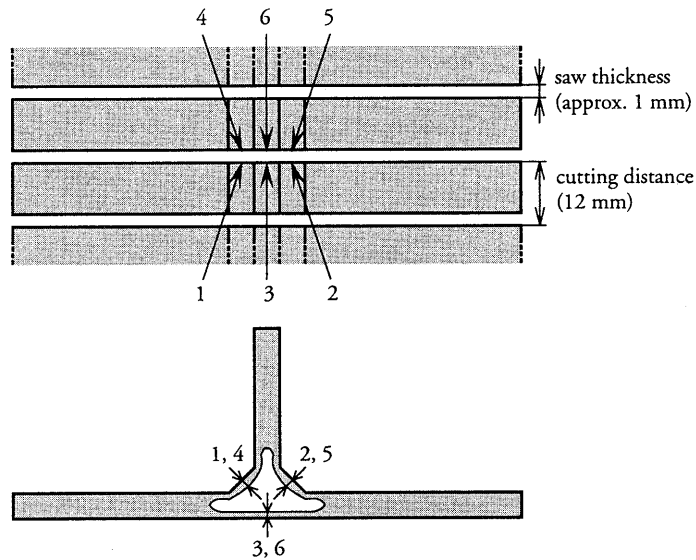


**Figure 4.11:** Locations of residual wall thickness measurements for the plaque-with-rib specimens: top view (top) and cross-sectional view (bottom). Note that for every cross section, two rib bottom thicknesses (positions 3 and 6) and four rib flank thicknesses (positions 1, 2, 4, and 5) are measured.

The mould geometry and computational mesh for the simulation of this experiment are depicted in Figure 4.12. This mesh is rather coarse as compared to the meshes used in the previous sections. Yet, it consists of 896 brick elements, which yield nearly 30 000 degrees of freedom for the Stokes equations. It took approximately  $2\frac{1}{2}$  days of CPU-time to simulate the experiment on a Silicon Graphics workstation with an R10000 processor.

The numerically and experimentally obtained gas core contours for this experiment, as shown in Figures 4.13 and 4.14, appear to match well. The numerical results also demonstrate that the contribution of the polymer shrinkage (also called ‘secondary gas penetration’) to the final gas core size proves to be significant: this is indicated by the area between the solid lines and the grey (polymer) area in Figure 4.13. In Figure 4.15 and Table 4.6, the residual wall thicknesses have been related to the hydraulic radius of the triangle that makes up the rib. The wiggles in the simulation results indicate that the mesh may have been too coarse to give accurate results. Still, there is a good quantitative agreement between numerical and experimental results. The slight under-prediction of the rib bottom wall thickness may be attributed to the mesh, which is coarser near the rib bottom than near the rib flank (see Figure 4.12).



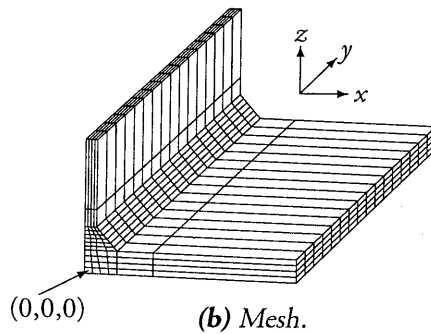
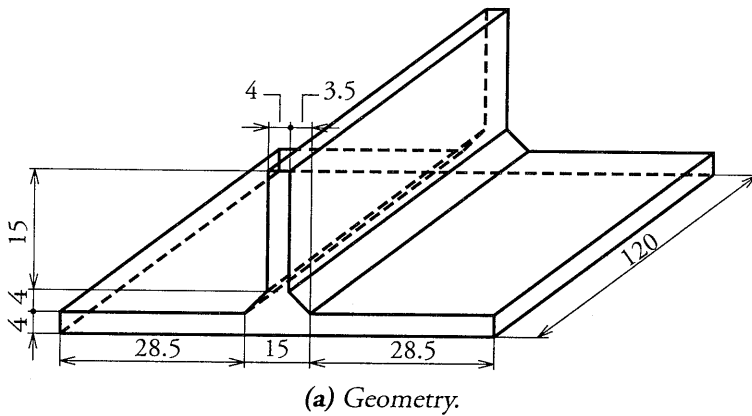


**Figure 4.12:** Plaque-with-rib geometry (dimensions in mm). For reasons of symmetry, only one half has to be meshed.

**Table 4.6:** Experimental and numerical residual wall thickness for gas injection into the plaque-with-rib mould. The values are averaged over the domain  $12 \text{ mm} \leq y \leq 84 \text{ mm}$ , where  $y$  is the axial distance from the gas injection point.

position	residual wall thickness [%]	
	experiment	simulation
rib bottom	$26.7 \pm 0.7$	21.0
rib flank	$24.3 \pm 0.6$	23.7

### 4.3.3 Discussion

Both isothermal and non-isothermal gas injection experiments in a cylinder mould were carried out to validate our model for gas-assisted injection moulding. The simulations

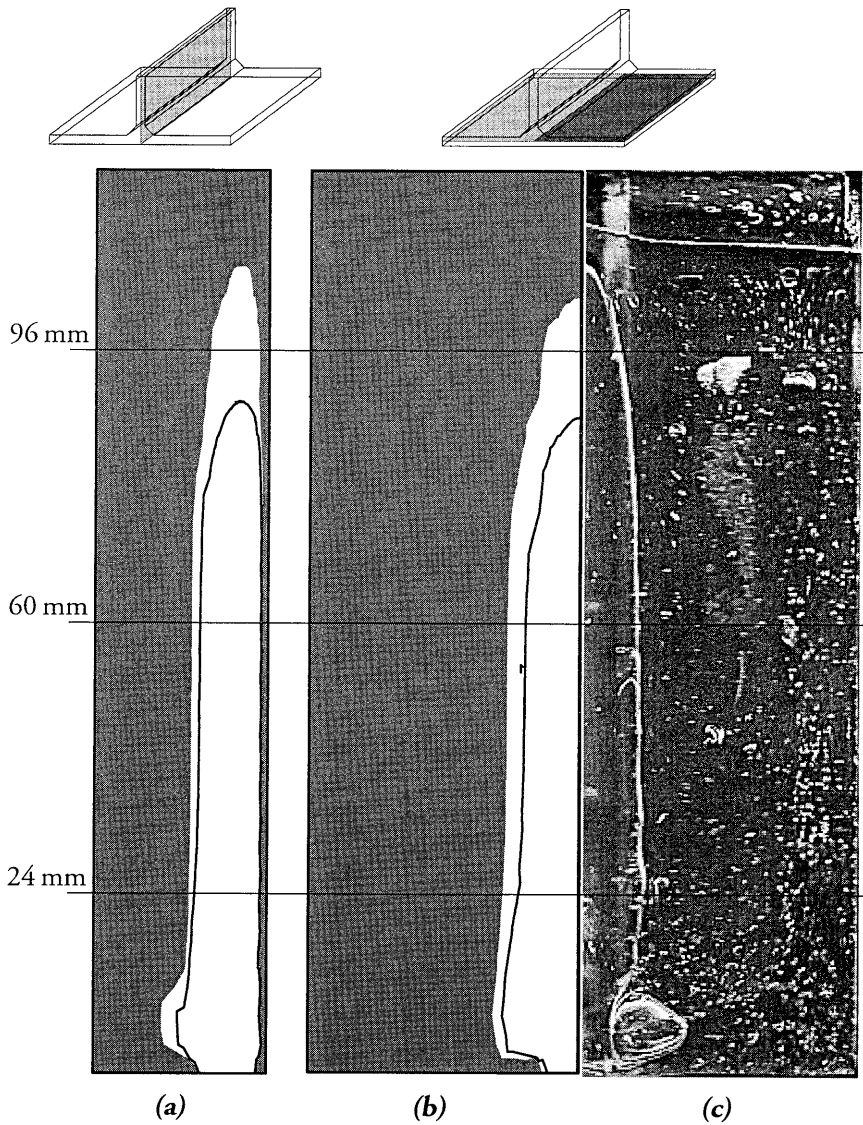


**Figure 4.13:** Isothermal gas injection simulation for the plaque-with-rib. **(a):** Simulation result for cross section  $x = 0$  mm. **(b):** Simulation result for cross section  $z = 2$  mm. **(c):** Photograph of the bottom ( $z = 0$  mm) of a transparent specimen (the nearly horizontal line just above the gas bubble contour is a crack). The lines in **(a)** and **(b)** depict the gas bubble contours at the end of the filling stage, i.e., before any shrinkage has occurred.

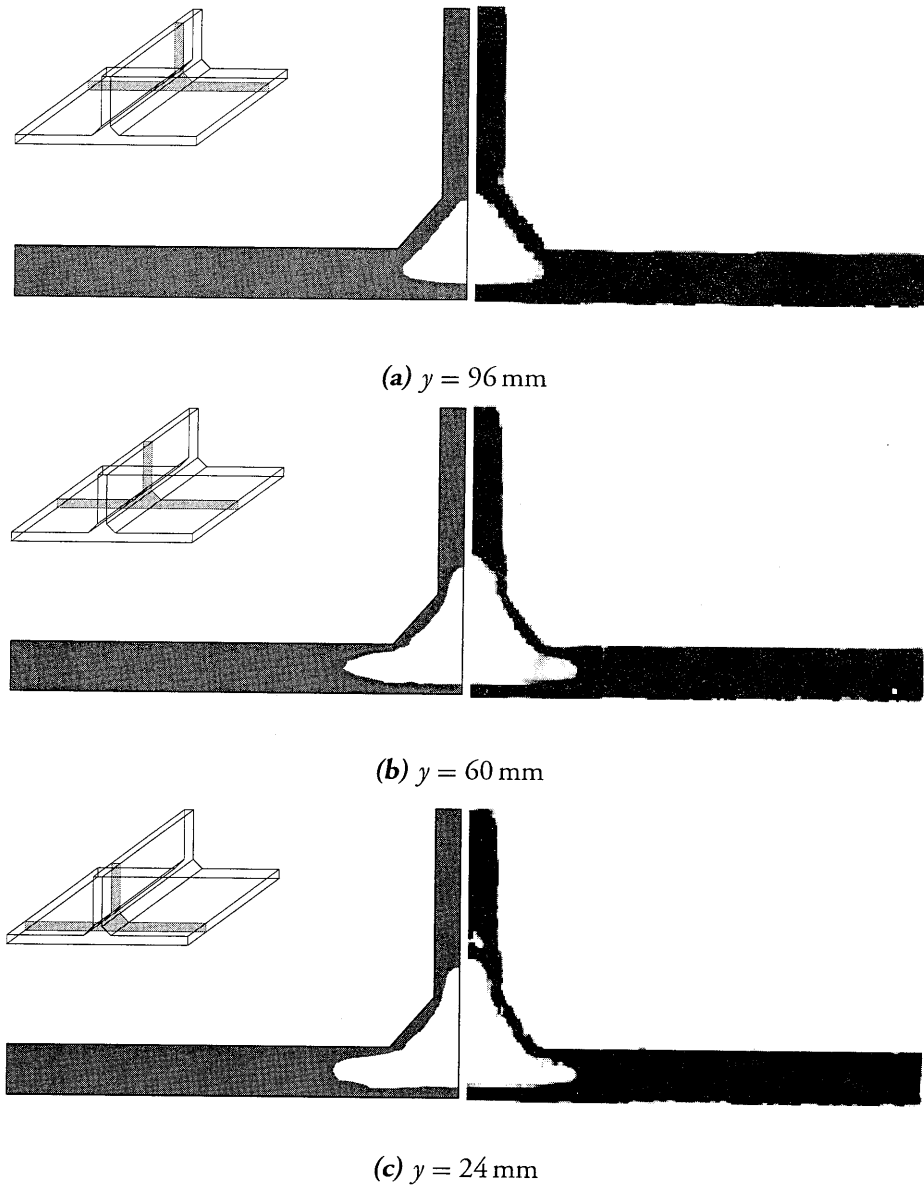


**Figure 4.14:** Isothermal gas injection for the plaque-with-rib: comparison of simulation (left) and experimental (right) results at different cross sections perpendicular to the  $y$ -direction (corresponding to the horizontal lines in Figure 4.13).

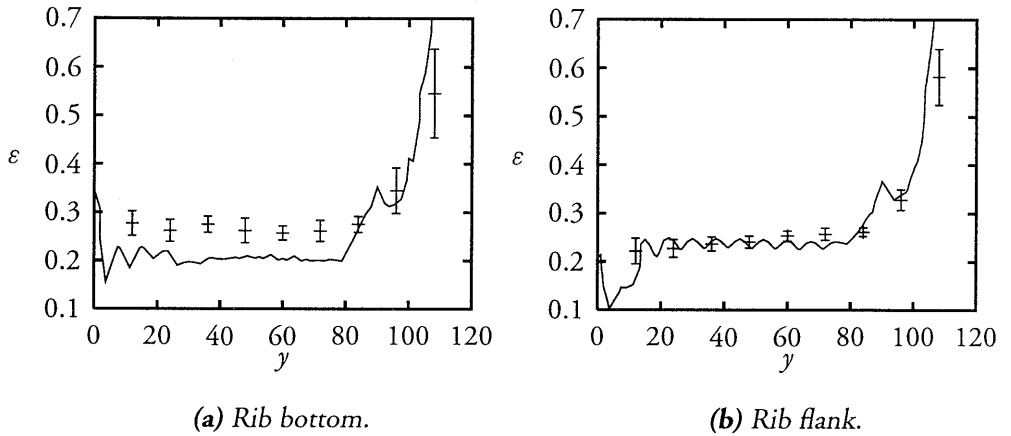


**Figure 4.15:** Comparison of experimental and numerical results for gas injection into a plaque with a triangular: residual wall thickness  $\varepsilon$  as a fraction of the hydraulic radius of the rib triangle ( $= 4.08$  mm) along the axial distance  $y$  from the gas injection point (error bars = experimental results; solid line = numerical result).

of the isothermal cases yielded results that agreed well with the experimental results. In particular, the effect of shear-thinning viscosity behaviour on the residual wall thickness was predicted correctly. For the non-isothermal experiment a qualitative agreement was found: mould cooling was seen to increase the residual wall thickness. The quantitative discrepancy between the numerical and experimental results for this case can, to a large extent, be attributed to experimental inaccuracies.

The simulation of an isothermal gas injection experiment in a plaque-with-rib mould demonstrated the model's ability to deal with three-dimensional geometries. Moreover, polymer shrinkage was found to have a significant effect on the final size of the gas core. Unfortunately, experimental difficulties related to the unstable nature of gas penetration prohibited reproducible non-isothermal experiments to be executed with the plaque-with-rib set-up. To facilitate such experiments, a real injection moulding machine with a gas injection unit is required. We would like to remark, however, that our conclusions regarding the modelling of GAIM are *not* affected by the absence of a fully three-dimensional, non-isothermal gas injection experiment: it has been pointed out earlier that the model does not treat two-dimensional (axisymmetric) gas-assisted injection moulding fundamentally different from its three-dimensional counterpart. Moreover, axisymmetric flow is only considered two-dimensional from a modelling perspective; the 'axisymmetric' cylinder validation experiments are as three-dimensional as any other GAIM experiment would be.

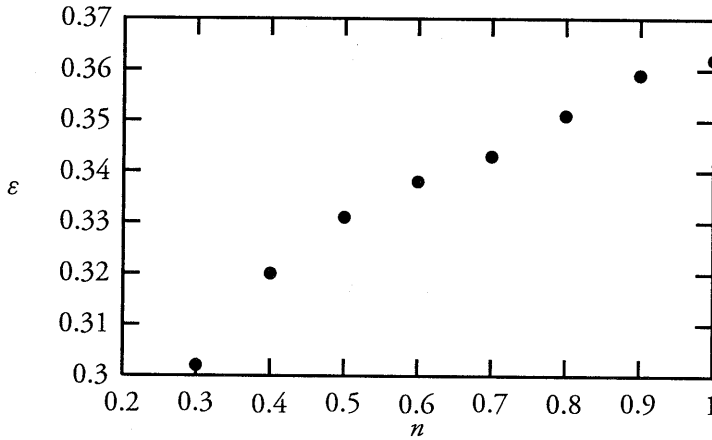


**Figure 4.16:** The effect of the power-law exponent  $n$  on the residual wall thickness  $\varepsilon$  for isothermal gas penetration into an axisymmetric cylinder (results from simulations).

This leads us to the three-dimensional nature of the gas penetration phenomenon. The residual wall thickness fraction is obviously the result of a force balance between the gas pressure and the (viscous) stresses in the penetrated liquid. Let us consider the penetration of an inviscid gas into an axisymmetric cylinder filled with a viscous liquid. For Newtonian liquids, the residual wall thickness fraction is approximately 0.36, irrespective of the liquid viscosity (or, equivalently, irrespective of the gas pressure). If the cylinder is filled with a power-law fluid, the residual wall thickness becomes a function of the power-law exponent, as is shown by the simulation results in Figure 4.16 and by the observations of Poslinski *et al.* (1995).

The residual wall thickness  $\varepsilon$  cannot be derived from the shear stress distribution far downstream of the gas front (which can be calculated from the Hagen-Poiseuille equation), since this distribution does *not* depend on the constitutive model for the viscosity. Consequently,  $\varepsilon$  is determined by the flow field at the gas front, which is three-dimensional, as advocated in Chapter 1 and shown in Section 4.2.1. One may try to predict this quantity from the two-dimensional Poiseuille flow characteristics of the penetrated liquid downstream of the gas front. However, such attempts are bound to lead to empirical relations (see, *e.g.*, Johannaber *et al.* (1995), Chen and Cheng (1996), and Poslinski *et al.* (1995)), which may not be generally applicable. For instance, Poslinski's relation (equation (1.8) in Section 1.3) has three material-dependent parameters. Those who persist in searching for an empirical relation should realise that the key parameter is the viscosity (or actually: the viscosity distribution), since this is the only parameter left

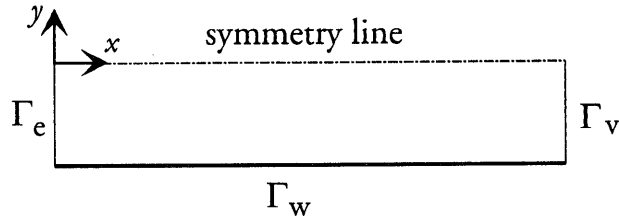


**Figure 4.17:** Two-dimensional parallel plate geometry; length = 100 mm, half height = 5 mm.

to vary in the Stokes equation that governs the gas penetration problem (equation 2.18). Nevertheless, as long as a reliable empirical relation is not available, accurate predictions of the gas distribution in GAIM products do require three-dimensional simulations.

#### 4.4 A test case for residual stress computations

The modelling and implementation of the residual stresses has not yet evolved sufficiently to show a complete residual stress computation. Nevertheless, a first indication of the potential of the algorithm described in Section 3.1.4 will be demonstrated in a two-dimensional test case, in which polystyrene melt is injected isothermally at 200°C between two parallel plates. The mould geometry, as depicted in Figure 4.17, is discretised using  $40 \times 10$  (length  $\times$  half height) elements. At the entrance a parabolic velocity profile is prescribed, such that the mould is filled in 1.0 s.

The generalised Newtonian viscosity of the polymer melt is related to the steady state behaviour of the Leonov model at simple shear through (Baaijens, 1991):

$$\hat{\eta}(\dot{\gamma}, T) = \eta_{sv} + \sum_{j=1}^m \frac{2\eta_j}{1 + X_j}, \quad X_j = \sqrt{1 + 4\dot{\gamma}^2 \theta_j^2}. \quad (4.2)$$

Hence, the viscoelastic ('flow-induced') stress computation using the Leonov model should yield a shear stress field that is approximately similar to the stress field from the moulding simulation with the generalised Newtonian model. The parameters for both models are given in Section 3.3.3. Only the first four modes of the viscoelastic model have been taken into account, as the contributions of the other two modes would relax almost instantaneously. The convective term in the Leonov model has been neglected.

In Figure 4.18 the shear stress fields are shown at 95% filling of the mould. The viscous and viscoelastic shear stress compare well indeed, yielding values of  $5.6 \cdot 10^4$  Pa and  $5.9 \cdot 10^4$  Pa, respectively, along the wall in the fully developed, steady shear flow

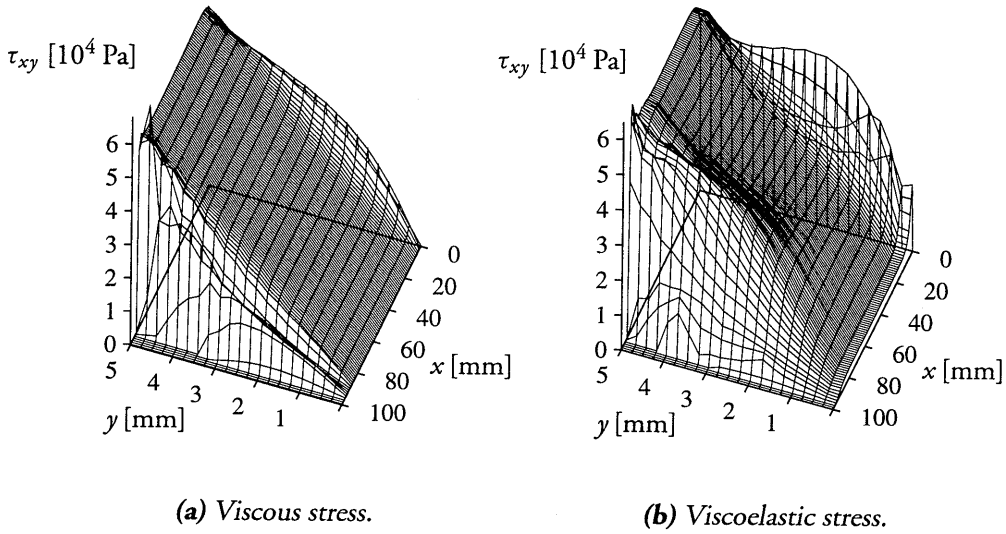


**Figure 4.18:** Viscous and viscoelastic shear stress  $\tau_{xy}$  for isothermal injection of polystyrene (Styron PS678E) at 200 °C between two parallel plates.

region. The deviations in the viscoelastic stress at the entrance ( $x = 0$  mm) and near the flow front ( $x \approx 90$  mm) can be attributed to the absence of the  $\mathbf{u} \cdot \nabla \bar{\mathbf{B}}_e$  term.





## Chapter 5

# Conclusions and Recommendations

A three-dimensional model has been developed for the simulation of gas-assisted injection moulding processes. It is based on a physical, rather than on an empirical approach, and has been implemented in a finite element package. To avoid elaborate three-dimensional remeshing, a pseudo-concentration method (or: fictitious fluid method) has been adopted, which employs a material label parameter to distinguish the polymer from the gas. Both two- and three-dimensional examples of characteristic GAIM phenomena were simulated to test whether the model is able to cover the important aspects of the process. Experiments on typical GAIM cases were carried out to validate the model. Finally, three-dimensional residual stress computations were added as a post-processing step to the moulding simulation, showing the main advantage of GAIM over conventional injection moulding.

### 5.1 Conclusions

**The three-dimensional nature of GAIM.** The first step towards gaining a better understanding of gas-assisted injection moulding, is the recognition that the process is governed by three-dimensional phenomena. This is, in the first place, due to the fact that the gas penetrates into the *thick-walled* parts of the mould, since these have a lower flow resistance than the thin-walled sections, which usually make up the larger part of an injection moulding product. Secondly, the velocity field near the advancing gas front exhibits significant velocity components in the thickness direction (*i.e.*, perpendicular to the main flow direction), even if the gas were to penetrate into thin-walled parts. Thus the important assumption underlying the Hele-Shaw approximation (*i.e.*, thin-walled geometries, resulting in negligible velocity components in thickness direction) loses its validity when one is modelling GAIM. Consequently, the  $2\frac{1}{2}$ -D approach that has been applied so successfully to many injection moulding processes, has to be abandoned.

**Modelling.** Since no appropriate analytical solution for the problem of gas penetration into a fluid in an arbitrary geometry is known, we have resorted to a full three-dimensional modelling of the GAIM process, employing a finite element method. To avoid elaborate remeshing, a pseudo-concentration method using a fixed mesh has been adopted. The essence of this method is, that a so-called material label is assigned to every particle in the computational domain to designate its material identity, which is either polymer or gas. As a consequence, the physical properties are also a function of the material label, and the equations governing the flow and the temperature have coefficients that are material-dependent.

Both the gas that is injected and the air downstream of the flow front are represented by a fictitious fluid. The main property of this fictitious fluid is that it should not contribute to the pressure build-up in the mould during filling. Therefore, its viscosity is set to a value at least  $10^3$  times smaller than the viscosity of the filling fluid. However, the viscosity of the fictitious fluid exceeds the real value for air (or nitrogen gas) by several orders to keep the Reynolds number small.

The filling of a mould is simulated in a series of time steps, for which a flow problem, a temperature problem, and a material label convection problem have to be solved to enable the fixed grid approach. On the fixed grid, the material labels are convected through the mould according to the instantaneous velocity field, in order to obey the 'conservation of identity' for each particle. A dimensional analysis has shown that the flow can be determined by solving the (quasi-stationary) Stokes equations on every time step. For the temperature, a (time-dependent) convection-diffusion equation is solved.

The fixed grid approach, however, raises a problem: how to deal with the advancement of the polymer flow front? This is in fact a moving boundary problem, which is characterised by the paradox of a fluid front that is moving along the mould wall at a finite velocity, while the fluid itself sticks to the wall. To overcome this problem, the boundary conditions at the mould walls are split into two parts: for the filling fluid region, a no-slip boundary condition has been imposed, whereas a free-slip boundary condition has been prescribed for the fictitious fluid region. Hence the wall boundary condition changes continuously during the filling stage of the process. Therefore, it has been implemented as a Robin boundary condition: depending on the local material label, it can be turned into a Dirichlet (no-slip) or a Neumann (free-slip) boundary condition. This procedure is a very rough approximation of the actual (small-scale) physics of moving contact lines: van der Zanden (1993) states that the macroscopic no-slip boundary condition breaks down only within molecular distances (*i.e.*, of the order of 1 nm) from the actual contact line, whereas in our procedure the no-slip boundary condition is abandoned at about half the element length (*i.e.*, of the order of several mm) from the contact line. Yet, our approach turns out to yield good results with respect to the flow front advancement.

**Testing and validation.** The model was first tested on three cases involving the isothermal filling of both two-dimensional and three-dimensional moulds with a Newtonian fluid (without gas injection). The results show that both the advancement of the flow front, including the moving contact points/lines, and the fountain flow effect, which is characteristic for viscous flow, emerge very clearly from the simulations. Hence the moving boundary problem appears to be approximated well.

Extending the simulations from injection moulding to gas-assisted injection moulding is merely a matter of adjusting the material label boundary condition at the inflow boundary in the appropriate manner, so that 'fictitious fluid' is injected into the polymer. Thus, gas-assisted injection moulding is not treated differently from (three-dimensional) conventional injection moulding, and no particular characteristics of GAIM — other than it being essentially three-dimensional — have been incorporated into the model *a priori*. Consequently, the gas penetration phenomenon is determined solely by the Stokes equation and its boundary conditions. Four test simulations have shown that this way of modelling successfully captures the important characteristics of GAIM: not only the residual fluid fraction for gas penetrating into a viscous (Newtonian) fluid is predicted correctly, also the qualitative effects of a sharp corner and a bifurcation on the gas flow are demonstrated by the simulations.

To validate the model, simulation results were compared with experimental results of gas injection into a cylinder and into a plaque with a rib that were both partially filled with polystyrene melt. In the cylinder mould set-up, temperature could be controlled to perform both isothermal and non-isothermal gas injection experiments. Furthermore, by varying the injection pressure in the isothermal experiments, the melt viscosity could either be kept Newtonian, or pushed into the shear-thinning regime.

For the isothermal gas injection experiments, an excellent agreement was found between the experimental and the numerical results, under both Newtonian and shear-thinning conditions. For the non-isothermal case, there was a qualitative agreement in the sense that trend in the residual wall thickness profile was predicted correctly, but the computed residual wall thickness was smaller than the actual experimental value. However, the experimentally obtained residual wall thickness suffered from a particular experimental error. The cylinder had been initially filled with a stack of polystyrene pills, which gives rise to contaminations and air gaps at the interfaces between these pills. It seems that under the high shear deformation, these pills prefer to break through instead of being sheared further. This 'local breakthrough' effect is accompanied by local increases in wall thickness at the transitions between pills, as can be observed in the specimens. Therefore, the measured residual wall thickness is larger than it should be under these non-isothermal conditions.

Due to experimental difficulties, which are related to the sensitivity to instabilities of the gas penetration, only isothermal gas injection experiments were carried out at the plaque-with-rib mould. Once again, the excellent agreement between experiments and

simulations for the plaque-with-rib mould showed, that the model is indeed capable of dealing with a typical, three-dimensional GAIM geometry.

**Residual stresses.** To extend the simulation program's possibilities with respect to the prediction of product properties, a proposal for the three-dimensional modelling of residual stresses is made. Decoupling the (viscoelastic) stress calculations from the (viscous) moulding simulation, the compressible Leonov model is used to model flow-induced stresses. The thermally and pressure-induced stresses are dominated by the pressure contribution, which has to be solved by time integration. The bottle-neck for such simulations is found in solving a (multi-mode) non-linear evolution equation for the Finger strain tensor. An explicit time integration scheme has been implemented to deal with this equation.

Unfortunately, the residual stress algorithm has not passed the testing stage yet, but further exploration of the proposed modelling is encouraged by preliminary results on flow-induced stresses.

**Final conclusion.** In conclusion, the model that has been developed for gas-assisted injection moulding, can predict the final gas distribution in a product and enhance the understanding of the process. In contradiction to other models that have been reported in the literature, this model yields the gas penetration from the actual process physics (not from a presupposed gas distribution), is able to deal with the three-dimensional character of the process, incorporates temperature effects and generalised Newtonian viscosity behaviour, and has been validated experimentally. As such, this model meets the requirements for successful simulations of industrial gas-assisted injection moulding processes.

## 5.2 Recommendations

Although the model that has been developed in this thesis, has proven to be successful in predicting such an important quantity as the residual wall thickness, there are still some challenges in converting this success to actual improvements in practical gas-assisted injection moulding processes and products. These challenges are outlined in the following recommendations:

- The validation experiments described in Sections 3.3 and 4.3 were designed to separate the influences of the parameters that govern the residual wall thickness (most notably shear rate and temperature). For this purpose those experiments served well. It is recommended to further evaluate the computational model by extending the simulations to GAIM under the 'practical' conditions of combined

high temperature gradients, high shear rates, and high pressures. Thus, the influence of the process parameters can be studied.

- One should keep in mind, though, that the *VIp3D* program that has been used to generate the results of Chapter 4, has *not* been designed to deal with complex (industrial) GAIM products. The objective of this thesis and of the *VIp3D* program is to gain understanding of the GAIM process, of the parameters that govern the process, and of the sensitivity of the final result to parameter variations, by simulating cases that represent typical GAIM conditions. Suggestions to exploit the model to simulate more complex GAIM processes are given below.
- The extension of the program to simulations involving complex GAIM products is obviously limited by CPU time and computer memory restrictions. Although these restrictions are becoming less severe due to the ongoing improvement in computer performance, optimisation of the *VIp3D* program may extend the program's possibilities as well. In this respect, the fixed grid approach, as it has been used in this thesis, is not particularly efficient: the velocity field is computed for the entire mould, although it is not of interest in the gas/air regions. To decrease the computing time, one might consider to interfere with the calculations on the element level by discarding the degrees of freedom in those elements that are either sufficiently far downstream of the polymer front, or upstream of gas flow front. Currently, three-dimensional remeshing for moving boundary problems is still considered troublesome and elaborate, but indications of progress in this area have been reported by Coupez (1995). If the problems in three-dimensional remeshing are overcome, it may provide a more efficient alternative to the fixed grid approach that has been adopted in this thesis.
- It has been shown that three-dimensional simulations are necessary for GAIM simulations, but only in the (thick-walled) parts that are subjected to gas penetration. As the larger part of a GAIM product usually still consists of thin-walled sections, a three-dimensional simulation for the complete product is unnecessary and inefficient. For such simulations, one would prefer to combine three-dimensional computations with 'traditional' moulding simulations based on the  $2\frac{1}{2}$ -D approach. A mesh for such a product can be thought to consist of 2-D elements for the thin-walled parts, and 3-D elements for the thick-walled parts. In that case, connection elements have to be developed to deal with the transitions from 2-D to 3-D elements.
- A different route to circumvent full 3-D simulations, particularly for complex GAIM products, may lie in finding an empirical relation for the residual wall thickness: the velocity, viscosity, and temperature fields downstream of the gas

front — which may well be approximated by a  $2\frac{1}{2}$ -D simulation — might contain sufficient information to give a useful estimation for the residual wall thickness. The downstream stress field apparently is not a good indicator, since fluids with different power-law exponents do yield different residual wall thicknesses, but give similar downstream stress distributions (see the analytical solutions for Poiseuille flow of power-law fluids). The three-dimensional model for GAIM simulations can be used to perform parameter studies in order to detect such an empirical relation.

- Another remark concerns the actual use of the *VIp3D* program itself. Not only the structure of this program resembles that of the *VIp* program (see Section 3.2), also the program input has been kept as consistent with the *VIp* input as possible. However, the problem definitions and boundary conditions have to be given in the SEPRAN manner (as described in the SEPRAN manual), which is a rather tedious task. This is a consequence of the boundary conditions at the mould walls that were described in Section 2.3.3.

Formally, all mould walls are impermeable to both polymer and air, except at specified air vents, where the fictitious fluid is allowed to escape. Consequently, at the mould walls the boundary conditions in tangential directions are different from the boundary condition in normal direction. However, if the air is allowed to leave the mould anywhere, the boundary conditions will be identical in all directions. This yields a major advantage from the programming point-of-view, since normal and tangential directions to the wall do not have to be determined explicitly anymore. As a result, designating the boundaries to be either injection gate or mould wall (= air vent) in the program input would suffice to take care of the appropriate boundary conditions. Simulations have shown that the effect of an over-all free outflow of air on the results is negligible.

- Finally, GAIM products have been reported to exhibit surface defects near the gas cores. It has been suggested that these defects are caused by strong, local orientation in the polymer skin. If this proves to be true, then the residual stress computations may provide useful information on such orientations. Furthermore, the computation of the product deformation (warpage) from the residual stress distributions is trivial, and can be performed by either SEPRAN or another package. Also shrinkage at the product's outer surface can be modelled in SEPRAN, by moving the mesh boundaries according to the 'shrinkage velocity' that results from the mass conservation equation.

## References

- Anders, S. and Sauer, R. (1991): Einflüsse von Werkstoff und Prozeßparametern bei der Gasinjektionstechnik. *Kunststoffe*, **81**(3), 205–207, (in German).
- Baaijens, F.P.T. (1991): Calculation of residual stresses in injection molded products. *Rheologica Acta*, **30**, 284–299.
- Barton, K.S. and Turng, L.S. (1994): General design guidelines for gas-assisted injection molding using a CAE tool. In: *ANTEC Proceedings*, pp. 421–425, Society of Plastics Engineers.
- Batchelor, G.K. (1967): *An Introduction to Fluid Mechanics*. Cambridge etc.: Cambridge University Press.
- Bensimon, D., Kadanoff, L.P., Liang, S., Shraiman, B.I., and Yang, C. (1986): Viscous flows in two dimensions. *Reviews of Modern Physics*, **58**(4), 977–999.
- Beris, A.N. (1987): Fluid elements deformation behind an advancing flow front. *Journal of Rheology*, **31**(2), 121–124.
- Bhattacharji, S. and Savic, P. (1965): Real and apparent non-Newtonian behavior in viscous pipe flow of suspensions driven by a fluid piston. *Proceedings of the 1965 Heat Transfer and Fluid Mechanics Institute*, pp. 248–262.
- Boshouwers, G. and van der Werf, J. (1988): Inject-3, a simulation code for the filling stage of the injection moulding process of thermoplastics. Ph.D. thesis, Eindhoven University of Technology.
- Brooks, A.N. and Hughes, T.J.R. (1982): Streamline Upwind/Petrov-Galerkin formulations for convection dominated flows with particular emphasis on the incompressible Navier-Stokes equations. *Computer Methods in Applied Mechanics and Engineering*, **32**(199-259).

- Caspers, L.W. (1995): *VI<sub>p</sub>*, an integral approach to the simulation of injection moulding: prediction of product properties. Ph.D. thesis, Eindhoven University of Technology.
- Castro, J.M. and Macosko, C.W. (1982): Studies of mold filling and curing in the reaction injection moulding process. *AIChE Journal*, **28**(2), 250–260.
- Chang, Y.C., Hou, T.Y., Merriman, B., and Osher, S. (1996): A level set formulation of Eulerian interface capturing methods for incompressible fluid flows. *Journal of Computational Physics*, **124**, 449–464.
- Chen, S.C. and Cheng, N.T. (1996): A simple model for evaluation of contribution factors to skin melt formation in gas-assisted injection molding. *International Communications in Heat and Mass Transfer*, **23**(2), 215–224.
- Chen, S.C., Cheng, N.T., and Hsu, K.S. (1995a): Simulation and verification of the secondary gas penetration in a gas-assisted-injection molded spiral tube. *International Communications in Heat and Mass Transfer*, **22**(3), 319–328.
- Chen, S.C., Hsu, K.F., and Hsu, K.S. (1995b): Analysis and experimental study of gas penetration in a gas-assisted injection-molded spiral tube. *Journal of Applied Polymer Science*, **58**, 793–799.
- Chen, S.C., Hsu, K.S., and Huang, J.S. (1995c): Experimental study on gas penetration characteristics in a spiral tube during gas-assisted injection molding. *Industrial and Engineering Chemistry Research*, **34**(1), 416–420.
- Chen, S.C., Cheng, N.T., and Hsu, K.S. (1996): Simulations of gas penetration in thin plates designed with a semicircular gas channel during gas-assisted injection molding. *International Journal of Mechanical Sciences*, **38**(3), 335–348.
- Chiang, H.H., Hieber, C.A., and Wang, K.K. (1991): A unified simulation of the filling and postfilling stages in injection molding. Part I: formulation. *Polymer Engineering and Science*, **31**, 116–124.
- Chuoque, R.L., van Meurs, P., and van der Poel, C. (1959): The instability of slow, immiscible, viscous liquid-liquid displacements in permeable media. *Petroleum Transactions AIME*, **216**, 188–194.
- Costa, F.S., Thompson, W., and Friedl, C. (1995): An adaptation of the boundary element method for modeling gas injection molding. In: S.-F. Shen and P. Dawson (eds.), *Simulation of Materials Processing: Theory, Methods and Applications (Numiform 95)*, pp. 1113–1118. Rotterdam: Balkema.



- Costa, F.S., Friedl, C., and Thompson, W. (1996): Gas injection molding simulation by the boundary element method. In: A.K. Easton and J.M. Steiner (eds.), *The Role of Mathematics in Modern Engineering*, pp. 179–186, 1st Biennial Engineering Mathematics Conference, 11-13 July, 1994, Melbourne, Australia. Lund, Sweden: Studentlitteratur/Chartwell-Bratt.
- Coupez, T. (1995): Automatic remeshing in three-dimensional moving mesh finite element analysis of industrial forming. In: S.-F. Shen and P. Dawson (eds.), *Simulation of Materials Processing: Theory, Methods and Applications (Numiform 95)*, pp. 407–412. Rotterdam: Balkema.
- Cox, B.G. (1962): On driving a viscous fluid out of a tube. *Journal of Fluid Mechanics*, **14**, 81–96.
- Cox, B.G. (1964): An experimental investigation of the streamlines in viscous fluid expelled from a tube. *Journal of Fluid Mechanics*, **20**, 193–200.
- Coyle, D.J., Blake, J.W., and Macosko, C.W. (1987): The kinematics of fountain flow in mold-filling. *AIChE Journal*, **33**(7), 1168–1177.
- Cuvelier, C., Segal, A., and van Steenhoven, A.A. (1986): *Finite Element Methods and Navier-Stokes Equations*. Dordrecht: Reidel.
- Douven, L.F.A. (1991): Towards the computation of properties of injection moulded products: flow- and thermally induced stresses in amorphous thermoplastics. Ph.D. thesis, Eindhoven University of Technology.
- Dubbel, (1995): *Dubbel Taschenbuch für den Maschinenbau*. Berlin etc.: Springer, 18th edition.
- Dussan V., E.B. (1979): On the spreading of liquids on solid surfaces: static and dynamic contact lines. *Annual Review of Fluid Mechanics*, **11**, 371–400.
- Eckardt, H. and Ehrhrt, J. (1989): Mit neuem Verfahren hochwertige Formteile wirtschaftlich herstellen (Airmould-Verfahren, Teil 1). *Plastverarbeiter*, **40**(1), 14–18, (in German).
- Eyerer, P., Märtins, R., and Bürkle, E. (1993): Spritzgießen mit Gasinnendruck. *Kunststoffe*, **83**(7), 505–517, (in German).
- Fairbrother, F. and Stubbs, A.E. (1935): Studies in electro-endosmosis. Part VI. The “bubble-tube” method of measurement. *Journal of the Chemical Society*, **1**, 527–529.
- Findeisen, H., Lanvers, A., Michaeli, W., Bender, K., and Kirberg, K. (1991): Gasinjektionstechnik transparent gemacht. Videotape IKV Aachen.

- Flaman, A.A.M. (1990): Build-up and relaxation of molecular orientation in injection moulding. Ph.D. thesis, Eindhoven University of Technology.
- Floryan, J.M. and Rasmussen, H. (1989): Numerical methods for viscous flows with moving boundaries. *Applied Mechanics Reviews*, **42**(12), 323–340.
- Fortin, A. (1997): personal communication, December 11.
- Fortin, A., Béliveau, A., and Demay, Y. (1995): Numerical solution of transport equations with applications to non-Newtonian fluids. In: M.D.P. Monteiro Marquez and J.F. Rodriguez (eds.), *Trends in Applications of Mathematics to Mechanics*. Longman.
- Gao, D.M., Nguyen, K.T., and Salloum, G. (1995): A numerical model for cavity filling during gas-assisted injection molding. In: S.-F. Shen and P. Dawson (eds.), *Simulation of Materials Processing: Theory, Methods and Applications (Numiform 95)*, pp. 1125–1130. Rotterdam: Balkema.
- Gao, D.M., Nguyen, K.T., Garcia Rejon, A., and Salloum, G. (1997): Numerical modelling of the mould filling stage in gas-assisted injection moulding. *International Polymer Processing*, **XII**(3), 267–277.
- de Gennes, P.G. (1985): Wetting: statics and dynamics. *Reviews of Modern Physics*, **57**(3), 827–863.
- Haagh, G.A.A.V. and van de Vosse, F.N. (1997): Simulation of three-dimensional mould filling processes using a pseudo-concentration method. *International Journal for Numerical Methods in Fluids*, (submitted).
- Haagh, G.A.A.V., Zuidema, H., van de Vosse, F.N., Peters, G.W.M., and Meijer, H.E.H. (1997): Towards a 3-D finite element method for the gas-assisted injection moulding process. *International Polymer Processing*, **XII**(3), 207–215.
- Halpern, D. and Gaver III, D.P. (1994): Boundary element analysis of the time-dependent motion of a semi-infinite bubble in a channel. *Journal of Computational Physics*, **115**, 366–375.
- Hétu, J.-F., Lauzé, Y., and Garcia-Rejon, A. (1995): Three-dimensional finite element simulation of mold filling processes. In: S.-F. Shen and P. Dawson (eds.), *Simulation of Materials Processing: Theory, Methods and Applications (Numiform 95)*, pp. 1135–1140. Rotterdam: Balkema.
- Hieber, C. and Shen, S. (1980): A finite-element/finite-difference simulation of the injection-molding filling process. *Journal of Non-Newtonian Fluid Mechanics*, **7**, 1–32.

- Hirt, C.W. and Nichols, B.D. (1981): Volume of Fluid (VOF) method for the dynamics of free boundaries. *Journal of Computational Physics*, **39**, 201–225.
- Hoffman, R.L. (1975): A study of the advancing interface. I. Interface shape in liquid-gas systems. *Journal of Colloid and Interface Science*, **50**(2), 228–241.
- Huh, C. and Scriven, L.E. (1971): Hydrodynamic model of steady movement of a solid/liquid/fluid contact line. *Journal of Colloid and Interface Science*, **35**(1), 85–101.
- Huzyak, P.C. and Koelling, K.W. (1997): The penetration of a long bubble through a viscoelastic fluid in a tube. *Journal of Non-Newtonian Fluid Mechanics*, **71**, 73–88.
- IKV, (1994): 17. IKV Kolloquium Aachen. Technical report, IKV Aachen, Block 3 & 7.
- Janeschitz-Kriegl, H. (1979): Injection moulding of plastics II. Analytical solution of heat transfer problem. *Rheologica Acta*, **18**, 693–701.
- Johannaber, F., Konejung, K., and Plaetschke, R. (1995): Zufall oder Vorsehung — Ausbildung der Wanddicke bei der Gas-Injektions-Technik. *Kunststoffe*, **85**(6), 763–770, (in German).
- Kennedy, P. (1993): *Flow Analysis Reference Manual*. Australia: Moldflow Pty. Ltd.
- Khayat, R.E., Derdouri, A., and Herbert, L.P. (1995): A three-dimensional boundary-element approach to gas-assisted injection molding. *Journal of Non-Newtonian Fluid Mechanics*, **57**, 253–270.
- Kolb, W.B. and Cerro, R.L. (1991): Coating the inside of a capillary of square cross-section. *Chemical Engineering Science*, **46**(9), 2181–2195.
- Kolb, W.B. and Cerro, R.L. (1993a): Film flow in the space between a circular bubble and a square tube. *Journal of Colloid and Interface Science*, **159**, 302–311.
- Kolb, W.B. and Cerro, R.L. (1993b): The motion of long bubbles in tubes of square cross section. *Physics of Fluids A*, **5**(7), 1549–1557.
- Leonov, A.I. (1976): Nonequilibrium thermodynamics and rheology of viscoelastic polymer media. *Rheologica Acta*, **15**, 85–98.
- Lewis, R.W., Usmani, A.S., and Cross, J.T. (1995): Efficient mould filling simulation in castings by an explicit finite element method. *International Journal for Numerical Methods in Fluids*, **20**, 493–506.

- Macosko, C.W. (1989): *RIM, Fundamentals of Reaction Injection Molding*. Munich: Hanser.
- Macosko, C.W. (1993): *Rheology: Principles, Measurements, and Applications*. New York: VCH.
- Manziona, L.T. (1987): *Applications of Computer Aided Engineering in Injection Moulding*. Munich: Hanser.
- Medale, M. and Jaeger, M. (1997): Numerical simulation of incompressible flows with moving interfaces. *International Journal for Numerical Methods in Fluids*, **24**, 615–638.
- Meridies, R. (1981): Verfahren zum Herstellen von Sandwich-Spritzgußteilen mit einem Gas als Kernkomponente. *Kunststoffe*, **71**(7), 420–424, (in German).
- Pearson, T. (1986): Formteilherstellung nach dem Cinpres-Verfahren. *Kunststoffe*, **76**(8), 667–670, (in German).
- Pittman, J.F.T (1989): Finite elements for field problems. In: C.L. Tucker III (ed.), *Computer Modelling for Polymer Processing*, chapter 6. Munich: Hanser.
- Poslinski, A.J., Oehler, P.R., and Stokes, V.K. (1995): Isothermal gas-assisted displacement of viscoplastic liquids in tubes. *Polymer Engineering and Science*, **35**(11), 877–892.
- Potente, H. and Hansen, M. (1993): The gas-assisted injection molding process: comparison between experiment and simulation. *International Polymer Processing*, **VIII**(4), 345–351.
- Press, W.H., Teukolsky, S.A, Vetterling, W.T., and Flannery, B.P. (1992): *Numerical Recipes in FORTRAN: the Art of Scientific Computing*. Cambridge, UK: Cambridge University Press, 2nd edition.
- Reijnierse, C.M.J. (1995): Development of a numerical model for the filling stage of reaction injection molding. Technical Report WFW-95.160, Eindhoven University of Technology.
- Reinelt, D.A. and Saffman, P.G. (1985): The penetration of a finger into a viscous fluid in a channel and tube. *SIAM Journal on Scientific and Statistical Computing*, **6**(3), 542–561.
- Rennefeld, C. (1996): Konstruktive Optimierung von Thermoplastformteilen und Spritzgießwerkzeugen für die Gasinnendrucktechnik. Ph.D. thesis, Universität-GH Paderborn.

- Rose, W. (1961): Fluid-fluid interfaces in steady motion. *Nature*, **191**, 242–243.
- Saffman, P.G. (1991): Selection mechanisms and stability of fingers and bubbles in Hele-Shaw cells. *IMA Journal of Applied Mathematics*, **46**, 137–145.
- Saffman, P.G. and Taylor, G.I. (1958): The penetration of a fluid into a porous medium or Hele-Shaw cell containing a more viscous liquid. *Proceedings of the Royal Society A*, **245**, 312–329.
- Schmidt, L.R. (1974): A special mold and tracer technique for studying shear and extensional flows in a mold cavity during injection molding. *Polymer Engineering and Science*, **14**(11), 797–800.
- Segal, A. (1993): Finite element methods for advection-diffusion equations. In: C.B. Vreugdenhil and B. Koren (eds.), *Numerical Methods for Advection-Diffusion Problems*, chapter 8, pp. 195–212. Braunschweig/Wiesbaden, Germany: Vieweg.
- Segal, A. and Vuik, C. (1995): A simple iterative linear solver for the 3D incompressible Navier-Stokes equations discretized by the finite element method. Technical Report 95-64, Delft University of Technology.
- Shakib, F. (1989): Finite element analysis of the compressible Euler and Navier-Stokes equations. Ph.D. thesis, Stanford University, Stanford, Ca.
- Shen, S.-F. (1992): Grapplings with the simulation of non-Newtonian flows in polymer processing. *International Journal for Numerical Methods in Engineering*, **34**, 701–723.
- Shewchuk, J.R. (1994): An introduction to the Conjugate Gradient method without the agonizing pain. Technical Report CMU-CS-94-125, Carnegie Mellon University, Pittsburgh, Pa.
- Sitters, C.W.M. (1988): Numerical simulation of injection moulding. Ph.D. thesis, Eindhoven University of Technology.
- Taylor, G.I. (1961): Deposition of a viscous fluid on the wall of a tube. *Journal of Fluid Mechanics*, **10**, 161–165.
- Thompson, E. (1986): Use of pseudo-concentrations to follow creeping viscous flows during transient analysis. *International Journal for Numerical Methods in Fluids*, **6**, 749–761.
- Turng, L.S. (1995): Development and application of CAE technology for the gas-assisted injection molding process. *Advances in Polymer Technology*, **14**(1), 1–13.

- Turng, L.S. and Wang, V.W. (1991): Simulation of co-injection and gas-assisted injection molding. In: *ANTEC Proceedings*, pp. 297–300, Society of Plastics Engineers.
- Usmani, A.S., Cross, J.T., and Lewis, R.W. (1992): A finite element method for the simulations of mould filling in metal casting and the associated heat transfer. *International Journal for Numerical Methods in Engineering*, **35**, 787–806.
- White, J.L. and Lee, B.-L. (1975): An experimental study of sandwich injection molding of two polymer melts using simultaneous injection. *Polymer Engineering and Science*, **15**(7), 481–485.
- Woods, J.T., Aslam, S., and Birnby, J. (1995): The stiffness and strength of gas-assisted ribbed parts: the effect of gas core size and its prediction. In: *ANTEC Proceedings*, pp. 3865–3873, Society of Plastics Engineers.
- Yang, S.Y. and Huang, F.Z. (1995a): Unstable gas penetrations in symmetrical rib channels during gas-assisted injection molding. *International Polymer Processing*, **X**(2), 186–187.
- Yang, S.Y. and Huang, F.Z. (1995b): A basic study of rib geometry for gas-assisted injection molding. In: *ANTEC Proceedings*, pp. 747–759, Society of Plastics Engineers.
- Yang, S.Y., Huang, F.Z., and Liao, W.N. (1996): A study of rib geometry for gas-assisted injection molding. *Polymer Engineering and Science*, **36**(23), 2824–2831.
- van der Zanden, A.J.J. (1993): The hydrodynamics of a moving fluid-liquid contact line. Ph.D. thesis, Eindhoven University of Technology.
- Zhao, H., Casademunt, J., Yeung, C., and Maher, J.V. (1992): Perturbing Hele-Shaw flow with a small gap gradient. *Physical Review A*, **45**(4), 2455–2460.
- Zoetelief, W.F. (1995): Multi-component injection moulding. Ph.D. thesis, Eindhoven University of Technology.
- Zoetelief, W.F., Peters, G.W.M., and Meijer, H.E.H. (1997): Numerical simulation of the multi-component injection moulding process. *International Polymer Processing*, **XII**(3), 216–227.
- Zuidema, H. (1995): Modelling of gas-assisted injection moulding. Technical Report WFW 95.144, Eindhoven University of Technology.
- Zuidema, H. (1996): Development of a numerical model for the filling stage of the gas-assisted injection moulding process. Master's thesis, Eindhoven University of Technology, WFW report 96.066.

## Appendix A

# The effect of compressibility on the momentum equation

In this section, we will show that for injection moulding of thermoplastics, the effect of compressibility on the momentum equation can be neglected. As we have introduced compressibility to calculate the polymer shrinkage, this section deals with the effect of polymer compressibility. By assigning a constant density to the fictitious fluid, the air is made *de facto* incompressible.

From equations (2.3) and (2.7a) to (2.7c), it is evident that compressibility only affects the elongational stresses:

$$\tau_{ii} = 2\eta \frac{\partial u_i}{\partial x_i} - \frac{2}{3}\eta (\text{tr}(\mathbf{D})) \quad \text{for } i = 1, 2, 3. \quad (\text{A.1})$$

Using the dimensionless variables defined in Table 2.1, the first term on the right hand side of equation (A.1) can be shown to be of order  $\frac{\eta_0 U}{L}$ , in which both  $U$  and  $L$  are related to the main flow direction. To estimate the order of the compressibility term in this equation, we rewrite the continuity equation as:

$$\text{tr}(\mathbf{D}) = \nabla \cdot \mathbf{u} = -\mathbf{u} \cdot \frac{1}{\rho} \nabla \rho - \frac{1}{\rho} \frac{\partial \rho}{\partial t}. \quad (\text{A.2})$$

Because of the inner product, the left side term is of order  $\frac{U}{L}$  (or equivalently:  $\frac{V}{H}$  or  $\frac{W}{H}$ ). The last term represents the relative change of density in time, which can be approximated by the polymer shrinkage  $\frac{\Delta \rho}{\rho}$  during the cooling time  $\tau$ . The shrinkage and the cooling time are typically of order 10% and 10 s, respectively.

The estimation of the second term in equation (A.2) requires a more elaborate approach. With regard to equation (2.6), we approximate this term by:

$$-\mathbf{u} \cdot \frac{1}{\rho} \nabla \rho = -\mathbf{u} \cdot \frac{1}{\rho} \frac{\partial \rho}{\partial T} \nabla T - \mathbf{u} \cdot \frac{1}{\rho} \frac{\partial \rho}{\partial p} \nabla p. \quad (\text{A.3})$$

With the thermal expansion coefficient  $\alpha$  and the compressibility coefficient  $\kappa$  given by equations (2.30) and (2.64), respectively, equation (A.3) can be written as:

$$-\mathbf{u} \cdot \frac{1}{\rho} \nabla \rho = \mathbf{u} \cdot \alpha \nabla T - \mathbf{u} \cdot \kappa \nabla p. \quad (\text{A.4})$$

Recognising the fact that  $\nabla T$  is largest in thickness directions, whereas  $\nabla p$  is largest in flow direction, we can estimate the order of the second term of equation (A.2) as:

$$-\mathbf{u} \cdot \frac{1}{\rho} \nabla \rho = \frac{\epsilon U \alpha \Delta T}{H} \mathbf{u}^* \cdot \nabla^* T^* - \frac{U^2 \kappa \eta_0}{L} \mathbf{u}^* \cdot \nabla^* p^*, \quad (\text{A.5})$$

in which, again, the dimensionless variables are indicated by an asterisk (\*).

Now that the different contributions to  $\text{tr}(\mathbf{D})$  have been identified, equation (A.1) can be written in its dimensionless form. Dividing by  $\frac{\eta_0 U}{L}$  facilitates the comparison of the first and second term on the right hand side:

$$\begin{aligned} \tau_{ii}^* &= 2\eta^* \frac{\partial u_i^*}{\partial x_i^*} - \frac{2}{3} \eta^* \text{tr}(\mathbf{D}^*) \quad \text{for } i = 1, 2, 3 \\ &= 2\eta^* \frac{\partial u_i^*}{\partial x_i^*} + \frac{2}{3} \eta^* \left( \alpha \Delta T \mathbf{u}^* \cdot \nabla^* T^* - U \kappa \eta_0 \mathbf{u}^* \cdot \nabla^* p^* + \frac{L}{U \tau \rho^*} \frac{\partial \rho^*}{\partial t^*} \right). \end{aligned} \quad (\text{A.6})$$

With characteristic values given in Table 2.2,  $\kappa$  being of the order of  $10^{-9} \text{ Pa}^{-1}$  for polymers and the estimate for the temporal density change given above, the dimensionless groups in the equation above are estimated to be of order:

$$\alpha \Delta T = 10^{-3} \quad (\text{A.7})$$

$$U \kappa \eta_0 = 10^{-6} \quad (\text{A.8})$$

$$\frac{L}{U \tau} \frac{\Delta \rho^*}{\rho^*} = 10^{-2}. \quad (\text{A.9})$$

Consequently, the influence of compressibility on the equation of conservation of momentum can be neglected.



# Appendix B

## Convergence test

Having developed a model for gas-assisted injection moulding and incorporated it into a finite element code, we have to investigate the effects of mesh coarseness and time step size on the simulation result. We therefore introduce the injection of gas into an axisymmetric tube that has been partially filled with liquid as a test problem.

The convergence of the simulation result is checked using the residual wall thickness as the main criterion, as this is the most important quantity to be predicted by the simulation program. Mass conservation of the initially present liquid will not be used as a convergence criterion in this particular test, because any mass gain or loss at the liquid flow front may be compensated by an opposite effect at the gas front.

The computational domain is identical to the one given in Figure 4.1(a) (with cylinder length  $L = 100$  mm and cylinder radius  $R = 5$  mm), and the initial state is depicted in Figure B.1(b); the liquid fraction is 62.5%. The viscosity ratio of the liquid and the gas is  $10^3$ . The initial conditions are defined by:

$$c(t=0) = \begin{cases} 1 & \text{for } 0 \leq z < z_{init} \\ 0 & \text{for } z_{init} < z \leq z_{max} \\ 0.5 & \text{for } z = z_{init} \cup z = 0 \end{cases} \quad (\text{B.1})$$

$$\mathbf{u}(t=0) = \mathbf{0} \quad \forall \mathbf{x} \in \Omega, \quad (\text{B.2})$$

whereas the boundary conditions are:

$$\begin{aligned} u_z(t) &= u_{max} \cdot \left(1 - \frac{r^2}{R_{inj}^2}\right) & \text{for } z = 0 \\ c(t) &= 0 & \text{for } z = 0 \cap r \leq R_{inj}, \end{aligned} \quad (\text{B.3})$$

in which  $z_{init} = 0.625L$ ,  $R_{inj} = 0.2R$ , and  $u_{max} = 3.2 \text{ m s}^{-1}$ . Consequently, the filling time for this case is 0.375 s.

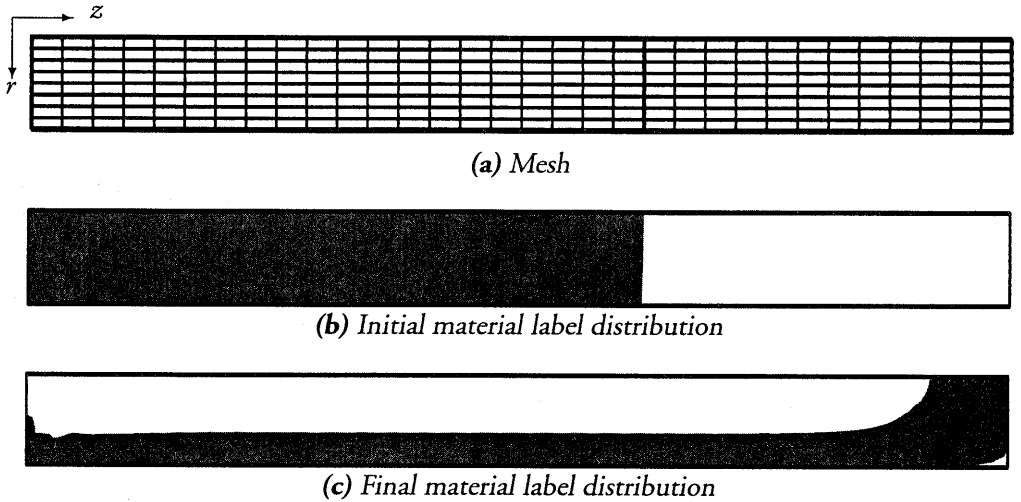


**Figure B.1:** Convergence test for gas penetration into a cylinder partially filled with a Newtonian liquid. Results for  $32 \times 8$  elements,  $\Delta t = 1.25 \cdot 10^{-3}$  s. Note that these figures are rotated over  $90^\circ$  clockwise with respect to Figure 4.1(a)

Assuming that a mesh of  $128 \times 32$  elements (over  $L$  and  $R$ , respectively) and a time step of  $3.125 \cdot 10^{-4}$  s yields a converged solution (which can be easily checked afterwards), we have carried out two sequences of simulations: one with increasing the time step, and another one with decreasing number of elements (keeping, respectively, the mesh and the time step constant). Having thus found that a mesh of  $32 \times 8$  elements yields a sufficiently converged result (see Table B.1), the time step has again been increased. A time step size of  $1.25 \cdot 10^{-2}$  for this mesh appears to be sufficient. Even a mesh of  $16 \times 8$  elements seems to yield a sufficiently converged solution, but gives rise to significant oscillations in the velocity field.

**Table B.1:** Residual wall thickness  $\varepsilon$  as a function of element size and time step for the gas penetration into a Newtonian liquid in a cylinder. Results marked with an asterisk exhibit oscillations in the velocity field.

# elements	time step [s]				
	$3.125 \cdot 10^{-4}$	$6.25 \cdot 10^{-4}$	$1.25 \cdot 10^{-3}$	$2.5 \cdot 10^{-3}$	$5 \cdot 10^{-3}$
128×32	0.368	0.365	0.354	0.329	
64×32	0.367				
64×16	0.368				
32×16	0.366				
32×8	0.364	0.362	0.362	0.353	0.333
16×8	0.365*	0.365*	0.364*		
16×4	0.377*				



## Appendix C

# The fingering effect

It was mentioned in Chapter 1, that when the gas front enters a thin-walled part of the mould, it is likely to become unstable. Usually, the gas is seen to proceed as irregularly shaped fingers into the part. This fingering effect is similar to the *viscous fingering* that can be observed when a fluid displaces another fluid with a higher viscosity in Hele-Shaw cell, which was investigated by Saffman and Taylor (1958) and Chuoke *et al.* (1959) (see also Bensimon *et al.* (1986) for a review). A short account of their stability analysis will be given here.

Consider a fluid 1 with viscosity  $\eta_1$  and density  $\rho_1$  displacing another fluid 2 with viscosity  $\eta_2$  and density  $\rho_2$  in a Hele-Shaw cell. Attach the coordinate system  $(x, y, z)$  to the interface between the two fluids, which moves uniformly with velocity  $U$  directed from fluid 1 to fluid 2, with  $x$  perpendicular to the interface (also directed from fluid 1 to fluid 2),  $y$  directed along the cell width, and  $z$  along the cell thickness  $b$ . Assume that the fluids are immiscible, and let the instantaneous interface between the two fluids be given by the plane  $x = 0$ . Suppose that this interface is slightly deformed by a wave-like disturbance of wavelength  $\lambda = 2\pi/k$  ( $k > 0$ ) given by:

$$x = ae^{iky+qt}. \quad (\text{C.1})$$

(It is assumed that the system is invariant in the  $z$ -direction, which implies, for instance, that fluid 2 is completely expelled over the cell thickness. Saffman and Taylor (1958) demonstrate that this assumption does not affect the stability analysis in a qualitative sense.)

Linear stability analysis now yields the following characteristic equation:

$$\frac{q}{k} \frac{12}{b^2} (\eta_2 + \eta_1) = \frac{12}{b^2} (\eta_2 - \eta_1) U + (\rho_2 - \rho_1) g \cos \beta, \quad (\text{C.2})$$

in which  $\beta$  is the angle between  $x$  and the vertical direction. Clearly, the disturbance will grow if  $q > 0$ , that is, if

$$\frac{12}{b^2}(\eta_2 - \eta_1)U + (\rho_2 - \rho_1)g \cos \beta > 0. \quad (\text{C.3})$$

Adding the effect of surface tension (which suppresses the instability) to equation C.2 yields:

$$\frac{q}{k} \frac{12}{b^2}(\eta_2 + \eta_1) = \frac{12}{b^2}(\eta_2 - \eta_1)U + (\rho_2 - \rho_1)g \cos \beta - \gamma k^2, \quad (\text{C.4})$$

from which it can be derived that the perturbation will grow if it contains wavelengths larger than the critical wavelength  $\lambda_c$  defined by

$$\lambda_c = 2\pi\sqrt{\gamma} \left\{ \frac{12}{b^2}(\eta_2 - \eta_1)U + (\rho_2 - \rho_1)g \cos \beta \right\}^{-\frac{1}{2}}. \quad (\text{C.5})$$

Substituting the characteristic values for gas-assisted injection moulding (see Table 2.2) into this equation yields a critical wavelength. Since, however, we are considering gas penetration into *thin-walled* geometries, the characteristic value for the thickness  $b$  should not be taken as the value for  $H$  from Table 2.2, as  $H$  applies to thick-walled channels. Instead,  $b$  is given a characteristic value of 1 mm for thin-walled parts. Consequently,  $\lambda_c$  is found to be of the order of  $10^{-5}$  m. As this value is small compared to the typical width of a thin-walled mould part, viscous fingering is likely to occur.

Another parameter that has been reported to affect the stability, is the gradient of the gap between the two plates in a Hele-Shaw cell (Zhao *et al.*, 1992). The interface was observed to be stabilised in a convex gap, and de-stabilised in a concave gap. In (gas-assisted) injection moulding, the actual boundaries of the flow are not the upper and lower mould walls, but the transitions from melt to solid layer. The analytical solution obtained by Janeschitz-Kriegl (1979) for the solid layer thickness along an injection moulded thin strip shows, that the actual flow channel is convex near the injection point and concave toward the end of the flow path. Hence, if gas penetrates into a thin-walled part of a GAIM mould, it will not have to become unstable immediately.

# Dankwoord

Graag wil ik hier iedereen bedanken die een bijdrage heeft geleverd aan het tot stand komen van dit proefschrift. Met name de enthousiaste manier waarop Frans van de Vosse, Gerrit Peters en Han Meijer mij bij mijn promotiewerk begeleid hebben, is voor mij zonder meer motiverend geweest.

Mijn dank gaat ook uit naar Carla Reijnierse, die met het werk voor haar ontwerpersopleiding een vliegende start van mijn promotie-onderzoek mogelijk heeft gemaakt, en naar Hans Zuidema en Gerald Croes, die hun afstudeeropdracht en stages hebben uitgevoerd in het kader van dit onderzoek.

Het regelmatige overleg met Will Balemans, Pieter Schoone, Marten Westerhof en Onno Hoitinga van Philips CFT, en hun kritische vragen met het oog op de praktische toepasbaarheid van mijn werk, heb ik altijd erg gewaardeerd. Frank Baaijens wil ik bedanken voor de discussies over restspanningen.

Verder ben ik dank verschuldigd aan de volgende mensen die op uiteenlopende manieren mijn promotiewerkzaamheden hebben ondersteund: Patrick Anderson, Leo Wouters, Patrick van Brakel, Ard Kuijpers, Marcel Heertjes, Toon van Gils, Sjef Garrenfeld, Rob van den Berg, Maykel Verschueren en Marcel van Gils; en aan mijn zus Mariska voor haar inbreng in het omslagontwerp.

Als dank voor hun morele ondersteuning draag ik de laatste stelling bij dit proefschrift op aan de leden van wielersclub-in-oprichting *'Eraf is eraf'*. Van mijn niet-wielrennende vrienden hoop ik dat ze mijn dank aanvaardden zonder een dergelijke opdracht.

Maar mijn dank gaat vooral uit naar mijn ouders, die me altijd onvoorwaardelijk hun steun en vertrouwen hebben gegeven.

Gerard Haagh  
Eindhoven, 5 maart 1998





# Curriculum Vitae

Gerard Haagh werd op 8 maart 1968 geboren te Dongen. Hij behaalde in 1986 het Gymnasium- $\beta$ -diploma aan het Theresialyceum in Tilburg, waarna hij werktuigbouwkunde ging studeren aan de Technische Universiteit Eindhoven. Na een stage van vier maanden aan het Georgia Institute of Technology in Atlanta (VS), rondde hij in 1992 zijn studie af met een opdracht op het gebied van de tribologie.

Vervolgens besloot hij de ontwerpersopleiding Computational Mechanics te volgen aan het Instituut voor Vervolgopleidingen van de TU Eindhoven, waardoor hij bij de vakgroep Fundamentele Werktuigkunde in aanraking kwam met de kunststoftechnologie. Zijn ontwerpoperdracht had betrekking op het modelleren van het spuitgieten van reagerende kunststoffen ten behoeve van de productie van hoogspanningsisolatoren, en werd uitgevoerd in samenwerking met Raychem Ltd in Swindon, Engeland. Aansluitend begon hij in 1995 bij dezelfde vakgroep het promotie-onderzoek dat in dit proefschrift beschreven is.